AD-A189 132   HF (HIGH FREQUENCY) MAXIMUM USABLE FREQUENCY (MUF)   1/2
MODEL UNCERTAINTY ASSESSMENT(U) NAVAL OCEAN SYSTEMS
CENTER SAN DIEGO CA T N ROY ET AL. JUN 87 NOSC/TR-1184

UNCLASSIFIED   F/G 20/14   NL

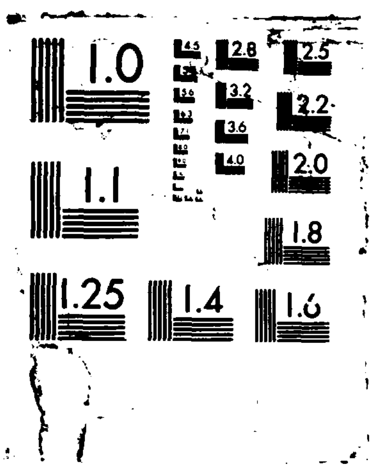
1.0
2.8
2.5
3.2
2.2
3.6
4.0
2.0
1.1
1.8
1.25
1.4
1.6

NOSC TR 1184

(4)

NOSC TR 1184

NOSC

NAVAL OCEAN SYSTEMS CENTER San Diego, California 92152-5000

Technical Report 1184
June 1987

HF Maximum Usable Frequency (MUF) Model Uncertainty Assessment

AD-A189 132

T. N. Roy
D. B. Sailors

UNITED STATES NAVY
NAVAL OCEAN SYSTEMS CENTER

Approved for public release; distribution is unlimited.

87 12 10 002

NAVAL OCEAN SYSTEMS CENTER

San Diego, California 92152-5000

E. G. SCHWEIZER, CAPT, USN
Commander

R. M. HILLYER
Technical Director

ADMINISTRATIVE INFORMATION

The work reported herein was performed by members of the Ionospheric Branch, Ocean and Atmospheric Sciences Division, Naval Ocean Systems Center, during the period October 1984 through September 1986. The project was sponsored by the U.S. Army Communication Electronics Command and Space and Naval Warfare Systems Command.

The authors wish to acknowledge various groups in the HF propagation community, too numerous to mention individually, for their assistance in accumulating more than 13,000 hours of oblique sounder propagation data for this report.

Released by
D.B. Sailors, Head
Ionospheric Sciences Branch

Under authority of
J.H. Richter, Head
Ocean and Atmospheric
Sciences Division

AS

UNCLASSIFIED
SECURITY CLASSIFICATION OF THIS PAGE

AD-A182 932

REPORT DOCUMENTATION PAGE

1a REPORT SECURITY CLASSIFICATION UNCLASSIFIED	1b RESTRICTIVE MARKINGS
2a SECURITY CLASSIFICATION AUTHORITY	3 DISTRIBUTION/AVAILABILITY OF REPORT Approved for public release; distribution is unlimited.
2b DECLASSIFICATION DOWNGRADING SCHEDULE	
4 PERFORMING ORGANIZATION REPORT NUMBER(S) NOSC TR 1184	5 MONITORING ORGANIZATION REPORT NUMBER(S)
6a NAME OF PERFORMING ORGANIZATION Naval Ocean Systems Center — 6b OFFICE SYMBOL (if applicable) NOSC	7a NAME OF MONITORING ORGANIZATION
6c ADDRESS (City, State and ZIP Code) San Diego, CA 92152-5000	7b ADDRESS (City, State and ZIP Code)
8a NAME OF FUNDING SPONSORING ORGANIZATION U.S. Army Communication Electronics Command — 8b OFFICE SYMBOL (if applicable) COM/ADP	9 PROCUREMENT INSTRUMENT IDENTIFICATION NUMBER
8c ADDRESS (City, State and ZIP Code) Ft. Monmouth, NJ 07703	10 SOURCE OF FUNDING NUMBERS PROGRAM ELEMENT NO: RDA; PROJECT NO: Army; TASK NO: 542-MP48; AGENCY ACCESSION NO: DN088 607

11 TITLE (include Security Classification)
HF Maximum Usable Frequency (MUF) Model Uncertainty Assessment

12 PERSONAL AUTHOR(S)
T.N. Roy, D.B. Sailors

13a TYPE OF REPORT	13b TIME COVERED	14 DATE OF REPORT (Year, Month, Day)	15 PAGE COUNT
Research	FROM Oct 1984 TO Sep 1986	June 1987	117

16 SUPPLEMENTARY NOTATION

17 COSATI CODES			18 SUBJECT TERMS (Continue on reverse if necessary and identify by block number)
FIELD	GROUP	SUB GROUP	HF propagation, MOF, maximum observable frequency, MUF, maximum usable frequency, HF model, MINIMUF

19 ABSTRACT (Continue on reverse if necessary and identify by block number)

A statistical analysis of observed oblique sounder median maximum observed frequencies (MOF) and predicted maximum usable frequencies (MUF) was used to assess the accuracy of high-frequency MUF prediction. A database of 13,054 hours of oblique sounder MOFs measured on 70 paths was compared with the predicted MUF values from MINIMUF-3.5, MINIMUF 85, and an unrelated MUF model, the HF Broadcast WARC Model (HFBC84). The data were screened into subsets to determine the effect of particular paths, path length and orientation, season, month, latitude, sunspot number, diurnal trends, geographic region, and sounder type. The accuracy of all three models was very close, with the MINIMUF-3.5 model having the lowest RMS error of 4.44 MHs. MINIMUF 85 was next, with an RMS error of 4.58 MHs, and HFBC84 was last, with an error of 4.67 MHs. The HFBC84 model had the lowest average residual (bias) of 1.17 MHs, with MINIMUF-3.5 next, with a bias of 1.26 MHs, and MINIMUF 85 last, with 1.28 MHs. Correlation was good for all three models. Correlation coefficients were .824, .819, and .827 for MINIMUF-3.5, MINIMUF 85, and HFBC84, respectively. Future improvements to the MINIMUF model are discussed and current MUF computer algorithms are included in the appendices.

20 DISTRIBUTION/AVAILABILITY OF ABSTRACT	21 ABSTRACT SECURITY CLASSIFICATION
☐ UNCLASSIFIED/UNLIMITED ☒ SAME AS RPT ☐ DTIC USERS	UNCLASSIFIED

22a NAME OF RESPONSIBLE INDIVIDUAL	22b TELEPHONE (include Area Code)	22c OFFICE SYMBOL
T.N. Roy	619-225-6822	Code 542

DD FORM 1473, 84 JAN — 83 APR EDITION MAY BE USED UNTIL EXHAUSTED. ALL OTHER EDITIONS ARE OBSOLETE

UNCLASSIFIED
SECURITY CLASSIFICATION OF THIS PAGE

CONTENTS

ILLUSTRATIONS

ILLUSTRATIONS, Continued

ILLUSTRATIONS, Continued

TABLES

SUMMARY

OBJECTIVE

Assess the accuracy of predicted MUFs from MINIMUF-3.5, MINIMUF 85, and HFBC84 MUF models, using a maximum observed frequency (MOF) database of 13,054 observed oblique sounder median MOFs from 70 paths.

RESULTS

The addition of 31 oblique sounder paths to the MOF database increased the total number of path-hours available for analysis from 7276 to 13054. Overall bias for MINIMUF-3.5 increased from 0.51 MHz for the 39-path database to 1.26 MHz for the new database; RMS error increased from 4.33 MHz to 4.44 MHz; and the correlation coefficient decreased slightly from .85 to .82. Overall bias for MINIMUF 85 also increased from 0.16 MHz to 1.28 MHz, RMS error increased from 4.19 MHz to 4.58 MHz and the correlation coefficient decreased from .86 to .82. For reference, the overall bias for the HFBC84 MUF model was 1.17 MHz, RMS error was 4.67 MHz, and the correlation coefficient was .83.

RECOMMENDATIONS

As a result of this study, the following recommendations are made:

(1) Use MINIMUF 85 instead of MINIMUF-3.5.

(2) Make additional improvements in the MINIMUF model by adding geographical and time dependencies not accounted for in the effective zenith angle in the model.

(3) Improve the M-factor representation by introducing the effects of the underlying layers on F-region M-factor estimation.

(4) Continue to enhance the MOF database for regions of the world not represented.

(5) Test the MINIMUF models in the south polar region.

(6) Use the MOF database to validate other ionospheric prediction models such as IONOCAP.

1.0 INTRODUCTION

The effective operation of long-distance, high-frequency (HF) communications systems has increased in proportion to the ability to predict variations in the ionosphere. These variations are affected in a complex manner by solar activity, seasonal and diurnal changes, as well as latitude and longitude. Such a predictive capability has permitted communicators to optimize frequencies, antennas, and other circuit parameters.

Initially, manual methods were developed for analyzing ionospheric variations on HF circuits of short, intermediate, and long distances (Reference 1). Because the manual methods were laborious and time consuming, various organizations developed computer programs to analyze HF circuit performance. A commonly predicted parameter in these programs is the maximum usable frequency (MUF). The MUF is the highest frequency that can be propagated by ionospheric refraction between points at a given time. Another commonly predicted parameter is the lowest usable frequency (LUF). The LUF is the lowest usable frequency propagated and is determined by the amount of D-region absorption. The LUF over any circuit path is established as a function of total path absorption with respect to such HF system parameters as transmitted power, signal-to-noise ratio, and antenna gains.

More recently, the Naval Ocean Systems Center (NOSC) has developed a series of ionospheric prediction programs that will run on portable microcomputers. MINIMUF, MINIMUF-3.5, and MINIMUF 85 are examples of this series of NOSC-developed models. The evolution of these models will be discussed in the next section.

This report will describe the uncertainty assessment of the MINIMUF and HF Broadcast Work (HFBC84) MUF models. The method of HF model uncertainty assessments starts with the construction of a database pertinent to each model. Each database containing observed ionospheric propagation data is edited for all propagation parameters to produce a modeled database. For each model, the observed and modeled data are compared using the Data Screen program. Error tables are produced as a function of all propagation parameters. At this point the model may be modified and retested to minimize the values in the error tables. A detailed description of this process is given in section 3.0.

Results are available from the analyses of the 70-path oblique sounder MOF database; 13,054 path hours were analyzed. The HFBC84 model had the lowest average residual (bias) of 1.17 MHz. MINIMUF-3.5 was next with a bias of 1.26 MHz and MINIMUF 85 was last with 1.28 MHz. MINIMUF-3.5 had the lowest rms error of 4.44 MHz with MINIMUF 85 next, 4.58 MHz and the HFBC84 model last with 4.67 MHz. Correlation coefficients for all three models were high, with the HFBC84 model correlation of .827, MINIMUF-3.5 with .824 and MINIMUF 85 with .819.

2.0 HISTORY OF HF PREDICTION

During the past 25 years, a steadily increasing dependence upon HF communications has resulted in the requirement for automated HF propagation predictions. Electronic computers are used today because of the speed with which they can handle the large volumes of data and lengthy computations needed for accurate predictions. Many different models of ionospheric radio propagation have been developed, ranging from extremely simple approximations to very complex ray-tracing techniques (References 2-22).

In 1978 NOSC developed a simplified HF MUF prediction algorithm called MINIMUF-3 (Reference 23). It was designed to complement existing large-scale HF propagation codes when computational resources were limited and when execution of large-scale codes was not feasible. It was based on the idea that f_0F2 can be modeled to a first approximation as the lagged response to a driving function proportional to $(\cos \chi)^n$, where χ is the instantaneous solar zenith angle and when the daytime lag is quite seasonally dependent. It was shown to be sufficiently accurate to provide an MUF prediction suitable for use on microcomputers. MINIMUF-3.5 allowed MINIMUF-3 to be used out to the antipodal point (Reference 24) as it formerly was constrained to be used in the 800- to 8000-km range. It also has been compared against short-range (192 km and 433 km) oblique sounder data (Reference 25). The most current model, called MINIMUF 85, extended MUF prediction to high latitudes.

3.0 MODEL UNCERTAINTY ASSESSMENT

3.1 DEVELOPMENT OF THE OBLIQUE SOUNDER DATABASE

The oblique sounder database assembled for this uncertainty assessment was derived from technical report graphs and sounder photographs, data printouts, and magnetic tapes. Digitization of the data was required in many cases and in others statistical tests were performed to determine if sufficient data were available to calculate an accurate monthly median value. Attempts were made to make the database as diverse as possible, including a variety of different path lengths, orientations, and geographical locations. The MOF database spans the period between 1960 and 1981, almost two complete solar sunspot cycles of propagation data. Figure 1 is a block diagram showing how data were prepared for the data screen comparison program. Observed oblique sounder data graphs and ionograms were digitized using the Tektronix 4596 digitizer and 4051 microcomputer. The digitized data were stored on magnetic tape in files containing additional data such as transmission-path parameters, solar activity indices, date/time, and transmitter-receiver specifications. Other data from technical report tables and printouts were entered into the database by hand using the MOF/LOF utility program. Existing data and new data on magnetic tape were combined with the digitized data and stored on 9-track magnetic tape. It was this MOF data tape that was used as input to the data screen comparison program.

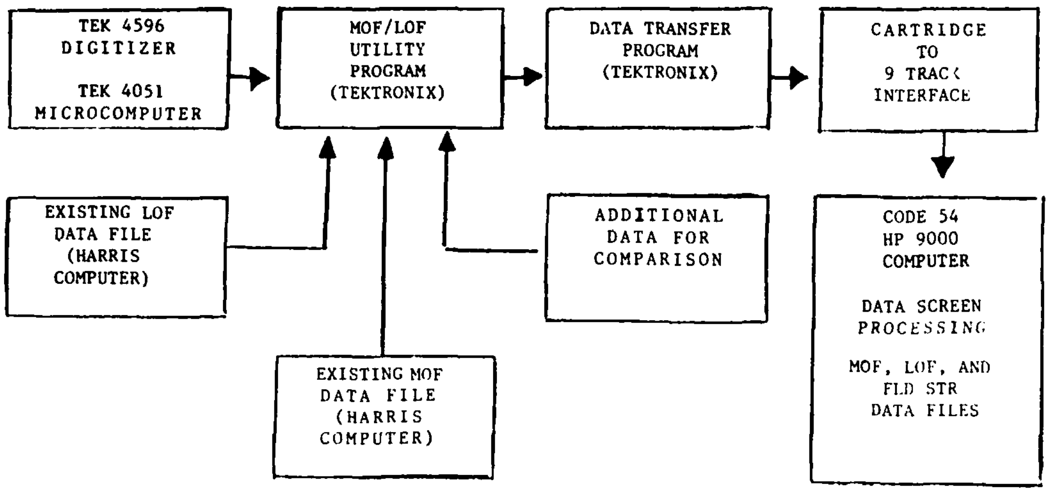

Figure 1. NOSC HF sounder database development.

The source of oblique sounder data is important because it influences the statistical significance of a given path-month measurement. The MOF sounder data were categorized into six sources: (1) NTSS-HFDR, (2) NTSS-strip chart, (3) non-NTSS, (4) Granger 900 series, (5) Modified C-3, and (6) BR Communications Chirpsounder.

The Navy's Tactical Sounder System (NTSS) consists of several shore-based sounder transmitters and a number of sounder receivers. AN/FPT-11 (XN-1) sounder transmitters were installed at selected naval communication stations. The system receiver and an AN/UPR-2 receiver were installed at selected naval communications stations, research installations, and aboard ships.

Once each minute the FPT-11 transmitter sequentially transmitted a double, biphase, Barker-coded pulse on each of 80 discrete frequencies between 2 and 32 MHz; the total scan consisted of 160 pulses lasting 16 s. The frequency range is divided into 4 octave bands, with 20 channels linearly spaced in each band. The 80 frequencies were spaced in 100-kHz increments in the 2- to 4-MHz range (Band A), 200-kHz increments from 4 to 8 MHz (Band B), 400-kHz increments from 8 to 16 MHz Band C), and 800-kHz increments from 16 to 32 MHz (Band D).

The UPR-2 receiver sequentially processed the pulse-train input by starting the gated receiver scan at the same time as the transmission. This was accomplished by synchronizing to a common timing source (i.e., WWV) and maintaining an accurate time-base generator in the receiver. Since each sounder signal is composed of a series of 13 Barker-coded subpulses, signal processing is required in the receiver. The process gain over noise is 11 dB. A permanent record of the daily variations of the scanned spectrum between 2 and 32 MHz is produced on strip charts. To supplement this capability, NOSC developed a method of digitizing the video output signal and recording it on magnetic tape. The HF digital recorder (HFDR) developed for this purpose operates concurrently with the AN/UPR-2 receiver and in no way affects normal operation. Hence, with the HFDR-equipped sounder receiver, all amplitude, time delay and frequency information are recorded once every minute, 24 hours a day.

Data collected prior to 1968 were measured on a variety of sounder systems. One system, used primarily by Stanford Research Institute, used the Model 900 series of sounders made by Granger Associates (Reference 26). These scanned the range of frequencies from approximately 4 to 64 MHz in four 1-octave bands of 40 linearly spaced channels each. The transmitted output is in pulses of 0.1 ms (short pulse) or 1.0 ms (long pulse) at 30 kW peak amplitude, repeated two or four times each channel. The long pulse is more appropriate for communication system sounding and also presents a higher average power, which is often needed on long paths. The short pulse is used for mode resolution and is normally made as narrow as possible within the limitations set by the length of the sounded path. The entire scan was completed in 29 s and was repeated every 20 min. Another sounder system, a modified C-3 ionosonde, transmitted 0.1-ms pulses; the transmitting frequency was swept linearly between 2 and 25 MHz (Reference 27). In some instances data were acquired by means of a Granger transmitter and UPR-2 receiver. Most of the recent sounder data were measured using BR Communications HF Chirpsounder System equipment. This system sweeps the range of frequencies from 2 to 30 MHz in 5 min. Each sweep is repeated every 15 min.

A path-month MOF curve from the NTSS-HFDR system is generally the product of approximately 40,000 digitally processed measurements (up to 1861 an hour over the month). The resolution of the NTSS-strip chart system limits this to about 2880 hand-scaled data points per path-month (120 per hour of the month). The Granger series data consisted of three scans per hour or 90 points per hour per month or 2160 data points per path-month. The modified C- 3 data consisted of one 7.5-min sweep every hour. This was equivalent to 720 points per path-month (30 per hour per month). The non-NTSS system consists of 180 points per hour or 4320 data points per month.

The data can also be categorized according to the frequency range of the sounder transmitter. In the first three categories, the sounder scanned the range from 2 to 32 MHz. The Granger 900 series scanned the range from 4 to 64 MHz, and the modified C-3 scanned the range from 2 to 25 MHz. The chirp sounder operates in the frequency range of 2 to 30 MHz.

3.2 DATA SCREENING

In the comparison of the models, it is highly desirable to subdivide the database into subsets according to variables influencing the predicted and observed results (e.g., path length, season, month, geomagnetic latitude, sunspot number (SSN), local time at path midpoint, etc.). To accomplish this, a computer program called DASCR3 (acronym for data screening 3) was used. The results, along with auxiliary information about the propagation situation (e.g., path length, local time of day, SSN, etc.), were stored in a data file to be used later by DASCR3.

DASCR3 is a program designed to perform data screening and statistical comparison on two large matrices of observations. For each set of matrices, up to 10 sets of information are read on propositions to be satisfied and limits placed on a selected variable. A portion of each matrix is read in and tested for each set of propositions in turn. For each subset satisfying a given set of conditions, the variable to be analyzed is stored temporarily on disc. The next portion of each matrix is then read in and screened, and the good observations are added to those already on disc. When the entire matrix has been screened, the screened data are then read into core, and the difference (or residual) between the two matrices is taken. These arrays are then sorted to ensure maximum computer efficiency for the statistical evaluation. Finally, a statistical evaluation is then performed of the screened data and their residuals.

An example of the output from DASCR3 is given in Figure 2. The variables being compared are the observed MOF and predicted MUF. In the printout the observed data are represented by column A, and the predicted values are represented by column B. The residual (the observed data minus the predicted value) is given by column D. The relative residual is given by column D/A, and the absolute relative residual by column ABS(D)/A. The left-hand side of the page shows the statistics calculated for each of these columns. In addition, the correlation coefficients between the observed and predicted data are given. Included also are the slope, intercept, and mean square error of linear regression.

Each computer model is run to produce a predicted database corresponding to the observed database. Auxiliary information output to be screened included universal time of propagation, month, year, 12-month running mean and monthly median SSN, path length in kilometers, geographic region of the path midpoint, the local time at the path midpoint, the path orientation with respect to north, the geomagnetic latitude at each of the control points, the predicted MUF, path identification number, and sounder type.

Before the actual data screening was begun, data points in both observed and predicted bases corresponding to observed values at the extremes of the particular measuring sounder were removed from the database.

3.3 ANALYSIS OF RESIDUALS BETWEEN PREDICTIONS AND OBSERVED DATA

An indication of the accuracy of the numerical predictions can be obtained from a study of the residuals between observed data and predicted values. The terms "residual," "relative residual," and "absolute relative residual" are used with the following standard meaning:

$$\text{residual} = (\text{observed datum}) - (\text{predicted value}) \tag{1}$$

$$\text{relative residual} = \frac{\text{residual}}{\text{observed datum}} \tag{2}$$

$$\text{absolute relative residual} = \frac{\text{absolute residual}}{\text{observed datum}} \tag{3}$$

DATA SCREENING PROBLEM : MINIMUF 85 by PATH ID

CONDITIONS TO BE SATISFIED
PATH ID (ckt#) EQ 15.00000

SUMMARY STATISTICS FOR VARIABLE 11 = OBSERVED MOF and 12 = PREDICTED MUF

STATISTIC	A	B	D	D/A	ABS(D)/A
TOTAL	10888.4	10417.4	471.000	-.508231	76.3940
POPULATION SIZE	528.000	528.000	528.000	528.000	528.000
AVERAGE	20.6220	19.7299	.892045	-.962559E-03	.144686
R.M.S. VALUE	22.1592	20.8402	3.45340	.223797	.223797
MEAN ABSOLUTE ERROR	7.48114	5.91034	2.59603	.144875	.914327E-01
STANDARD DEVIATION	8.10949	6.71149	3.33620	.223795	.170737
3RD MOMENT ABOUT MEAN	-82.2755	-31.9005	-25.9860	-.336463E-01	.224938E-01
4TH MOMENT ABOUT MEAN	6219.11	3525.85	607.085	.408768E-01	.238888E-01
5TH MOMENT ABOUT MEAN	-20400.3	-3899.01	-4890.03	-.480450E-01	.254993E-01
6TH MOMENT ABOUT MEAN	689601.	333793.	70073.0	.587637E-01	.278409E-01
LOWER DECILE	9.50361	10.2975	-2.48047	-.213048	.203342E-01
LOWER QUARTILE	12.9002	13.5347	-.978994	-.752745E-01	.547460E-01
MEDIAN QUARTILE	20.6030	20.5049	.804528	.395371E-01	.117313
UPPER QUARTILE	28.8161	25.3232	3.12725	.135213	.179880
UPPER DECILE	30.1711	28.3732	4.87759	.193257	.240361
.00TH PERCENTILE	.000000E+00	.000000E+00	.000000E+00	.000000E+00	.000000E+00
.00TH PERCENTILE	.000000E+00	.000000E+00	.000000E+00	.000000E+00	.000000E+00
SEMI-INTERQUARTILE RANGE	7.95794	5.89426	2.05312	.105244	.625669E-01
COEFFICIENT OF VARIATION	.393245	.340168	3.73995	-232.500	1.18005
MINIMUM	7.10000	7.50000	-12.8000	-1.37647	.000000E+00
MAXIMUM	31.6000	32.2000	9.10000	.307432	1.37647
COEFFICIENT OF SKEWNESS	-.154273	-.105521	-.699812	-3.00184	4.51942
COEFFICIENT OF EXCESS	-1.56202	-1.26225	1.90048	13.2959	25.1117
INTERVAL SIZE	12.2500	12.3500	10.9500	.841952	.688235
GIVEN LOWER BOUND	.000000E+00	.000000E+00	.000000E+00	.000000E+00	.000000E+00
GIVEN UPPER BOUND	.000000E+00	.000000E+00	.000000E+00	.000000E+00	.000000E+00
CORRELATION COEFFICIENT	.915705				

A MATRIX = OBSERVED

LINEAR REGRESSION ESTIMATE OF Y=AX+B

MEAN SQUARE ERROR	10.619847
STANDARD ERROR OF ESTIMATE	3.258811
EST. OF THE STANDARD ERR. OF THE MEAN	.141822
MEASURE OF ERR. IN REGRES COEF. B	.145366
SLOPE	1.106446
INTERCEPT	-1.208141

MEAN-SQUARE ESTIMATE OF Y=AX

MEAN SQUARE ESTIMATE	10.788754
STANDARD ERROR OF THE ESTIMATE	3.284624
SLOPE	1.045212

END OF PROBLEM

Figure 2. Example output from DASCR3.

Certain statistical measures of these terms have proved useful in past ionospheric studies in comparing predicted and observed data. These include:

(1) The average residual (av. res.).
(2) Root mean square residual (RMS res.).
(3) The mean absolute error of the residual (mae res).
(4) The average relative residual (av. rel. res.).
(5) The root mean square relative residual (RMS rel. res.).
(6) The mean absolute error of the relative residual (mae rel. res.).
(7) The average absolute relative residual (ave. abs. rel. res.).
(8) Correlation coefficient between observed and predicted values.
(9) The standard error of the estimate of linear regression.

Values of each of these parameters are produced by DASCR3 as can be seen by examining Figure 2. Examples of these statistical parameters plotted from DASCR3 analysis results for the MINIMUF-3.5 model are shown in the following figures. The results when MINIMUF-3.5 was compared against a 25-path database is discussed in Reference 28.

The average residual and the average relative residual locate the center of the distributions of error and are sometimes referred to as the bias in the estimate. Figures 3 and 4 illustrate the average residual and average relative residual, respectively, as a function of month for the three MUF models tested.

The mean absolute errors of the residual and relative residual are a measure of the range of the error and are the first moments about the average residual and average relative residual, respectively. They provide information about the range of variation. Figures 5 and 6 are examples of these two parameters, respectively, for MINIMUF-3.5. They are displayed as bars about the average residual (bias) as a function of month. The mean absolute error of the relative residual is rather uniform as a function of month as shown in Figure 6. However, Figure 5 shows that the range of variation of the mean absolute error during the equinox months March and September to be greater than the other months.

The average absolute relative residual is a measure of the average magnitude of the error. Figure 7 shows a plot of the average absolute relative residual as a function of month for MINIMUF-3.5.

The RMS residual and relative residuals are measures of the dispersion in the error. In fact, the RMS residual and RMS relative residual are the standard deviations of the error about the origin (zero bias) and are related to the standard deviation about the mean according to

$$\sigma^2 = \nu_2 - \nu_1^2, \tag{4}$$

where ν_2 the mean square error (the square of the RMS error), and ν_1 is the bias. When the bias is small or nearly zero, the standard deviation and the RMS error are nearly the same. Otherwise, the RMS error is larger than the standard deviation. Figures 8 and 9 are examples of the RMS residual and RMS relative residual, respectively, plotted as a function of month.

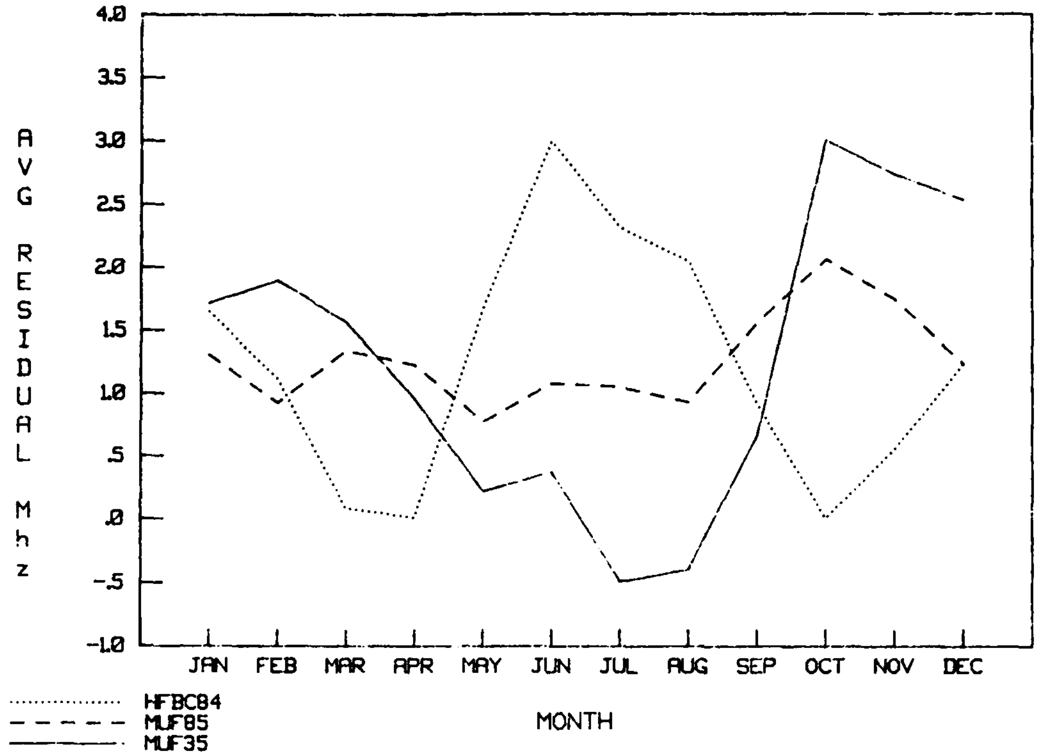

Figure 3. Average residual (bias) as a function of month.

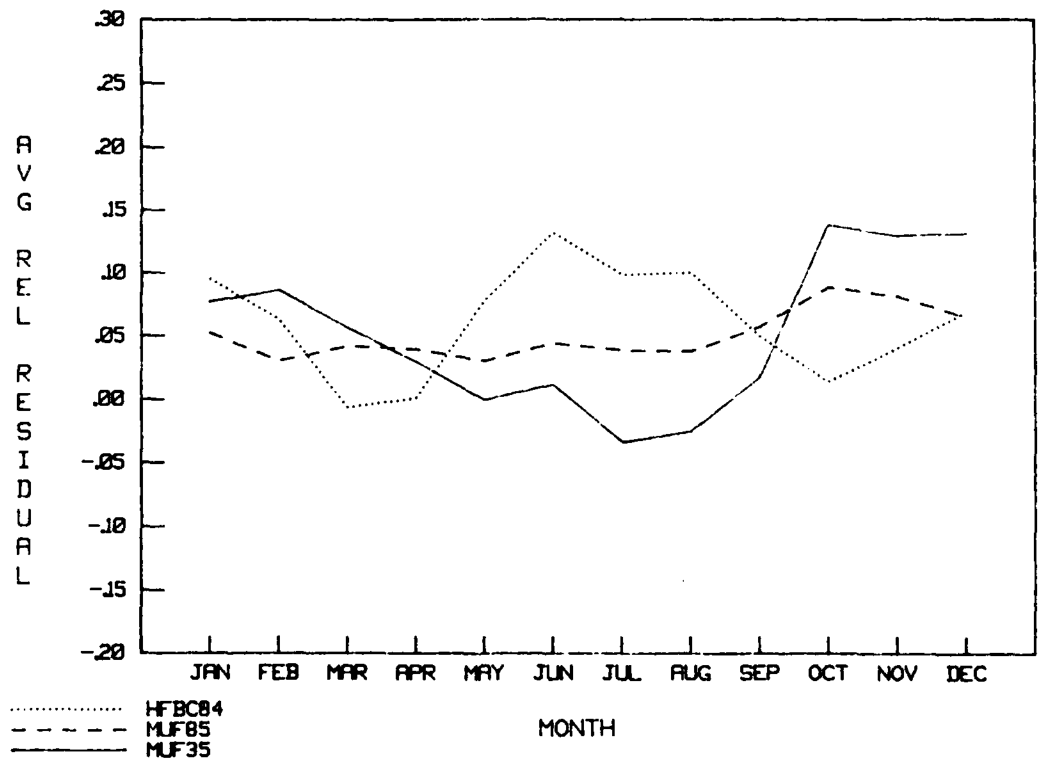

Figure 4. Average relative residual (relative bias) as a function of month.

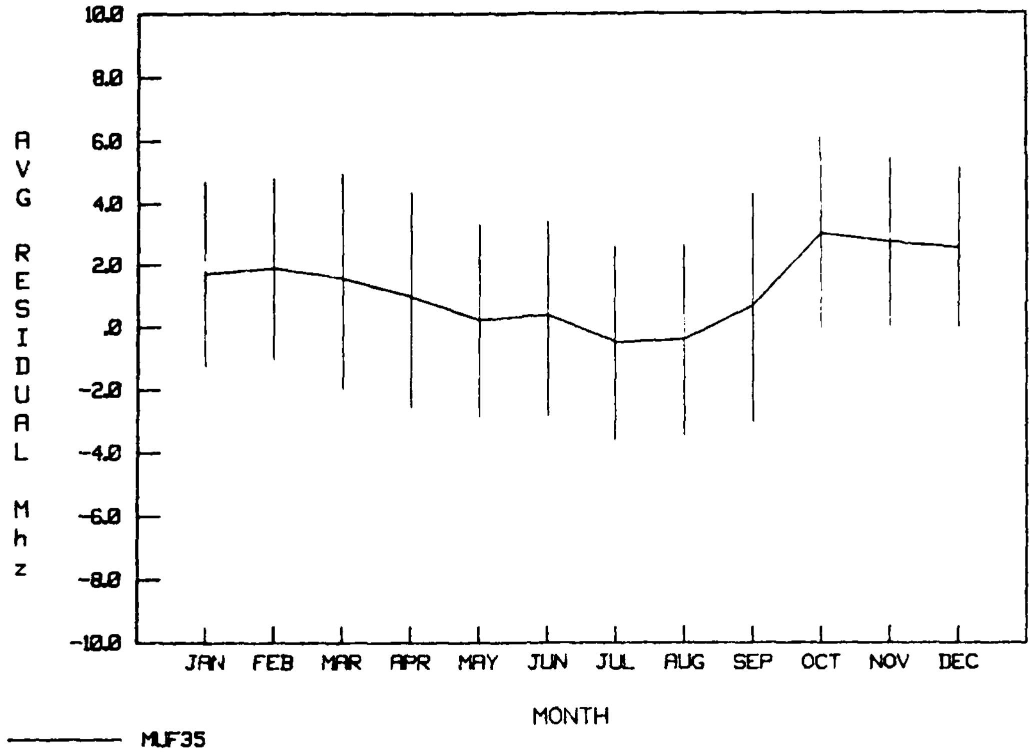

Figure 5. Average residual (bias) for MINIMUF-3.5 with the mean absolute error about the average residual.

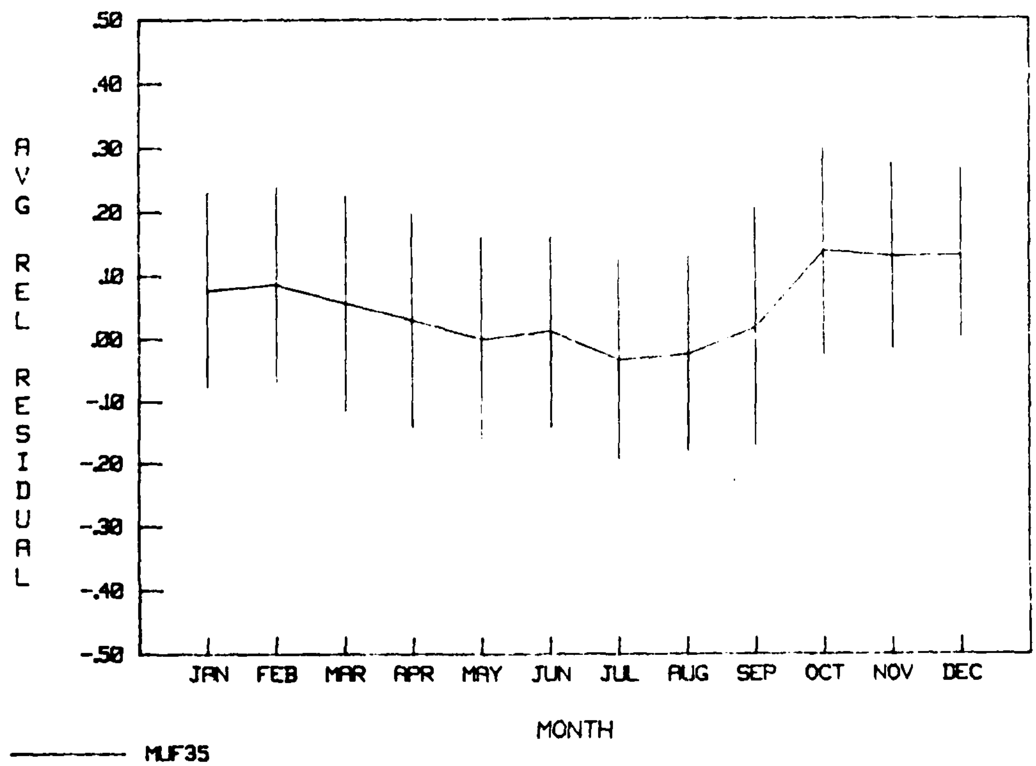

Figure 6. Average relative residual (relative bias) for MINIMUF-3.5.

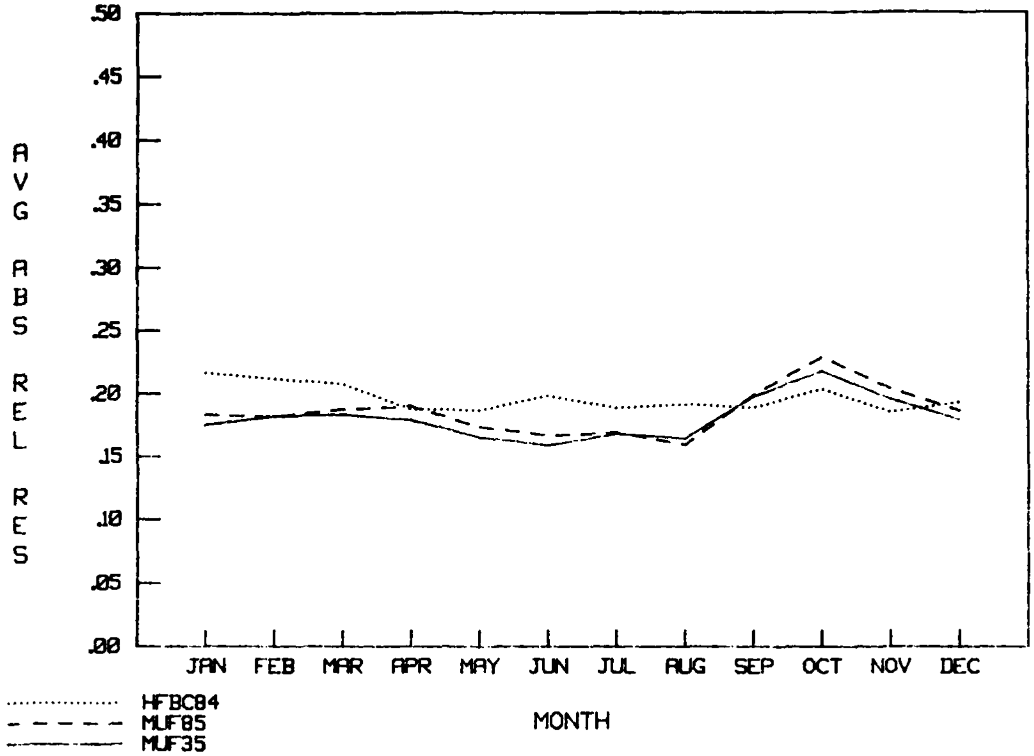

Figure 7. Magnitude of the error (average absolute relative residual) as a function of month.

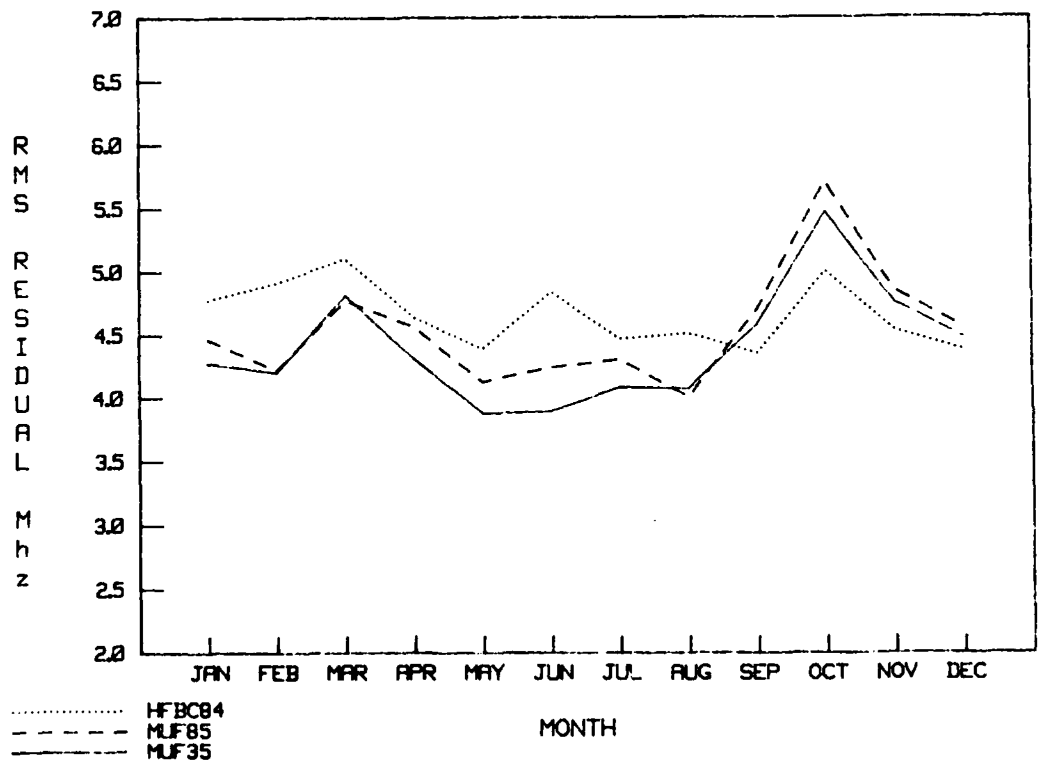

Figure 8. RMS error in MHz as a function of month.

MINIMUF-3.5 has the lowest RMS error in May and reaches its highest value of 5.5 MHz during October.

A measure of the degree of association or the closeness of fit between variables is given by the correlation coefficient. It indicates the strength of the tendency for high (or low) values of one variable to be associated with high (or low) values of the other variable. Figure 10 is an example of the correlation coefficients as a function of month.

A description of the nature of the relationship between variables is called regression analysis (Reference 29). Regression analysis is concerned with the problem of describing or estimating the value of one variable, called the dependent variable, on the basis of one or more other variables, called independent variables. In other cases, regression may be used merely to describe the relationship between known values of two or more variables.

Regression analysis that involves the determination of a linear relationship between two variables is referred to as simple linear regression. Here, the variable y is given as $y = a + bx$, where x is the independent variable and y is the dependent variable. The coefficients a and b are determined in the regression analysis. A measure of the success of linear regression analysis is the standard error of the estimate given by

$$S_{y.x} = (\sigma_y^2(1 - \gamma^2))^{1/2}, \tag{5}$$

where σ_y is the standard deviation in the observed datum and γ is the correlation coefficient between the observed data and predicted values. If the relationship is truly linear, then the bias of the estimate should be removed (or made nearly zero). An estimate of the standard error of mean is given by

$$S_{y.x} = \frac{S_{y.x}}{\sqrt{n}}. \tag{6}$$

A measure of the error in the regression coefficient b is given by

$$S_b = \sqrt{\frac{S_{\bar{y}.x}}{\sigma_x}}, \tag{7}$$

where σ_x the standard deviation in the predicted values. The above values are also calculated in the DASCR3 program and are shown in Figure 2.

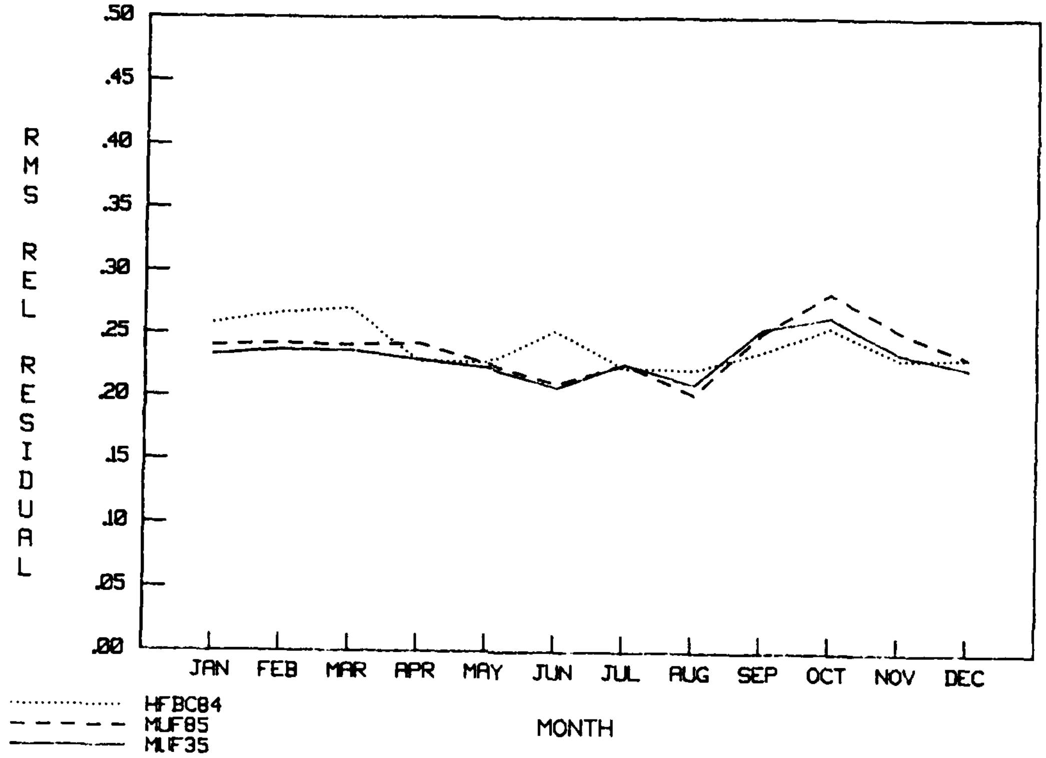

Figure 9. RMS relative error in percent as a function of month.

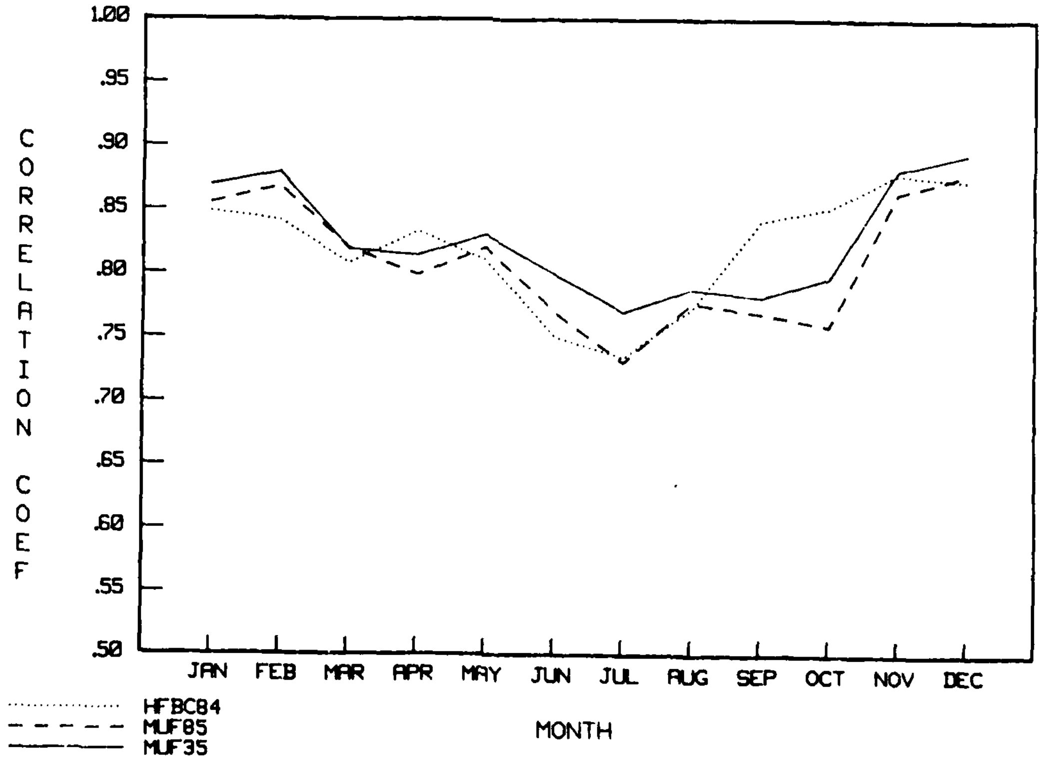

Figure 10. Correlation coefficients as a function of month.

4.0 MODELING THE MUF

A central task of long-term statistical HF propagation forecasting is the prediction of MUF. The MUF, in turn, is principally controlled by the critical frequency of the F_2 layer of the ionosphere, f_oF_2, and it is the success in predicting this quantity that primarily determines the accuracy of the MUF forecast. Unlike the E and F_1 layers, which can be modeled quite well as a function of a single parameter, cos χ (the cosine of the instantaneous solar zenith angle), proportional to the solar intensity, the physics of the F_2 layer is generally believed to involve an interaction of photochemical and transport processes sufficiently complex that diurnal, seasonal, and geographic f_oF_2 variations cannot be simply accommodated through the corresponding variations in cos χ. Indeed, one even speaks of F_2 layer "anomalies" when comparing observed f_oF_2 with expectations based on the instantaneous cos χ. For example, f_oF_2 can be higher at midday in winter than in summer ("seasonal" anomaly), and on a given day can peak in late afternoon rather than at midday ("diurnal" anomaly).

Therefore, while f_oF_2 cannot be modeled as a function of the instantaneous cos χ, the possibility remains that it could be modeled as the response of a dynamic system "driven" by a function of cos χ. Examination of the shape of observed f_oF_2 diurnal profiles, for example, suggests that a simple relaxation model, according to which f_oF_2 represents a lagged response to the instantaneous solar intensity, may be useful as a first approximation. Allowing the lag time constant to be long (~10 hours) in summer and short (~1 hour) in winter at middle and equatorial latitudes could then at least partially reproduce both the seasonal and diurnal anomalies.

A semiempirical model for f_oF_2, MINIMUF-3, was developed based on the analogy to a single-lag linear system (e.g., an RC circuit) driven by a forcing function proportional to the instantaneous cos χ. Further simplifying assumptions of the model were as follows:

(1) The lag time constant during the day is a simple monotonic function of the midday solar zenith angle.

(2) The time constant at night is a constant (2 hours) independent of season or geographical location.

As with other semiempirical models of complex geophysical processes, no attempt was made to justify the model in terms of the underlying physical mechanisms. Rather, the model served to provide a mathematical framework for force-fitting to empirical data. Of course, if the model was successful in fitting a large database with reasonable accuracy and relatively few adjustable constants, the physical reality of the assumed relaxation process gains credibility and may guide the understanding of the underlying mechanisms.

A key feature of the MINIMUF f_oF_2 model was that seasonal and geographical variations of the predicted f_oF_2 arose only from the corresponding variations in the midday solar zenith angle, in marked contrast to the customary procedure of numerically mapping f_oF_2 by fitting appropriate mathematical functions to observed ionospheric sounding data collected from a worldwide net of vertical sounders. Furthermore, by making simple analytical approximations to the dynamic solutions of the model (i.e., the diurnal response function), a simple closed-form expression for f_oF_2 as a function of midday solar zenith angle, SSN, and time relative to local sunrise and sunset was obtained. By appending simple approximations for the M-factor (i.e., MUF/f_oF_2) and for solar zenith angle as a function of location and time, a model for MUF which is sufficiently compact to be coded for computation on a minicomputer or desktop microcomputer was developed.

4.1 MINIMUF-3.5

MINIMUF-3.5 is a semiempirical model developed in 1978 (the initial algorithm was called MINIMUF-3) to provide an MUF prediction capability suitable for use on small (micro) computers, where time and storage limitations exist. The theory and method used in the development of the MINIMUF-3.5 algorithm has been documented in several earlier reports and will not be presented here (References 23, 24 and 28).

The expression for the MUF used in a MINIMUF-3.5 is given by

$$MUF = M \cdot f_oF2\,, \tag{8}$$

where M is the obliquity, or M-factor, which reflects the dependence of the MUF on transmission path length. The parameter f_oF2 is the critical or penetration frequency at vertical incidence for the F2 layer.

In particular, we have

$$M = \{1 + 2.5\,[\sin(2.54\psi)]^{3/2}\} \cdot G_1 \cdot G_2 \cdot G_3\,, \tag{9}$$

where ψ is the minimum great circle distance between transmitter and receiver. The various constants in the bracketed term in Equation (9) were determined by fitting this expression, without the G_i, $i = 1,2,3$, to an exact transmission curve for a parabolic layer height of 290 km and a ratio of height of maximum of electron density to half-width of the F2 layer of 0.4. The multipliers G_i provide small corrections to the MUF for known systematic departures from the median behavior under certain conditions of path geography or season.

The expression for the critical frequency used in MINIMUF-3.5 is

$$f_oF_2 = \left(1 + \frac{R}{R_o}\right)\left[A_o + A_1\sqrt{\cos\chi_{eff}}\right]^{1/2}, \tag{10}$$

where R_o A_o, A_1 are constants and R is the 12-month running mean SSN. The constants in Equation (10) were determined by iteratively adjusting the model in a "real time" mode, to 36 path-months of data chosen to represent a range of transmission path types.

In Equation (10), χ_{eff} is an "effective" solar zenith angle. Cos χ_{eff} is modeled as the lagged response of a dynamic linear system "driven" by the instantaneous value of cos χ. By using an effective value of the zenith angle, recognition is given to the fact that the F2 layer, unlike the E and D layers, does not show a relatively simple cos $n\chi$ diurnal dependence on χ. The dynamical behavior of the F2 layer is more complicated because various other dependencies make simple, accurate modeling more difficult. In keeping with the simplistic nature of the model, defining an effective χ allows relatively accurate modeling without explicitly including these other dependencies.

4.2 MINIMUF 85

An improved version of MINIMUF-3.5, called MINIMUF 85, was developed to predict accurate MUFs under conditions of anomalously high SSNs, to predict values of f_oF2 suitable for ray-tracing applications, to predict M3000 factor values usable for determining the mirror height of reflection for oblique incidence propagation, and to predict accurate MUFs for paths having a portion of the path in the polar region. This version includes SSN dependence in both the f_oF2 and the M-factor calculations and provides a natural saturation in the MUF vs. SSN curve, reducing the error in predicted MUF values under very high SSN conditions. The polar and nonpolar f_oF2 models are combined by means of a folding function.

The theory and method used in the development of the MINIMUF 85 model is documented in Reference 30. However, a brief review of these improvements follows.

The choice of control points was modified in MINIMUF 85 to place control points at the path midpoint for path lengths less than or equal to 4000 km, control points located 2000 km from either terminus for path lengths greater than 4000 km, but less than or equal to 6000 km, and control points located at 1/4, 1/2 and 3/4 of the great circle path length for path lengths greater than 6000 km.

The geomagnetic latitude dependence was modified to reduce the bias at high latitudes by adding one-half the gyrofrequency to the f_oF2 value at latitudes greater than 55° N geomagnetic.

A new critical frequency model was developed to reduce the error at high SSN. A different multiplier, A_1, shown below, was developed

$$(f_oF2_d)^2 - A_o = A_1(SSN)\sqrt{\cos \chi_{eff}}, \quad (11)$$

where $A_1\,(SSN) = (0.814)R + 22.23$.

The new expression provides a saturation effect in the behavior of the critical frequency as a function of SSN.

The M-factor model was modified to incorporate SSN, and seasonal and diurnal dependencies. Again, using the data screen analysis technique, multipliers for the M-factor model were developed.

For sunspot dependence the equation

$$MOF_d = A_2(SSN)\, M \left[A_o + A_1(SSN)\sqrt{\cos \chi_{eff}}\right]^{1/2} \quad (12)$$

where $A_2(SSN) = 1.3022 - (0.00156)R$,

shows a monotonically decreasing behavior as a function of SSN.

For seasonal dependence an additional multiplier was added to the expression

$$Mof_d = A_3(month)\, A_2(SSN)\, M\, f_oF2, \tag{13}$$

where $A_3(month) = 0.9925 + 0.011 \sin m + 0.087 \cos m$

$$\begin{aligned}&- 0.043 \sin 2m + 0.003 \cos 2m\\ &- 0.013 \sin 3m - 0.022 \cos 3m\\ &+ 0.003 \sin 4m + 0.005 \sin 5m\\ &+ 0.018 \cos 6m\end{aligned}$$

and $m = \frac{2\pi\ month}{12}$.

This seasonal dependence factor allows higher frequencies to propagate on a given transmission path during the winter months.

For time dependence an additional multiplier was added to the expression

$$MOF_d = A_4(time)\, A_3(month)\, A_2(SSN)\, f_oF2, \tag{14}$$

where $A_4(time) = 1.11 - 0.01t_{local}$,

which adequately fits daytime data.

For night it was necessary to introduce a new time coordinate, hours after sunset, and use a sixth-order Fourier series to fit the data. The night multiplier is

$$A_4(time) = 1.0195 \tag{15}$$

$$\begin{aligned}&- 0.06 \sin 2t - 0.037 \cos 2t\\ &+ 0.018 \sin 4t - 0.003 \cos 4t\\ &+ 0.025 \sin 6t + 0.018 \cos 6t\\ &+ 0.007 \sin 8t - 0.005 \cos 8t\\ &+ 0.006 \sin 10t + 0.017 \cos 10t\\ &- 0.009 \sin 12t - 0.004 \cos 12t,\end{aligned}$$

where $t = t_{local} - t_{sunset}$.

The Chiu polar model (Reference 31) for the F2 layer, developed to predict electron density, was used for a polar model. The basis of the model is an analysis by Yonezawa and Arima (Reference 32) of variations of electron density into seasonal and annual categories. The first version of a global model as developed by Ching and Chiu (Reference 33) separates the global variations into polar and nonpolar regimes. The polar and nonpolar functions describing each regime are linked by a folding function.

The folding function determines when polar effects (particle precipitation) become dominant. It is a function of geomagnetic latitude and SSN. Figure 11 is a plot of the folding function for an SSN of zero. When the folding function is near one, particle precipitation effects are supposed to dominate. When the folding function is near zero, solar zenith angle is the major factor in causing ionization. In between, there exists a fairly narrow transition region where both sources of free electrons are significant.

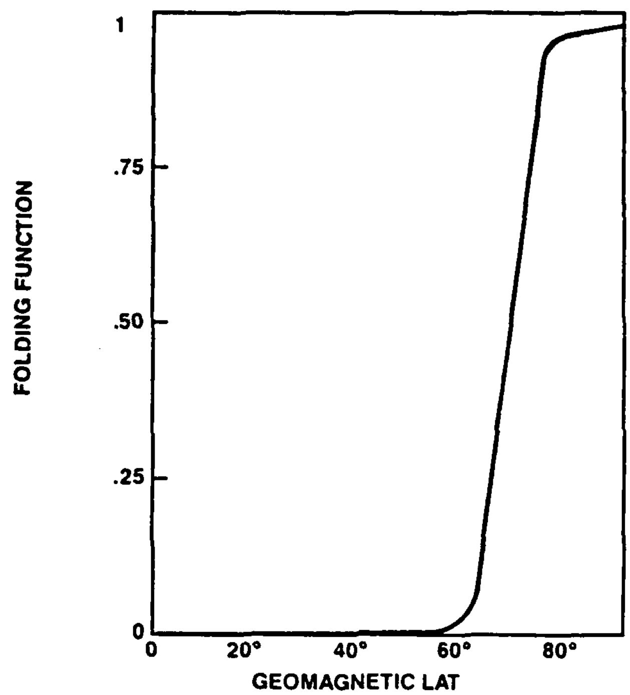

Figure 11. The folding function for monthly smoothed SSN = 0.

In folding a polar function into MINIMUF, it is necessary to isolate that portion of MINMUF which calculates f_0F2 and then converts the value of f_0F2 into electron density. MINIMUF's f_0F2 was found by dividing its calculated value for the MUF at each control point by the range-dependent portion of the M factor. Note that the G-factors, which are empirically latitude-dependent adjustments to MINIMUF, remain in the value F_0F2 produced by MINIMUF. f_0F2 is then converted to electron density using the equation

$$f_0F2(\mathrm{MHz}) = 2.85\, N^{1/2}\, (\mathrm{electrons/cm^3})\,. \tag{16}$$

The electron density from MINIMUF is multiplied by a factor of one minus the folding function and then added to the product of the folding function and the Chiu polar model electron density as shown in the equation

$$N_{total} = (1-f)N_{MINIMUF} + f\,N_{polar}\,. \tag{17}$$

The total electron density at the control point is then converted back to f_oF2 at the control point using Equation (16). Finally, the MUF is obtained by multiplying the value of f_oF2 by the range-dependent portion of the M-factor.

4.3 DISCUSSION OF SYSTEMATIC ERRORS

In a recent evaluation of MINIMUF-3.5 (Reference 34), J. Carnana and M.W. Fox confirm a definite geomagnetic latitude dependence. This might imply that the $f_oF2 \sim (\cos \chi_{eff})^m$, where m is a function of geomagnetic latitude and SSN, and would be less than one-quarter on some occasions.

In addition, they found a systematic difference of about 24 min between MINIMUF-3.5 estimates for the length of the F2-layer day and the true values, with MINIMUF-3.5 values being too low. This means that MINIMUF-3.5 predicted sunrise and sunset times are too late and too early by 12 min. However, they found this discrepancy not to be a major source of error.

5.0 DESCRIPTION OF THE OBLIQUE SOUNDER MOF DATABASE

The final oblique sounder data set consists of median hourly MOF values derived from 70 different HF transmission paths. The longest path was 10,576 km and the shortest path was 196 km. The set contains a cross section of transmission paths, including midlatitude, transauroral, transequatorial, all seasons, and all solar SSNs. The final number of hourly values in the MOF database was 13054 points. Table 1 lists all transmission paths in the 70-path database, Figures 12 and 13 show the geographical locations except for the shortest paths (the scale is too large to illustrate them). Note the lack of data in South America and in southern Africa.

Table 1. 70-Path oblique sounder MOF database.

ID	Transmission Path	Latitude	Longitude	Path Length(km)	Sunspot Number Smoothed	Sunspot Number Monthly Median	Years	# of months	Data type
1	GUAM	13.47N	144.79E	2505	71-107	60-110	1968-71	13	NTSS-SC
	YOKOHAMA	35.48N	139.47E		12-34	5-56	1974-76		NTSS-HFDR
2	FORT MONMOUTH	40.19N	74.03W	4132	26-50	20-50	1961-63	6	GRANGER 900
	PALO ALTO	37.26N	122.10W						
3	GUAM	13.47N	144.79E	6102	71-106	61-98	1969-71	24	NTSS-SC
	HONOLULU	21.51N	158.00W		13-33	5-34	1974-76		NTSS-HFDR
4	GUAM	13.47N	144.79E	7141	71-106	60-98	1969-71	6	NTSS-SC
	KODIAK	57.67N	152.46W						
5	HONOLULU	21.42N	158.14W	4057	71-106	60-98	1969-71	6	NTSS-SC
	KODIAK	57.67N	152.46W						
6	HONOLULU	21.42N	158.14W	7808	10	6-9	1964	4	GRANGER 900
	WASHINGTON	38.75N	76.85W						
7	MCCLELLAN	38.50N	121.68W	3939	10	6-9	1964	4	GRANGER 900
	HONOLULU	21.51N	158.00W						
8	PALO ALTO	37.26N	122.10W	3503	10	9	1964	1	GRANGER 900
	FAIRBANKS	64.89N	147.79W						
9	BOULDER	40.00N	105.30W	4482	144-120	110-122	1960	3	Modified C-3
	BARROW	71.10N	156.79W						
10	HONOLULU	21.42N	158.14W	6196	104-107	81-127	1968	7	NTSS-SC
	YOKOHAMA	35.48N	139.47E		13-15	5-14	1974-76		NTSS-HFDR
11	PHILIPPINES	15.35N	120.37E	2936	105-107	96-110	1968	2	NTSS-SC
	YOKOHAMA	35.48N	139.47E						
12	PHILIPPINES	15.35N	120.37E	4243	104-111	86-136	1968-69	16	NTSS-SC
	HEH	22.32S	114.15E						
13	GUAM	13.47N	144.79E	5195	71-110	61-136	1968-71	18	NTSS-SC
	HEH	22.32S	114.15E						
14	DAVIS	38.32N	121.47W	3113	104-108	91-136	1969	10	NTSS-SC
	KODIAK	57.76N	152.52W						
15	HONOLULU	21.42N	158.14W	4199	104-107	91-136	1968-70	21	NTSS-SC
	CORONA	33.86N	117.55W						
16	ANDOYA	69.00N	15.00E	3208	10-20	9-18	1964	6	GRANGER 900
	THESSALONIKI	40.38N	22.56E						
17	MCCLELLAN	38.50N	121.68W	803	65-69	52-82	1971	6	NTSS-SC
	LA POSTA	32.67N	116.43W						
18	FRANCE	43.00N	2.00E	1923	15-28	12-25	1974-75	4	NTSS HFDR
	GREECE	38.09N	2.39E						

Table 1. 70-Path oblique sounder MOF database, continued.

ID	Transmission Path	Latitude	Longitude	Path Length(km)	Sunspot Number Smoothed	Sunspot Number Monthly Median	Years	# of months	Data type
19	HONOLULU	21.42N	158.14W	4286	12-35	5-40	1974-76	14	NTSS HFDR
	LA POSTA	32.67N	116.43W						
20	COCO SOLO	9.37N	79.88W	3764	31-75	24-111	1966-67	12	GRANGER 900
	STOCKBRIDGE	43.00N	75.50W						
21	ANDOYA	69.00N	15.00E	5923	11-24	10-23	1963-64	7	GRANGER 900
	NEW DELHI	28.59N	77.20E						
22	PALO ALTO	37.26N	122.10W	5070	10-18	9-18	1964	2	GRANGER 900
	THULE	76.50N	68.80W						
23	FRANCE	43.00N	2.00E	2806	12-22	5-28	1975-76	13	NTSS HFDR
	ICELAND	63.98N	22.59W						
25	FORT MONMOUTH	40.19N	74.03W	196	105	107	1970	1	Non-NTSS
	ABERDEEN	39.50N	76.14W						
26	FORT MONMOUTH	40.19N	74.03W	445	71	72	1971	1	Non-NTSS
	CAMP DRUM. NY	44.00N	75.69W						
27	PUERTO RICO	18.25N	67.16W	2717	28-70	24-57	1966	8	GRANGER 900
	MAYNARD, MA	42.41N	71.45W						
28	THULE	76.50N	68.80W	3739	73-79	70-111	1966-67	3	GRANGER 900
	STOCKBRIDGE	43.00N	75.50W						
29	ANDOYA	69.00N	15.00E	5533	15-20	9-24	1965	3	GRANGER 900
	MAYNARD, MA	42.41N	71.45W						
30	BANGKOK	12.50N	102.10E	219	37	49	1966	1	GRANGER 900
	CHANTABURI	13.70N	100.50E						
31	OTTAWA	45.40N	75.90W	5628	52-131	46-146	1959-61	16	Non-NTSS
	THE HAGUE	52.10N	4.40E						
32	WINNIPEG	49.90N	97.40W	2760	122-146	102-146	1959	6	Non-NTSS
	RESOLUTE BAY	74.70N	94.90W						
33	OTTAWA	45.40N	75.90W	3387	52-88	46-90	1960-61	11	Non-NTSS
	RESOLUTE BAY	74.70N	94.90W						
34	OKINAWA	26.30N	127.80E	6876	45-87	48-112	1966-67	15	GRANGER 900
	ST. KILDA	34.70S	138.50E		57-89	61-95	1970-71		
35	OKINAWA	26.30N	127.80E	5443	68-87	57-112	1966-67	9	GRANGER 900
	TOWNSVILLE	19.16S	146.49E		57-89	52-95	1970-71		
36	YAMAGAWA	31.12N	130.38E	7368	52-89	50-95	1970-72	16	GRANGER 900
	ST. KILDA	34.70S	138.50E						
37	YAMAGAWA	31.12N	130.38E	5850	52-89	50-95	1970-72	14	GRANGER 900
	TOWNSVILLE	19.16S	146.49E						

Table 1. 70-Path oblique sounder MOF database, continued.

ID	Transmission Path	Latitude	Longitude	Path Length(km)	Sunspot Number Smoothed	Sunspot Number Monthly Median	Years	# of months	Data type
38	MONROVIA	6.23N	10.75W	3409	24	23	1963	1	Non-NTSS
	ROTA, SPAIN	36.62N	6.35W						
39	MONROVIA	6.23N	10.75W	2899	24	23	1963	1	Non-NTSS
	LAMY, CHAD	12.17N	14.98E						
40	TRIPOLI	32.92N	13.42E	3331	51	39	1961	1	Non-NTSS
	ACCRA, GHANA	5.75N	.13W						
41.	OKINAWA	26.50N	127.80E	9277	11-31	9-40	1962-64	12	GRANGER 900
	THESSALONIKI	40.38N	22.56E						
42	OKINAWA	26.50N	127.80E	4958	10-20	9-18	1964	6	GRANGER 900
	NEW DELHI	28.59N	77.20E						
43	SAPPORO	43.00N	141.21E	8899	92-106	87-128	1969-70	18	BR CHIRP
	AVIANO	46.30N	12.35E						
44	SAPPORO	43.00N	141.21E	7813	92-106	87-128	1969-70	18	BR CHIRP
	KASSEL	51.19N	9.32E						
45	SAPPORO	43.00N	141.21E	8753	96-106	91-128	1969-70	17	BR CHIRP
	THETFORD	52.25N	.44E						
46	PHILIPPINES	15.35N	120.37E	9944	96-111	86-136	1968-70	24	BR CHIRP
	BRINDIS	40.39N	17.55E						
47	PHILIPPINES	15.35N	120.37E	10135	96-111	86-136	1968-70	24	BR CHIRP
	AVIANO	46.30N	12.35E						
48	PHILIPPINES	15.35N	120.37E	10576	92-111	87-136	1968-70	25	BR CHIRP
	THETFORD	52.25N	.44E						
49	TOKOROZAWA	35.47N	139.28E	9642	105-111	86-136	1968-69	10	BR CHIRP
	BRINDIS	40.39N	17.55E						
50	TOKOROZAWA	35.47N	139.28E	9486	103-111	86-127	1968-69	12	BR CHIRP
	AVIANO	46.30N	12.35E						
51	TOKOROZAWA	35.47N	139.28E	8488	105-111	81-136	1968-69	13	BR CHIRP
	KASSEL	51.19N	9.32E						
52	TOKOROZAWA	35.47N	139.28E	9430	106-111	886-136	1968-69	12	BR CHIRP
	THETFORD	52.25N	.44E						
53	THULE	76.50N	68.80W	3930	10-18	3-19	1964	8	GRANGER 900
	PULLMAN	46.75N	117.50W						
54	ANDOYA	69.00N	15.00E	6530	10-18	3-19	1964	10	GRANGER 900
	PULLMAN	46.75N	117.50W						
55	BROME	18.00S	122.20E	1850	38-55	42-88	1971-72	11	GRANGER 900
	MIRIKATA	29.85S	135.20E						

Table 1. 70-Path oblique sounder MOF database, continued.

ID	Transmission Path	Latitude	Longitude	Path Length(km)	Sunspot Number Smoothed	Sunspot Number Monthly Median	Years	# of months	Data type
56	ADELAIDE	35.00S	135.50E	1946	38-110	42-136	1969-72	14	GRANGER 900
	TOWNSVILLE	19.00S	146.50E						
57	KOLSAAS	60.00N	10.30E	340	150	155	1980	1	BR CHIRP
	USS MT WHITNEY	63.00N	8.40E						
58	SOL BUCHAN	57.30N	1.50W	830	150	155	1980	1	BR CHIRP
	USS MT WHITNEY	63.00N	8.40E						
59	DRIVER, VA	36.82N	76.50W	260	143	128	1980	1	BR CHIRP
	FT. BRAGG	35.15N	78.98W						
60	HURLBERT FLD	30.30N	86.40W	904	143	128	1981	1	BR CHIRP
	FT. BRAGG	35.10N	78.60W						
61	SHAW AFB	34.97N	80.48W	226	143	128	1981	1	BR CHIRP
	FT. BRAGG	35.15N	78.98W						
62	MACDILL	27.85N	82.48W	915	143	128	1981	1	BR CHIRP
	FT. BRAGG	35.15N	78.98W						
63	DRIVER, VA	36.82N	76.50W	29	143	128	1981	1	BR CHIRP
	NORFOLK	36.67N	76.23W						
64	HURLBERT FLD	30.30N	86.40W	1176	143	128	1981	1	BR CHIRP
	NORFOLK	36.67N	76.23W						
65	SHAW AFB	34.97N	80.48W	500	143	128	1981	1	BR CHIRP
	NORFOLK	36.67N	76.23W						
66	MACDILL	27.85N	82.48W	1163	143	128	1981	1	BR CHIRP
	NORFOLK	36.67N	76.23W						
67	CAMP LEJUNE	34.67N	77.35W	245	143	128	1981	1	BR CHIRP
	NORFOLK	36.67N	76.23W						
68	ROBINS	32.60N	83.60W	820	139	138	1981	1	BR CHIRP
	NORFOLK	36.90N	76.30W						
69	ISABELA	18.08N	67.05W	2280	139	138	1981	1	BR CHIRP
	NORFOLK	36.90N	76.30W						
70	R/V MOANA WAVE	30.30N	61.50W	1640	139	138	1981	1	BR CHIRP
	NORFOLK	36.90N	76.30W						

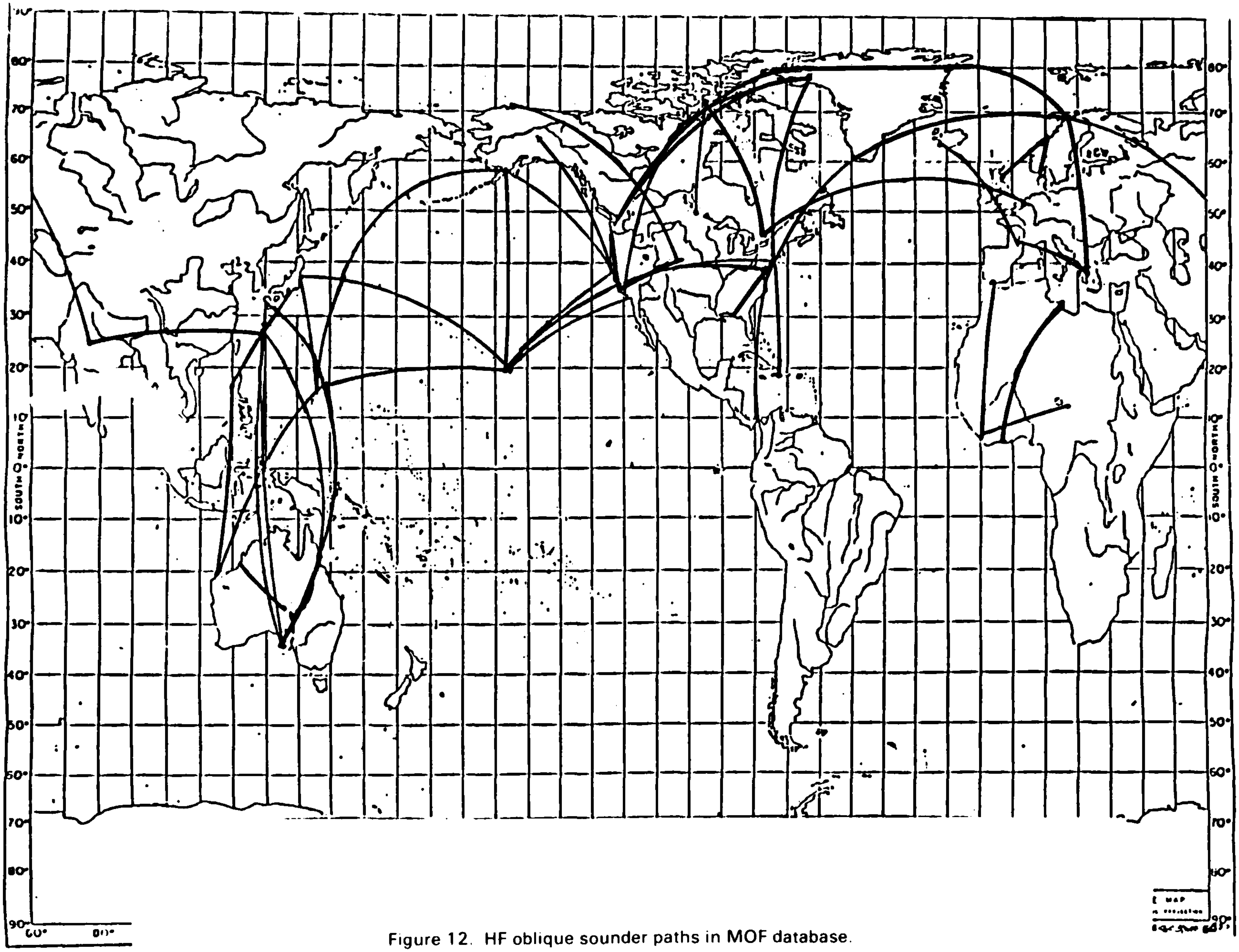

Figure 12. HF oblique sounder paths in MOF database.

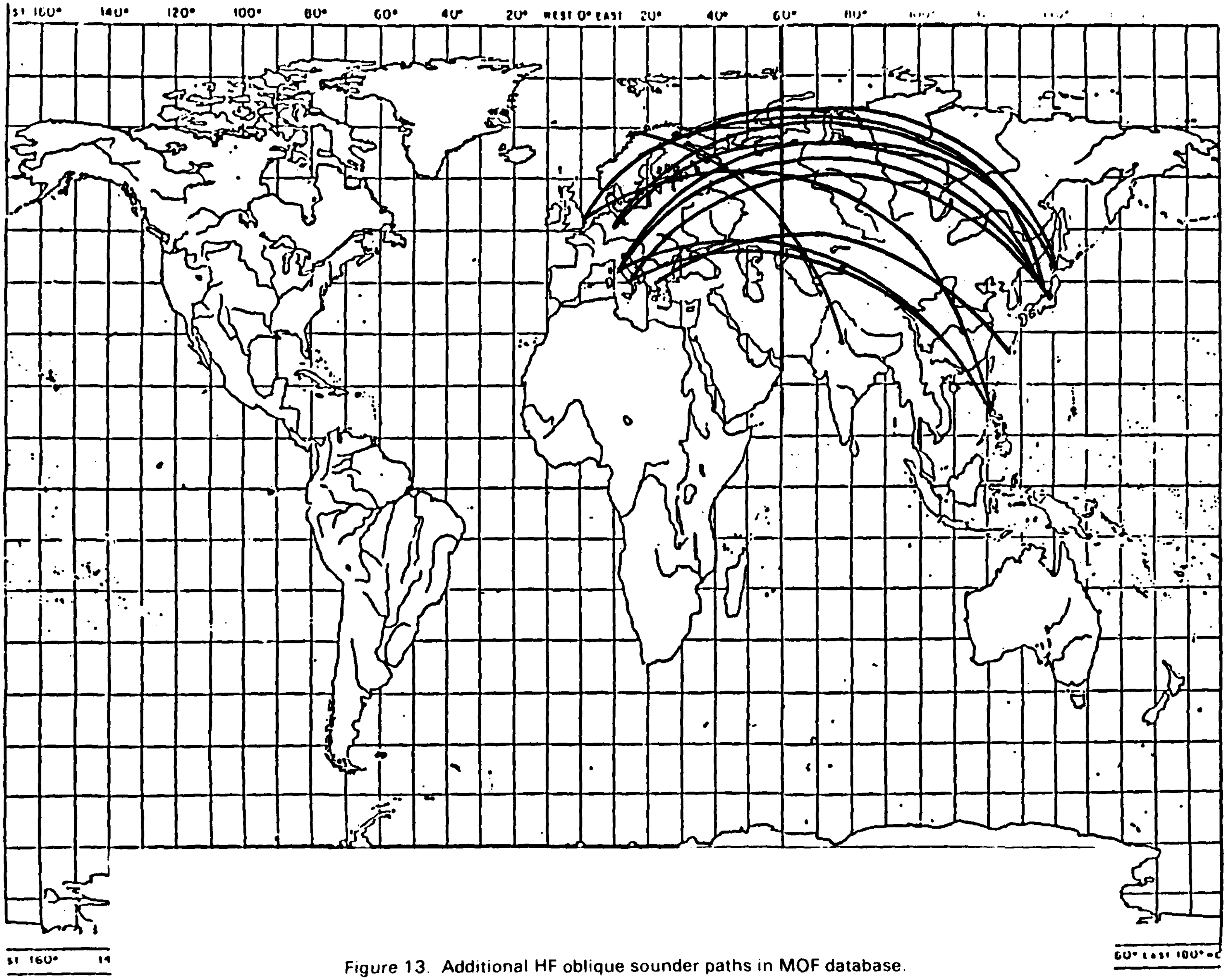

Figure 13. Additional HF oblique sounder paths in MOF database.

Tables 2 through 11 show the composition of the MOF oblique sounder database. Sample path-hours and the percent of sample are shown for sounder type, path length, path orientation, season, geomagnetic latitude, yearly running mean, and monthly median SSNs and geographic region categories.

Table 2. Sample path-hours and percentage of sample for each sounder type in the MOF database.

Sounder Type	Path-Hours	Percentage of Sample
NTSS - HFDR	1416	10.9
NTSS - strip chart	2388	18.3
Non-NTSS	927	7.1
Granger 900 Series	3816	29.2
Modified C-3	72	0.5
BR Chirpsounder	4435	34.0

Table 3. Sample path-hours and percentage of sample for each path-length range.

Path Length (km)	Path-Hours	Percentage of Sample
$L \leq 1000$	396	3.0
$1000 < L \leq 2000$	737	5.6
$2000 < L \leq 3000$	1014	7.8
$3000 < L \leq 4000$	1254	9.6
$4000 < L \leq 5000$	1738	13.3
$5000 < L \leq 6000$	1581	12.1
$6000 < L \leq 7000$	1291	9.9
$7000 < L \leq 8000$	1054	8.1
$8000 < L \leq 9000$	1169	9.0
$9000 < L \leq 10000$	1630	12.5
$10000 < L \leq 11000$	1190	9.1

Table 4. Sample path-hours and percentage of sample in path orientation categories.

Path Orientation	Path-Hours	Percentage of Sample
NORTH/SOUTH	1777	13.6
EAST/WEST	6367	48.8
OTHER	4910	37.6

Table 5. Sample path-hours and percentage of sample for each season.

Season	Path-Hours	Percentage of Sample
WINTER	4252	32.6
SPRING	2232	17.1
SUMMER	4213	32.3
AUTUMN	2357	18.0

Table 6. Sample path-hours and percentage of sample for each month.

Month	Path-Hours	Percentage of Sample
January	907	6.9
February	1120	8.6
March	1160	8.9
April	1072	8.2
May	1128	8.6
June	1033	7.9
July	1017	7.8
August	1035	7.9
September	1166	8.9
October	1191	9.1
November	1255	9.6
December	970	7.4

Table 7. Sample path-hours and percentage of sample in geomagnetic latitude categories.

Geomagnetic Latitude	Path-Hours	Percentage of Sample
Transequational	2631	20.2
Low Latitude	1114	8.5
Midlatitude	4350	33.3
High Latitude	4045	31.0
Transauroral	914	7.0

Table 8. Sample path-hours and percentage of sample for smoothed (12-month running mean) SSNs.

Smoothed SSN (Cycle Phase)	Path-Hours	Percentage of Sample
0-30 (minimum)	2638	20.2
31-60 (rise and decline)	1476	11.3
61-90 (near maximum)	1955	15.0
91-120 (maximum)	6445	49.4
121-180 (high maximum)	540	4.1

Table 9. Sample path-hours and percentage of sample for unsmoothed (monthly median) SSNs.

Unsmoothed SSN (Cycle Phase)	Path-Hours	Percentage of Sample
0-30 (minimum)	2514	19.3
31-60 (rise and decline)	1469	11.3
61-90 (near maximum)	2207	16.9
91-120 (maximum)	5293	40.5
121-180 (high maximum)	1571	12.1

Differences in the SSN categories reflect the averaging process used in calculating a yearly running mean for the smoothed SSN versus a monthly median value for the unsmoothed SSN.

Table 10. Sample path-hours and percentage of sample in geographic region categories.

Geographic Region	Path-Hours	Percentage of Sample
Continental	6370	48.8
Ocean	3442	26.4
Other	3242	24.8

Table 11. Sample path-hours and percentage of sample for midpath local time.

Midpath Local Time	Path-Hours	Percentage of Sample
1	510	3.9
2	527	4.0
3	540	4.1
4	538	4.1
5	532	4.1
6	542	4.1
7	537	4.1
8	544	4.2
9	544	4.2
10	541	4.1
11	549	4.2
12	548	4.2
13	549	4.2
14	546	4.2
15	543	4.2
16	544	4.2
17	548	4.2
18	548	4.2
19	550	4.2
20	551	4.2
21	549	4.2
22	550	4.2
23	546	4.2
24	544	4.2

6.0 DISCUSSION OF ACCURACY

For each MUF model being compared, Tables 12-14 list the paths and the bias, the RMS error, the average magnitude of the error, and the correlation coefficient between the observed MOFs and the calculated MUFs for each path. The data contained in these tables will be discussed in the section on sounder path ID (section 6.9).

Discussion of the results shown in the following tables and graphs will be concerned with comparison of the MINIMUF models to the unrelated HFBC84(MUF) model and to previous MUF accuracy studies reported in References 28 and 30. In Reference 28, MINIMUF-3.5 was tested using a 25-path database, and in Reference 30, MINIMUF 85 was tested using a 39-path database.

Table 12. MINIMUF-3.5 comparison by sounder path.

ID	Transmission Path		Bias error Mhz	Bias error %	RMS error Mhz	RMS error %	Magni- tude,%	Corre- lation Coeffi- cient
1	GUAM	YOKOHAMA	.03	-7.2	5.15	34.8	25.0	.665
2	FORT MONMOUTH	PALO ALTO	1.73	6.5	4.12	22.2	18.8	.818
3	GUAM	HONOLULU	.34	-.3	3.00	16.8	13.2	.884
4	GUAM	KODIAK	-2.14	-11.4	3.87	20.4	16.1	.872
5	HONOLULU	KODIAK	.08	-1.4	2.40	13.2	10.5	.928
6	HONOLULU	WASHINGTON	2.24	12.6	3.61	20.3	16.9	.881
7	MCCLELLAN	HONOLULU	-1.14	-6.9	3.29	21.3	17.2	.862
8	PALO ALTO	FAIRBANKS	.83	2.9	2.17	11.8	9.4	.747
9	BOULDER	BARROW	-.01	-1.8	4.21	24.7	20.4	.386
10	HONOLULU	YOKOHAMA	-2.31	-14.0	4.32	28.1	19.1	.863
11	PHILIPPINES	YOKOHAMA	-.33	-.3	3.55	15.0	13.4	.877
12	PHILIPPINES	HEH	1.49	5.7	4.31	17.5	14.2	.767
13	GUAM	HEH	-1.55	-6.4	4.67	19.1	15.5	.797
14	DAVIS	KODIAC	-2.07	-17.3	5.29	38.5	28.6	.713
15	HONOLULU	CORONA	1.25	1.0	3.33	19.4	14.2	.947
16	ANDOYA	THESSALONIKI	3.99	17.0	5.06	20.9	18.0	.447
17	MCCLELLAN	LA POSTA	1.40	13.6	2.46	24.2	19.9	.734
18	FRANCE	GREECE	-2.99	-31.2	4.05	44.4	31.2	.820
19	HONOLULU	LA POSTA	-.79	-6.5	2.70	24.1	16.0	.827
20	COCO SOLO	STOCKBRIDGE	-.39	-2.7	2.66	15.0	10.5	.925
21	ANDOYA	NEW DELHI	2.78	18.5	3.52	23.2	20.0	.884
22	PALO ALTO	THULE	2.77	17.7	3.33	21.3	18.3	.913
23	FRANCE	ICELAND	1.42	10.1	2.46	17.7	13.6	.896
25	FORT MONMOUTH	ABERDEEN	-1.46	-18.8	1.89	24.3	21.7	.806
26	FORT MONMOUTH	CAMP DRUM	-1.17	-16.1	1.61	24.6	16.9	.875
27	PUERTO RICO	MAYNARD	.61	3.2	2.75	15.6	12.1	.897
28	THULE	STOCKBRIDGE	7.77	31.4	8.90	33.8	32.2	.916
29	ANDOYA	MAYNARD	2.48	7.6	6.31	43.0	36.7	.185
30	BANGKOK	CHANTABURI	2.40	27.0	2.61	28.7	27.0	.837
31	OTTAWA	THE HAGUE	2.85	13.1	5.46	25.0	21.2	.711
32	WINNIPEG	RESOLUTE BAY	2.24	11.4	5.25	29.1	25.6	.607
33	OTTAWA	RESOLUTE BAY	-.12	-1.9	4.59	25.5	22.1	.593
34	OKINAWA	ST.KILDA	-2.16	-10.1	4.64	20.8	16.3	.839
35	OKINAWA	TOWNSVILLE	3.16	9.5	5.55	17.4	13.5	.826
36	YAMAGAWA	ST.KILDA	-.43	-4.4	4.52	19.2	14.6	.845
37	YAMAGAWA	TOWNSVILLE	3.09	6.5	5.79	21.8	16.8	.860
38	MONROVIA	ROTA,SPAIN	9.46	29.9	10.68	36.0	34.8	.880
39	MONROVIA	LAMY,CHAD	3.91	15.9	7.24	28.7	24.3	.223
40	TRIPOLI	ACCRA,GHANA	13.32	33.4	15.50	39.2	36.0	.621
41	OKINAWA	THESSALONIKI	3.55	18.6	4.91	25.8	22.9	.811

Table 12. MINIMUF-3.5 comparison by sounder path, continued.

ID	Transmission Path		Bias error Mhz	Bias error %	RMS error Mhz	RMS error %	Magni-tude,%	Corre-lation Coeffi-cient
42	OKINAWA	NEW DELHI	1.87	9.5	2.95	15.4	12.5	.917
43	SAPPORO	AVIANO	3.19	16.4	4.84	23.6	19.9	.807
44	SAPPORO	KASSEL	3.47	17.5	5.28	25.4	21.6	.759
45	SAPPORO	THETFORD	3.06	16.3	5.04	25.9	22.4	.736
46	PHILIPPINES	BRINDIS	-.53	-1.3	5.51	24.2	19.6	.744
47	PHILIPPINES	AVIANO	2.45	12.4	3.95	19.3	15.5	.892
48	PHILIPPINES	THETFORD	1.85	8.5	4.08	23.1	16.9	.829
49	TOKOROZAWA	BRINDIS	3.60	19.0	4.98	25.1	21.9	.830
50	TOKOROZAWA	AVIANO	2.67	13.8	4.65	23.1	19.3	.798
51	TOKOROZAWA	KASSEL	3.14	16.3	5.21	25.9	22.6	.738
52	TOKOROZAWA	THETFORD	3.35	17.7	5.18	26.6	23.2	.750
53	THULE	PULLMAN	-1.56	-9.6	2.99	20.5	18.1	.776
54	ANDOYA	PULLMAN	4.15	24.9	5.82	34.0	28.1	.312
55	BROME	MIRIKATA	.82	4.5	2.11	13.7	10.5	.917
56	ADELAIDE	TOWNSVILLE	.88	4.3	3.07	15.9	12.4	.842
57	KOLSAAS	USS MT WHITNEY	1.52	16.2	2.33	28.2	26.1	.738
58	SOL BUCHAN	USS MT WHITNEY	1.09	10.6	1.52	16.9	15.7	.962
59	DRIVER	FT. BRAGG	-1.03	-10.4	1.57	16.6	13.4	.922
60	HURLBERT FLD	FT. BRAGG	.74	5.4	2.66	19.5	17.6	.581
61	SHAW AFB	FT. BRAGG	-1.10	-14.3	1.46	18.1	15.3	.953
62	MACDILL	FT. BRAGG	-1.71	-16.0	2.60	23.9	19.7	.928
63	DRIVER	NORFOLK	2.76	23.3	3.13	26.7	23.3	.674
64	HURLBERT FLD	NORFOLK	-.12	-.3	1.75	11.3	9.4	.835
65	SHAW AFB	NORFOLK	-.22	-.9	1.33	13.5	11.4	.908
66	MACDILL	NORFOLK	1.88	10.9	3.10	18.6	15.0	.693
67	CAMP LEJUNE	NORFOLK	.35	3.0	1.95	16.6	14.5	.647
68	ROBINS	NORFOLK	4.00	28.2	4.30	29.8	28.5	.963
69	ISABELA	NORFOLK	3.58	17.6	4.68	21.9	19.1	.916
70	R/V MOANA WAVE	NORFOLK	6.00	26.7	6.28	28.3	26.7	.956

Table 13. MINIMUF 85 comparison by sounder path.

ID	Transmission Path		Bias error Mhz	Bias error %	RMS error Mhz	RMS error %	Magni-tude,%	Corre-lation Coeffi-cient
1	GUAM	YOKOHAMA	-.08	-8.8	5.28	35.1	25.9	.636
2	FORT MONMOUTH	PALO ALTO	1.43	2.8	4.36	25.2	19.8	.772
3	GUAM	HONOLULU	.83	.7	3.21	18.7	14.5	.873
4	GUAM	KODIAK	-1.00	-4.8	3.14	17.9	14.3	.892
5	HONOLULU	KODIAK	.52	.5	2.87	16.4	12.9	.897
6	HONOLULU	WASHINGTON	2.46	11.0	3.90	19.3	16.2	.814
7	MCCLELLAN	HONOLULU	-.44	-5.6	2.88	19.6	13.5	.846
8	PALO ALTO	FAIRBANKS	2.49	11.1	3.68	18.9	17.2	.392
9	BOULDER	BARROW	.76	1.6	4.69	26.8	22.4	.191
10	HONOLULU	YOKOHAMA	-1.08	-8.3	3.42	23.4	16.2	.881
11	PHILIPPINES	YOKOHAMA	1.43	6.6	3.71	16.4	13.1	.813
12	PHILIPPINES	HEH	1.12	4.9	3.91	16.1	13.1	.828
13	GUAM	HEH	-1.67	-6.0	4.45	17.2	14.0	.857
14	DAVIS	KODIAC	-1.90	-15.8	5.21	38.6	28.4	.728
15	HONOLULU	CORONA	.89	-.1	3.45	22.4	14.5	.916
16	ANDOYA	THESSALONIKI	5.26	22.5	6.26	25.4	22.7	.265
17	MCCLELLAN	LA POSTA	1.15	11.4	2.35	22.2	18.6	.746
18	FRANCE	GREECE	-3.25	-37.2	4.23	47.8	38.0	.716
19	HONOLULU	LA POSTA	-.50	-6.2	2.38	20.4	14.4	.825
20	COCO SOLO	STOCKBRIDGE	-1.16	-6.3	3.29	16.9	12.6	.907
21	ANDOYA	NEW DELHI	2.55	14.7	3.38	19.4	17.3	.887
22	PALO ALTO	THULE	1.86	6.8	3.35	23.2	20.8	.823
23	FRANCE	ICELAND	1.07	4.1	2.54	17.4	14.5	.855
25	FORT MONMOUTH	ABERDEEN	-1.32	-17.3	1.71	22.6	19.5	.730
26	FORT MONMOUTH	CAMP DRUM	-1.55	-21.8	2.07	31.7	22.7	.801
27	PUERTO RICO	MAYNARD	.15	.4	2.39	13.6	10.2	.915
28	THULE	STOCKBRIDGE	4.18	10.6	7.03	26.8	22.9	.836
29	ANDOYA	MAYNARD	1.20	-3.4	5.68	41.0	35.7	.016
30	BANGKOK	CHANTABURI	1.94	21.3	2.20	23.7	21.3	.820
31	OTTAWA	THE HAGUE	2.29	8.3	5.19	24.1	20.2	.706
32	WINNIPEG	RESOLUTE BAY	1.56	5.2	3.96	19.6	16.6	.682
33	OTTAWA	RESOLUTE BAY	-.51	-7.5	3.65	23.7	18.3	.641
34	OKINAWA	ST.KILDA	-3.45	-14.0	5.00	19.7	16.6	.907
35	OKINAWA	TOWNSVILLE	.62	.2	4.73	16.0	11.9	.822
36	YAMAGAWA	ST.KILDA	-1.75	-8.4	3.80	16.8	12.8	.918
37	YAMAGAWA	TOWNSVILLE	1.10	-.4	5.01	20.4	15.4	.854
38	MONROVIA	ROTA	7.25	20.2	9.05	32.2	29.4	.850
39	MONROVIA	LAMY	1.93	6.8	6.07	23.5	19.8	.219
40	TRIPOLI	ACCRA	11.06	26.1	13.67	35.1	31.2	.607
41	OKINAWA	THESSALONIKI	3.45	18.2	4.81	25.5	22.5	.817

Table 13. MINIMUF 85 comparison by sounder path, continued.

ID	Transmission Path		Bias error Mhz	Bias error %	RMS error Mhz	RMS error %	Magni- tude,%	Corre- lation Coeffi- cient
42	OKINAWA	NEW DELHI	1.97	10.1	3.05	15.9	13.0	.914
43	SAPPORO	AVIANO	4.12	20.8	5.71	27.3	23.3	.771
44	SAPPORO	KASSEL	4.21	20.9	6.09	28.8	24.6	.711
45	SAPPORO	THETFORD	3.83	20.0	5.82	29.0	25.4	.680
46	PHILIPPINES	BRINDIS	.07	1.5	5.69	24.8	20.6	.737
47	PHILIPPINES	AVIANO	3.14	15.6	4.76	22.5	18.2	.858
48	PHILIPPINES	THETFORD	2.94	13.5	5.48	28.4	21.4	.738
49	TOKOROZAWA	BRINDIS	4.04	21.4	5.23	26.5	23.5	.843
50	TOKOROZAWA	AVIANO	3.44	17.8	5.22	25.5	21.4	.784
51	TOKOROZAWA	KASSEL	3.70	19.2	5.76	28.2	24.9	.716
52	TOKOROZAWA	THETFORD	3.87	20.4	5.79	28.9	25.8	.711
53	THULE	PULLMAN	-2.10	-13.3	3.32	22.5	19.7	.768
54	ANDOYA	PULLMAN	4.14	24.7	5.83	33.8	28.7	.283
55	BROME	MIRIKATA	.65	3.4	2.19	14.1	10.6	.905
56	ADELAIDE	TOWNSVILLE	.90	4.3	3.15	16.4	12.6	.835
57	KOLSAAS	USS MT WHITNEY	1.27	13.1	2.16	26.7	24.6	.744
58	SOL BUCHAN	USS MT WHITNEY	.75	6.7	1.29	15.0	12.5	.963
59	DRIVER	FT. BRAGG	-.65	-6.2	1.27	13.8	10.9	.919
60	HURLBERT FLD	FT. BRAGG	1.28	9.3	2.77	20.3	17.1	.581
61	SHAW AFB	FT. BRAGG	-.77	-9.7	1.17	14.5	12.1	.951
62	MACDILL	FT. BRAGG	-1.24	-11.2	2.21	20.4	17.0	.926
63	DRIVER	NORFOLK	3.12	26.4	3.44	29.1	26.4	.675
64	HURLBERT FLD	NORFOLK	.56	3.6	1.77	11.5	9.1	.833
65	SHAW AFB	NORFOLK	.20	3.0	1.25	13.4	11.1	.908
66	MACDILL	NORFOLK	2.51	14.5	3.46	20.5	16.9	.691
67	CAMP LEJUNE	NORFOLK	.84	6.9	2.02	17.1	14.6	.649
68	ROBINS	NORFOLK	4.10	28.9	4.41	30.5	29.2	.962
69	ISABELA	NORFOLK	3.66	18.0	4.73	22.2	19.3	.916
70	R/V MOANA WAVE	NORFOLK	6.06	27.0	6.34	28.6	27.0	.956

Table 14. HFBC84 comparison by sounder path.

ID	Transmission Path		Bias error Mhz	Bias error %	RMS error Mhz	RMS error %	Magnitude,%	Correlation Coefficient
1	GUAM	YOKOHAMA	-1.22	-11.2	5.67	39.4	25.5	.695
2	FORT MONMOUTH	PALO ALTO	.97	3.4	3.22	18.1	14.3	.883
3	GUAM	HONOLULU	-2.59	-11.8	4.74	23.8	18.6	.915
4	GUAM	KODIAK	-2.12	-12.9	3.40	20.2	15.7	.892
5	HONOLULU	KODIAK	-2.49	-16.6	4.40	25.7	21.5	.837
6	HONOLULU	WASHINGTON	5.59	29.5	6.41	33.3	30.8	.813
7	MCCLELLAN	HONOLULU	.89	5.5	2.98	18.0	14.5	.893
8	PALO ALTO	FAIRBANKS	4.68	24.8	4.90	25.5	24.8	.873
9	BOULDER	BARROW	2.57	13.3	3.33	16.8	14.3	.767
10	HONOLULU	YOKOHAMA	-2.63	-14.0	4.33	24.2	17.5	.899
11	PHILIPPINES	YOKOHAMA	1.14	4.9	2.20	9.0	7.2	.886
12	PHILIPPINES	HEH	-5.92	-23.6	7.52	30.9	25.1	.774
13	GUAM	HEH	-3.91	-16.1	5.12	21.9	18.2	.871
14	DAVIS	KODIAC	.96	1.4	5.20	27.8	20.9	.681
15	HONOLULU	CORONA	-4.79	-28.2	5.79	34.7	29.4	.927
16	ANDOYA	THESSALONIKI	5.56	24.6	6.51	27.4	24.9	.425
17	MCCLELLAN	LA POSTA	2.38	22.9	2.88	27.5	23.2	.818
18	FRANCE	GREECE	3.48	34.1	4.19	37.6	35.0	.657
19	HONOLULU	LA POSTA	-4.55	-31.7	5.76	42.4	32.5	.878
20	COCO SOLO	STOCKBRIDGE	2.14	10.1	3.33	15.5	13.0	.935
21	ANDOYA	NEW DELHI	1.78	12.9	2.87	20.6	17.4	.904
22	PALO ALTO	THULE	2.45	13.7	3.51	21.7	18.8	.833
23	FRANCE	ICELAND	2.61	18.2	3.51	23.9	20.7	.850
25	FORT MONMOUTH	ABERDEEN	.95	12.7	1.10	14.7	12.7	.811
26	FORT MONMOUTH	CAMP DRUM	.65	7.4	.95	12.2	10.8	.938
27	PUERTO RICO	MAYNARD	3.14	16.7	3.87	20.1	17.2	.923
28	THULE	STOCKBRIDGE	5.60	24.1	6.30	26.7	24.3	.946
29	ANDOYA	MAYNARD	3.03	14.2	5.14	31.2	28.2	.548
30	BANGKOK	CHANTABURI	.18	2.1	.92	11.9	8.7	.894
31	OTTAWA	THE HAGUE	1.64	9.8	3.21	17.6	13.7	.924
32	WINNIPEG	RESOLUTE BAY	2.00	12.2	2.54	16.0	13.5	.959
33	OTTAWA	RESOLUTE BAY	2.14	12.6	2.62	14.8	13.2	.948
34	OKINAWA	ST.KILDA	1.76	4.8	3.77	14.6	12.6	.874
35	OKINAWA	TOWNSVILLE	2.67	5.4	5.84	19.8	15.9	.783
36	YAMAGAWA	ST.KILDA	2.69	7.8	4.99	16.7	14.2	.869
37	YAMAGAWA	TOWNSVILLE	3.10	6.4	5.79	21.5	17.0	.877
38	MONROVIA	ROTA	2.47	8.6	3.28	13.2	11.0	.975
39	MONROVIA	LAMY	4.05	17.3	5.12	21.1	17.9	.690
40	TRIPOLI	ACCRA	4.87	11.0	6.95	19.5	15.2	.873
41	OKINAWA	THESSALONIKI	2.10	11.9	3.13	16.9	13.7	.918

Table 14. HFBC84 comparison by sounder path, continued.

ID	Transmission Path		Bias error Mhz	Bias error %	RMS error Mhz	RMS error %	Magni-tude,%	Corre-lation Coeffi-cient
42	OKINAWA	NEW DELHI	-2.98	-13.7	4.84	23.4	19.5	.941
43	SAPPORO	AVIANO	4.48	22.3	4.91	24.1	22.8	.915
44	SAPPORO	KASSEL	4.90	23.9	5.36	25.8	24.1	.894
45	SAPPORO	THETFORD	4.50	22.9	4.92	24.9	23.2	.893
46	PHILIPPINES	BRINDIS	.14	2.2	5.32	24.0	18.9	.774
47	PHILIPPINES	AVIANO	.08	7.3	4.52	20.2	17.5	.867
48	PHILIPPINES	THETFORD	2.14	1.0	4.43	22.8	7.8	.841
49	TOKOROZAWA	BRINDIS	3.25	18.1	4.26	22.6	20.2	.911
50	TOKOROZAWA	AVIANO	3.64	19.0	4.31	21.9	19.9	.908
51	TOKOROZAWA	KASSEL	4.32	22.2	4.83	24.9	22.6	.897
52	TOKOROZAWA	THETFORD	4.70	24.2	5.14	26.4	24.4	.887
53	THULE	PULLMAN	2.37	16.0	2.64	18.1	16.0	.893
54	ANDOYA	PULLMAN	4.57	27.0	4.94	28.5	27.1	.646
55	BROME	MIRIKATA	2.52	14.1	3.18	17.7	15.8	.922
56	ADELAIDE	TOWNSVILLE	2.27	11.6	3.08	15.3	12.8	.915
57	KOLSAAS	USS MT WHITNEY	1.22	11.8	1.64	15.4	13.3	.990
58	SOL BUCHAN	USS MT WHITNEY	1.09	6.7	1.92	14.9	13.0	.980
59	DRIVER	FT. BRAGG	.50	5.6	.78	8.7	7.0	.895
60	HURLBERT FLD	FT. BRAGG	2.80	20.4	3.12	22.7	20.4	.788
61	SHAW AFB	FT. BRAGG	-.58	-8.5	.77	11.1	10.3	.922
62	MACDILL	FT. BRAGG	.03	.7	.70	7.4	5.5	.925
63	DRIVER	NORFOLK	3.78	31.3	3.98	32.5	31.3	.607
64	HURLBERT FLD	NORFOLK	3.28	19.8	3.35	20.6	19.8	.966
65	SHAW AFB	NORFOLK	1.80	17.2	1.94	18.5	17.2	.881
66	MACDILL	NORFOLK	4.24	24.8	4.38	26.0	24.8	.921
67	CAMP LEJUNE	NORFOLK	3.83	30.5	4.04	31.7	30.5	.628
68	ROBINS	NORFOLK	2.82	20.9	2.99	22.0	20.9	.983
69	ISABELA	NORFOLK	1.38	9.4	3.56	17.5	15.7	.960
70	R/V MOANA WAVE	NORFOLK	2.86	14.2	2.97	16.3	14.2	.994

Table 15 summarizes the analysis statistics for all 70 paths for all three models tested.

Table 15. 70-path statistical analysis summary for MINIMUF-3.5, MINIMUF 85, and HFBC84 models.

Analysis	MINIMUF-3.5	MINIMUF 85	HFBC84
Total path-hours	13054	13054	13054
Average residual	1.26	1.28	1.17
RMS residual	4.44	4.58	4.67
Ave. rel. residual	.053	.051	.059
RMS rel. residual	.232	.239	.242
Ave. abs. rel. res.	.201	.208	.217
Std. error of est.	3.92	3.97	3.89
Correlation coefficient	.824	.819	.827

As shown in Table 15, the performance of all three MUF models was almost identical overall. Bias was lowest for the HFBC84 model: 1.17 MHz compared to 1.26 MHz for MINIMUF-3.5 and 1.28 MHz for MINIMUF 85. RMS error was lowest for MINIMUF-3.5: 4.44 MHz compared to 4.58 MHz for MINIMUF 85 and 4.67 MHz for HFBC84. The correlation was best for HFBC84; MINIMUF-3.5 was next; and MINIMUF 85 was last. The correlation of the three models differed by only 1 percent.

6.1 DATA TYPE

A critical part of any investigation involving the use of observed measurements is the quality and time resolution of the measurements. This is particularly important when multiple samples are merged into mean values, as was the case with the oblique sounder data. As discussed in the section on data preparation, there were six types of sounder data used: (1) NTSS-HFDR, (2) NTSS-strip chart, (3) non-NTSS, (4) Granger 900 series, (5) modified C-3 and (6) BR Communications Chirpsounder. The number of data points per hour per month determining the hourly medians were: 160, 4, 6, 3, 1, and 4 for the six data categories, respectively.

Figures 14 and 15 show the average residual (bias) and average relative residual, respectively, as a function of date type for the three models tested. MINIMUF-3.5 and MINIMUF 85 models have the lowest bias for the NTSS-strip chart data. The HFBC84 model has its lowest bias for the NTSS-HFDR data. All three models had their highest bias for the BR Chirpsounder data.

Figures 16 and 17 show the RMS error and relative RMS error, respectively. The MINIMUF models had their lowest RMS error for the NTSS-HFDR data while the HFBC84 model had the lowest RMS error for non-NTSS data. The relative RMS error was about 25 percent for the MINIMUF models and between 15 and 35 percent for the HFBC84 model for all data types. The MINIMUF models have their lowest relative RMS error for the Granger

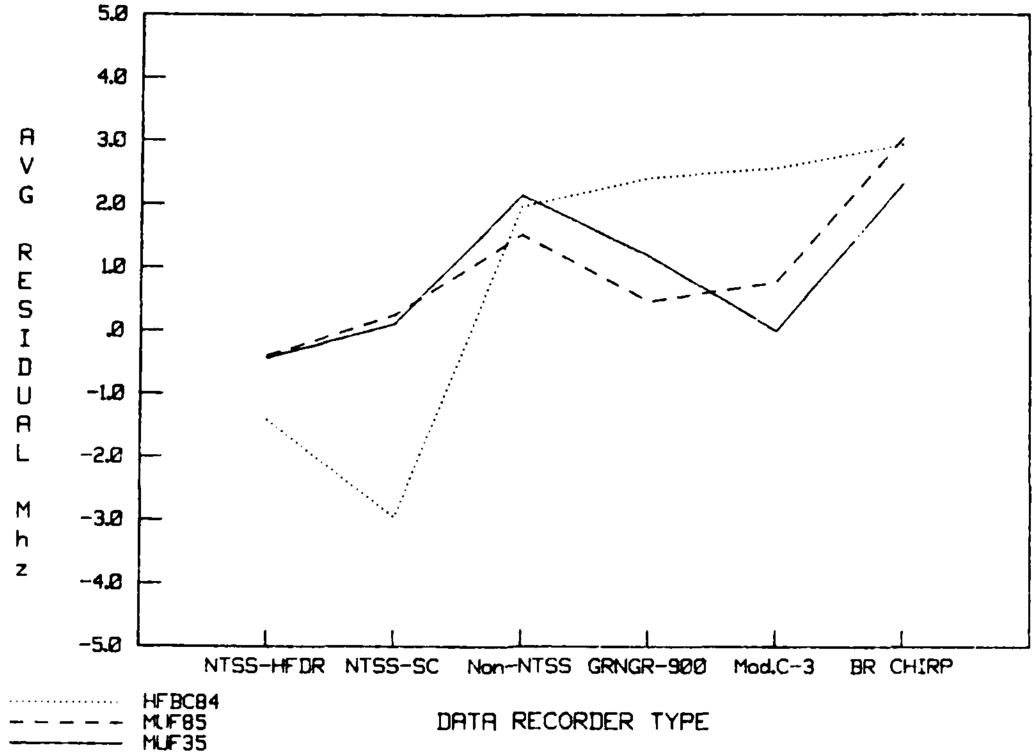

Figure 14. Average residual (bias) as a function of data type.

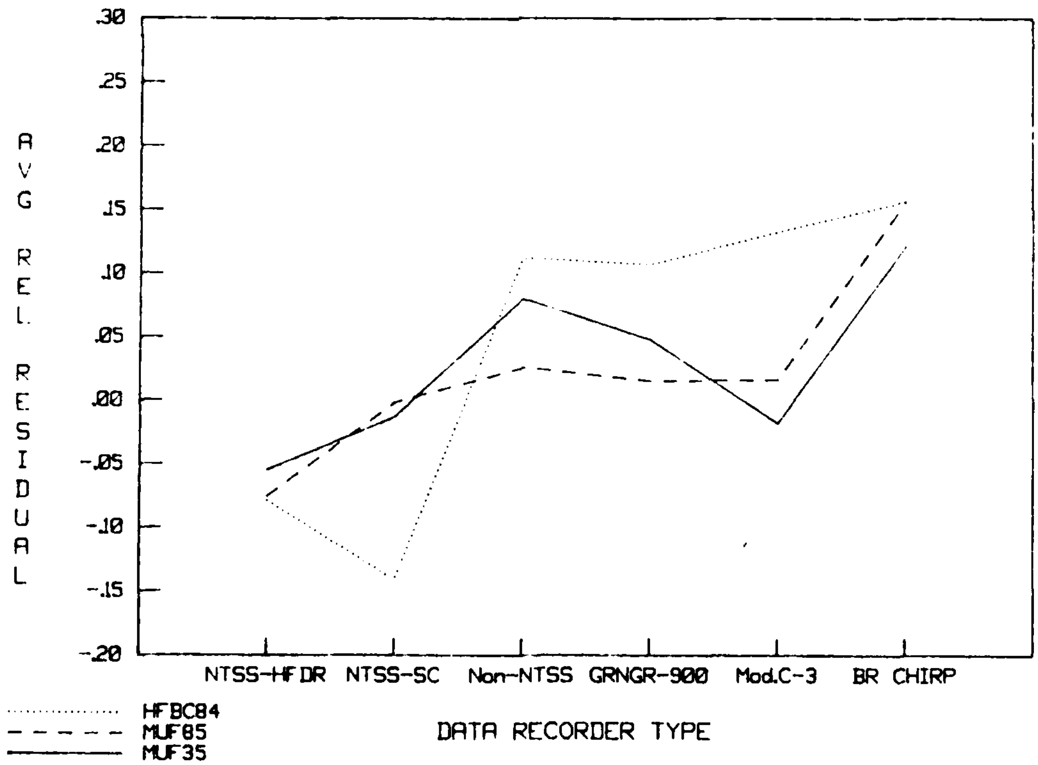

Figure 15. Average relative residual (relative bias) as a function of data type.

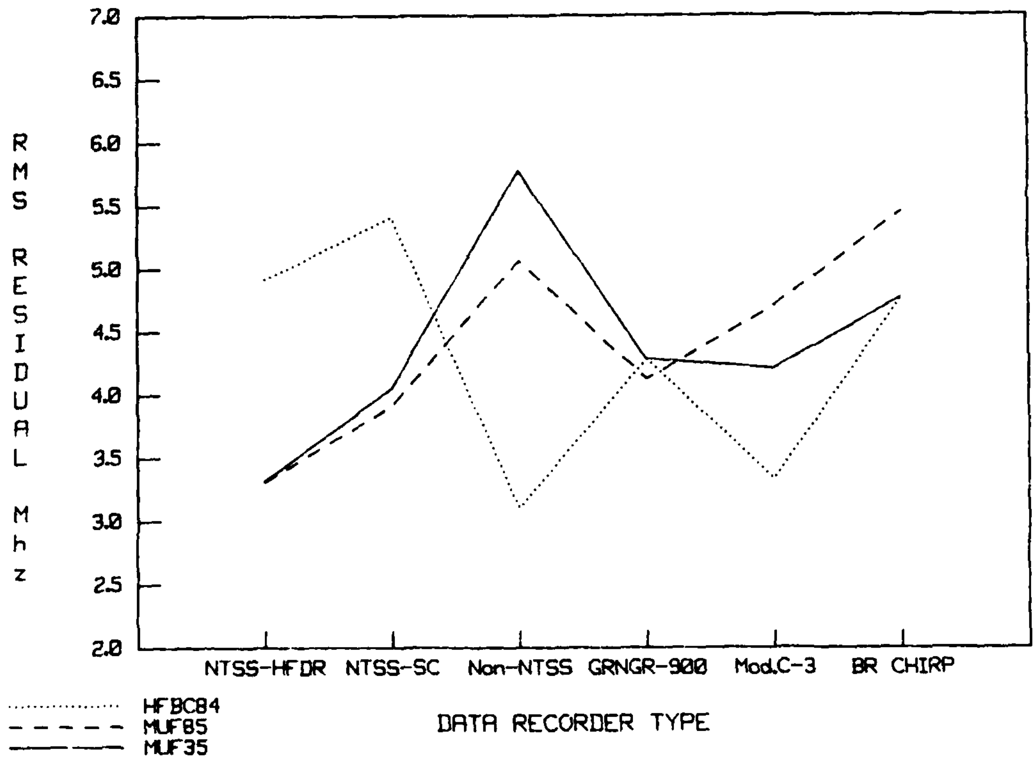

Figure 16. RMS error in MHz as a function of data type.

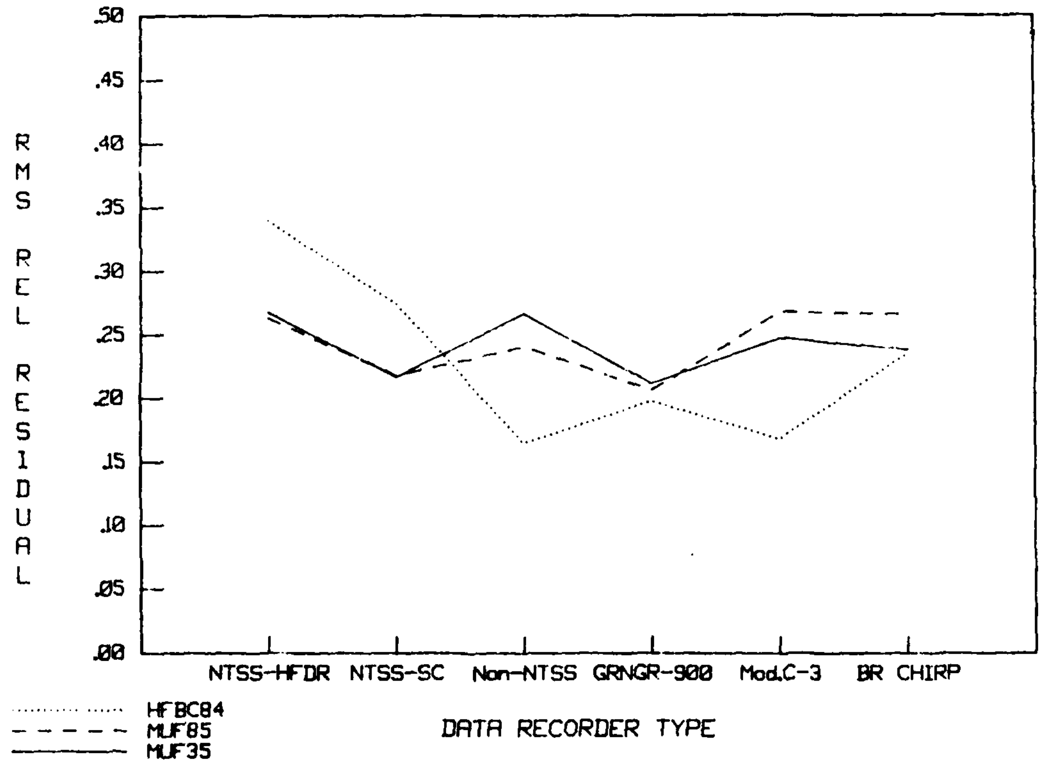

Figure 17. Relative RMS error as a function of data type.

900 data and the NTSS-strip chart data. The HFBC84 model has its lowest error for the modified C-3 data.

Figure 18 shows the magnitude of the error for the three models tested. MINIMUF error ranges between 15 and 20 percent; HFBC84 ranges between 15 and 25 percent.

Figure 19 shows the correlation coefficient of the predicted MUF and observed MOF as a function of data type for all three models. It indicates the generally high correlation for all data types except for the limited modified C-3 data set.

6.2 PATH LENGTH

Figures 20-25 show the distribution of MUF prediction error as a function of path length. Figures 20 and 21 show the average residual and average relative residual, respectively. The MINIMUF models have the lowest residuals in general, particularly for path lengths less than 5000 km. The HFBC84 model has its lowest residual in the 6000- to 7000-km path-length range, similar to the MINIMUF models; but unlike the MINIMUF models, the HFBC84 model has a large negative bias at 4000-5000 km. However, the MINIMUF models have another minimum in the 3000 to 4000 km path-length range. Figure 21 shows that MINIMUF 85 has the lowest average relative residual, 20 percent or less for all path-length ranges. Figures 22 and 23 show the RMS error and the relative RMS error, respectively. The figures show error to generally increase with path length. Note the large reduction in RMS error at 4000-5000 km for the MINIMUF models. The average magnitude of the error is shown in Figure 24. As can be seen, the error is 25 percent or less for all path-length ranges, with slightly lower values for shorter path lengths. The large error at 2000 km reported in Reference 28 has been eliminated. Figure 25 shows the model correlation as a function of path length. The HFBC84 model has the highest correlation overall. When the MINIMUF models are compared to previous results reported in Reference 28, an improvement in correlation can be seen at all path lengths except the 4000 km, where there is a very slight decrease.

6.3 PATH ORIENTATION

Figures 26-31 summarize the performance of the models as a function of path orientation. This categorization is important to assure that the sunrise/sunset reactions are correct for varying degrees of path illumination. The north-south (N-S) paths are those which lie nominally within ±15° of a 0° or 180° bearing. The east-west (E-W) paths are those which fall nominally within ±15° of a 90° or 270° bearing. The paths which did not meet either criterion were put in the "other" category. Table 16 indicates which paths in the MOF database are in each of the path orientation categories.

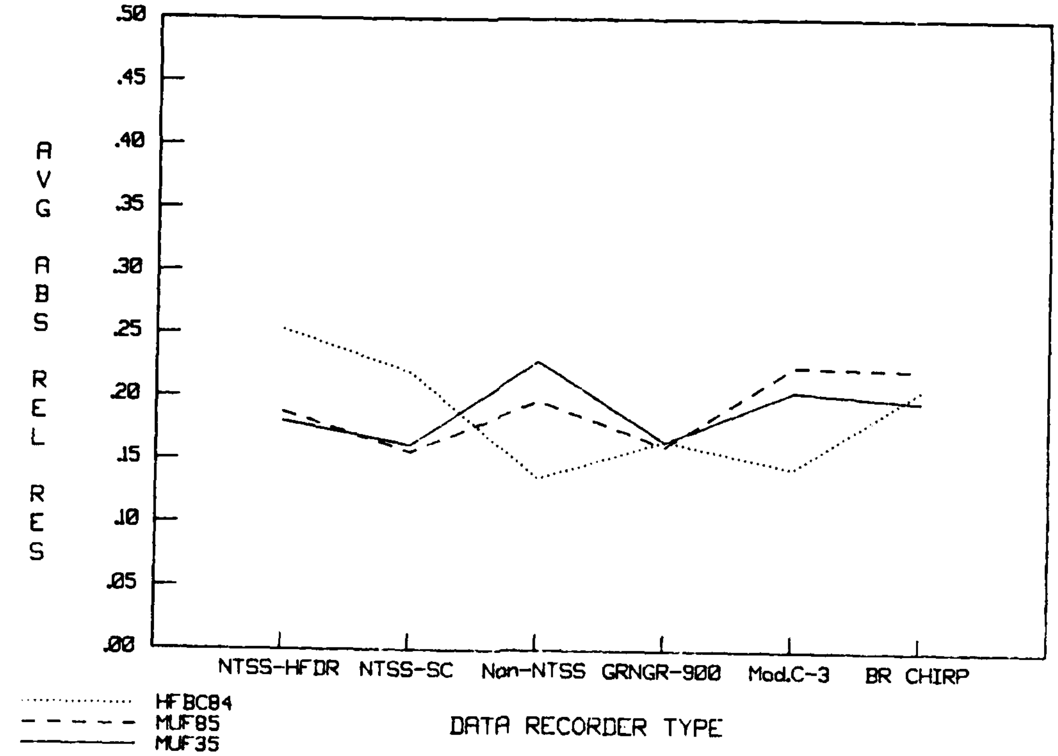

Figure 18. Magnitude of the error (average absolute relative residual) as a function of data type.

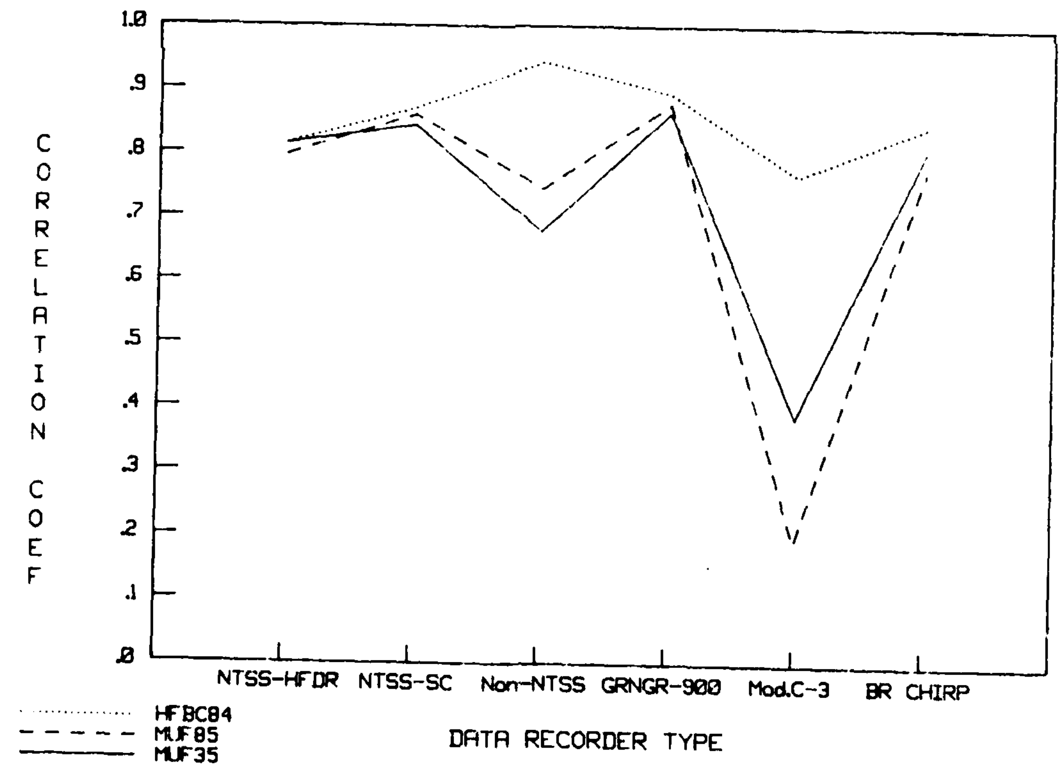

Figure 19. Correlation coefficients as a function of data type.

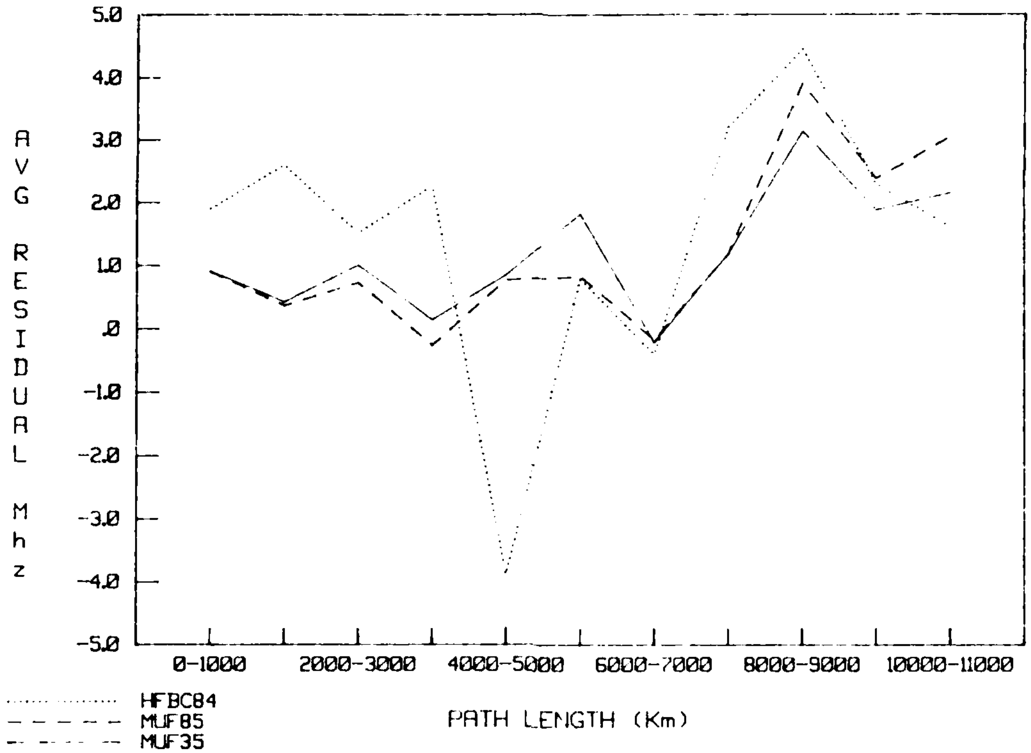

Figure 20. Average residual (bias) as a function of path length.

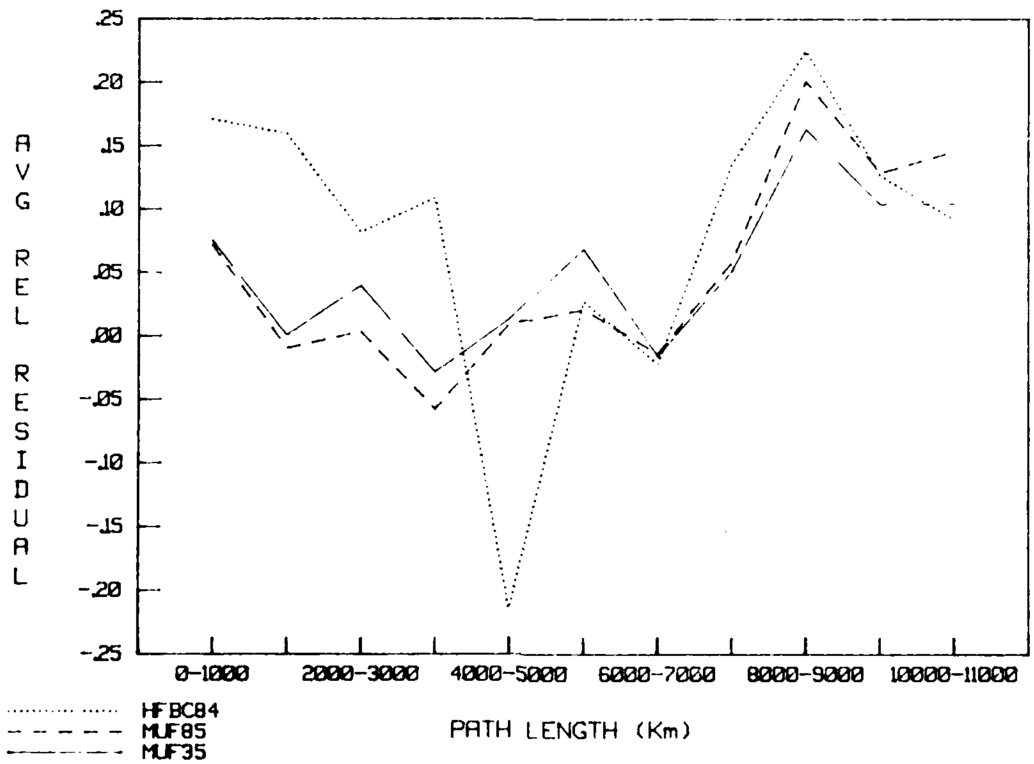

Figure 21. Average relative residual (relative bias) as a function of path length.

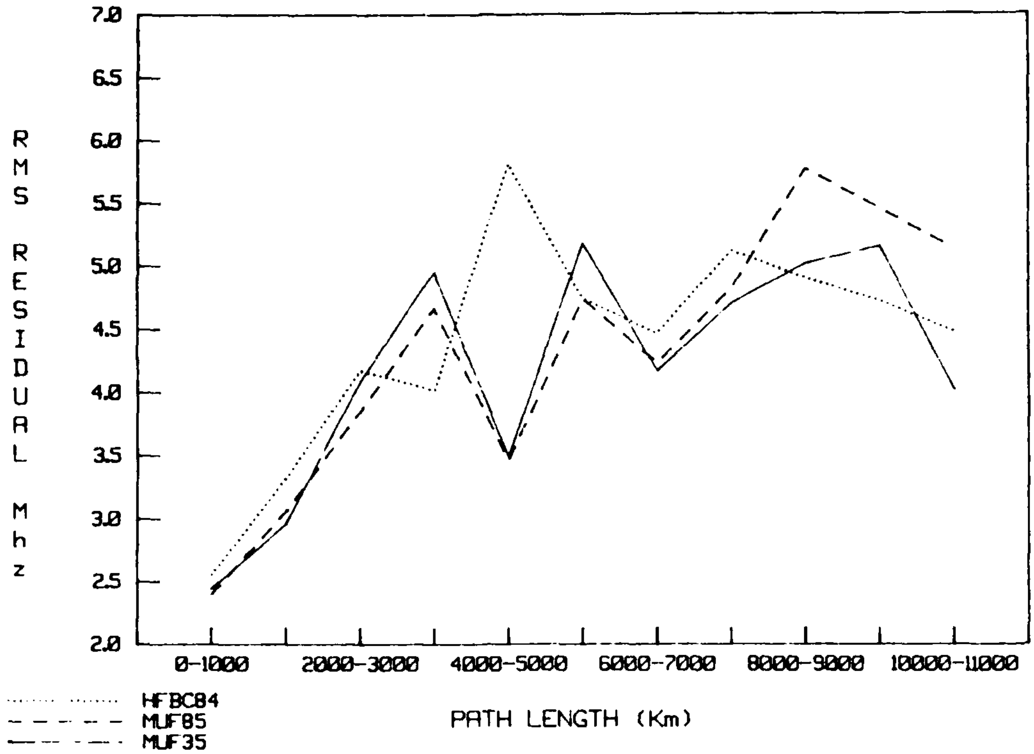

Figure 22. RMS error in MHz as a function of path length.

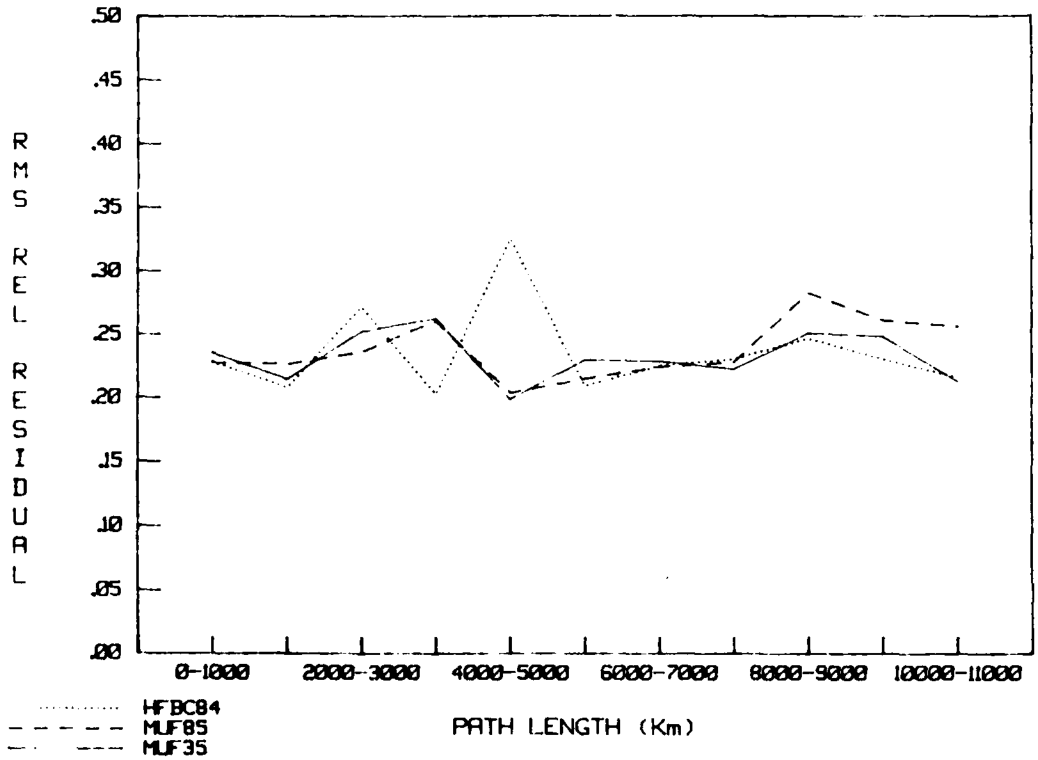

Figure 23. Relative RMS error as a function of path length.

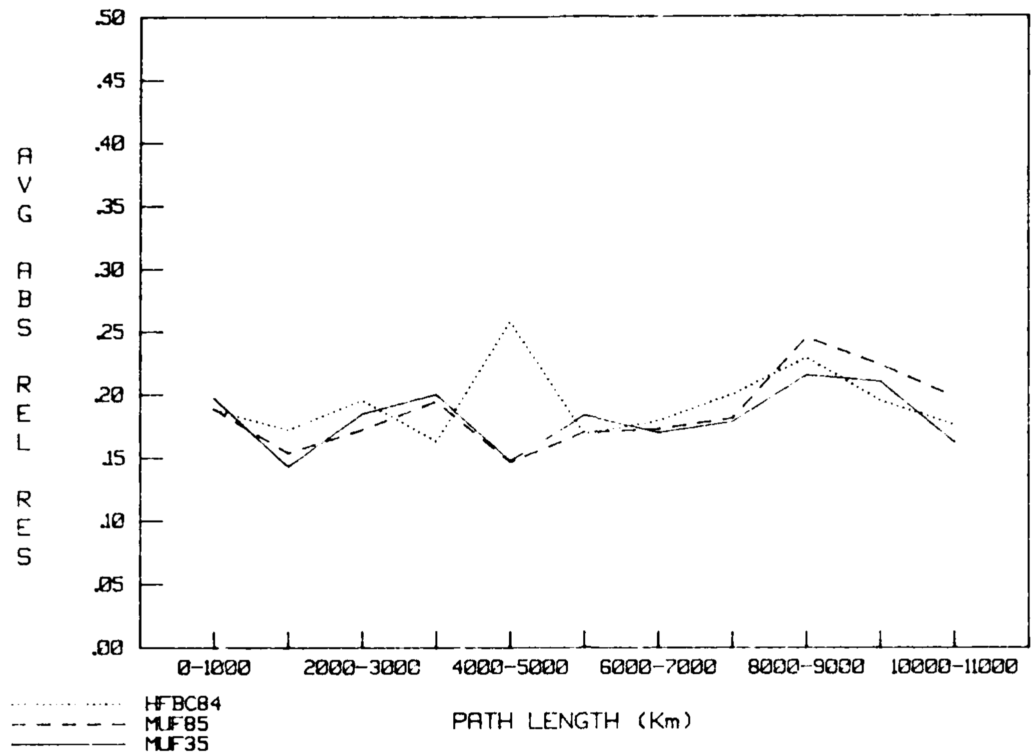

Figure 24. Magnitude of the error (average absolute relative residual) as a function of distance.

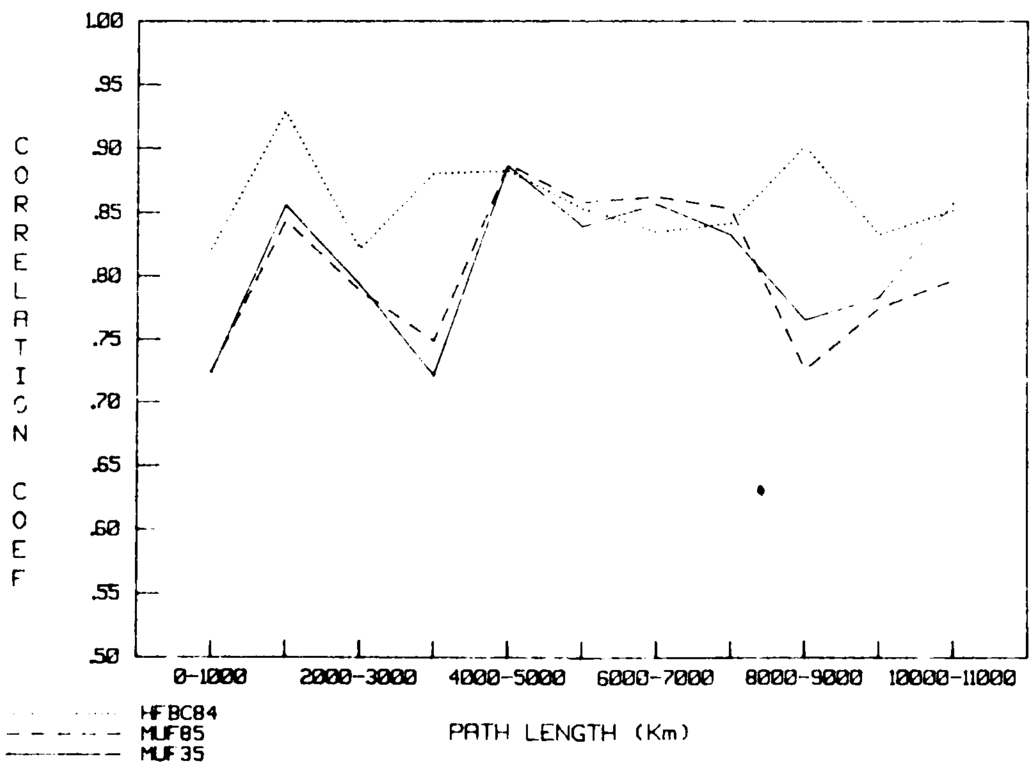

Figure 25. Correlation coefficients as a function of path length

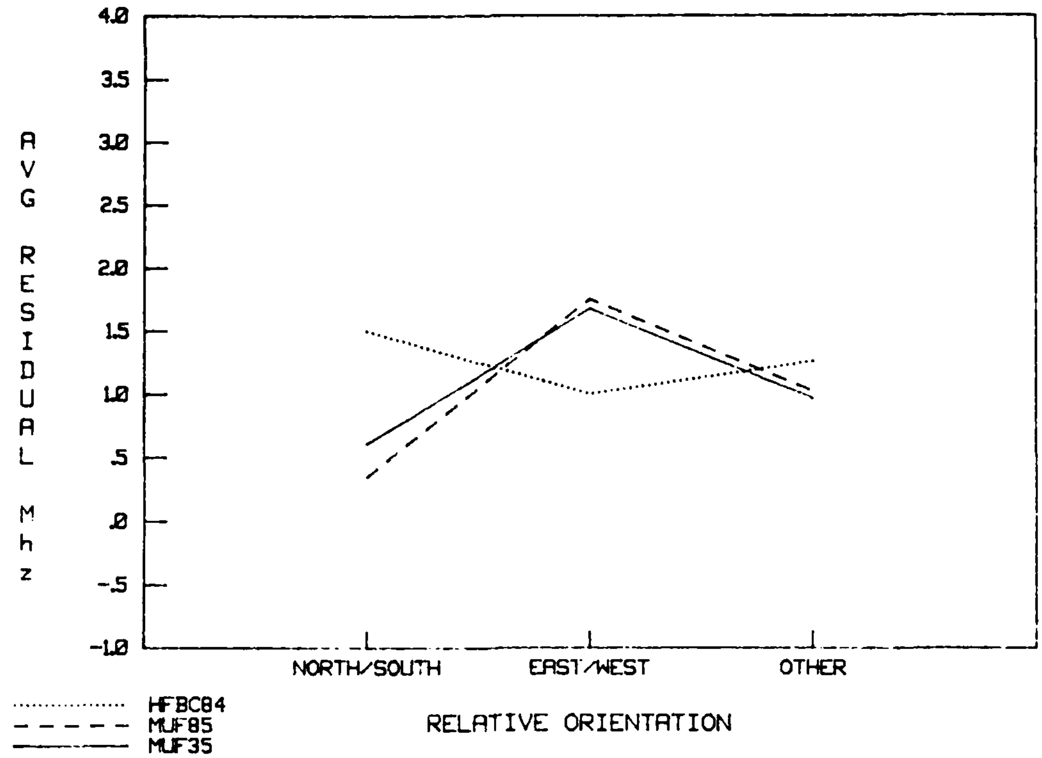

Figure 26. Average residual (bias) as a function of path orientation.

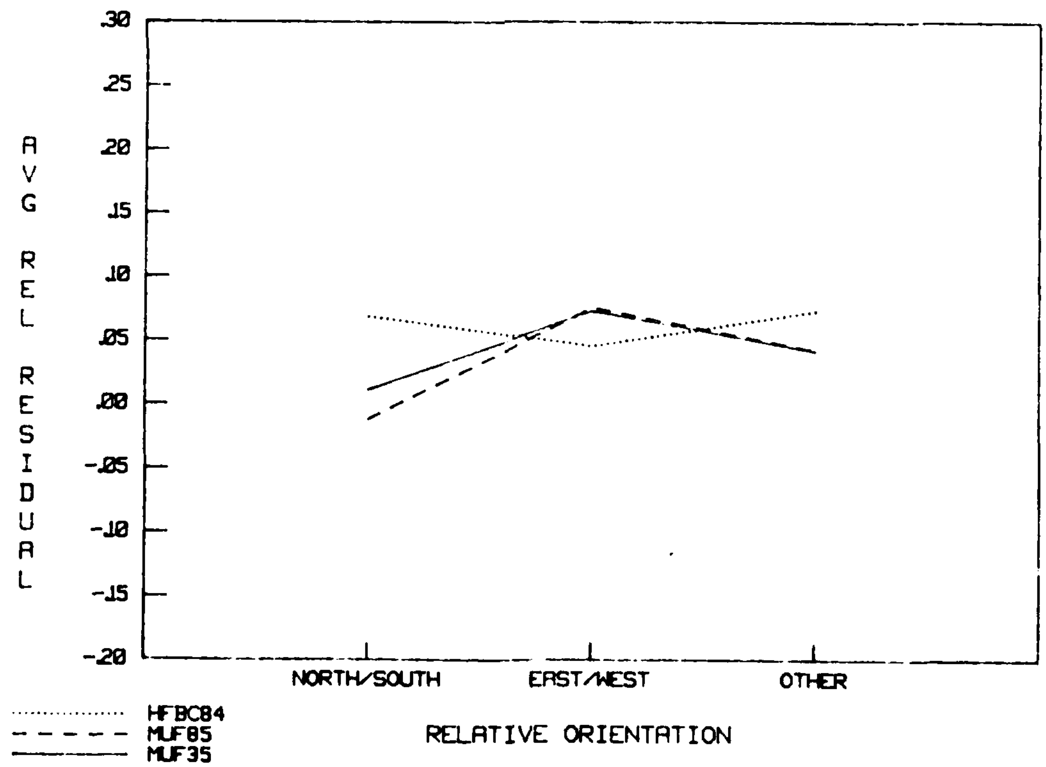

Figure 27. Average relative residual (relative bias) as a function of orientation.

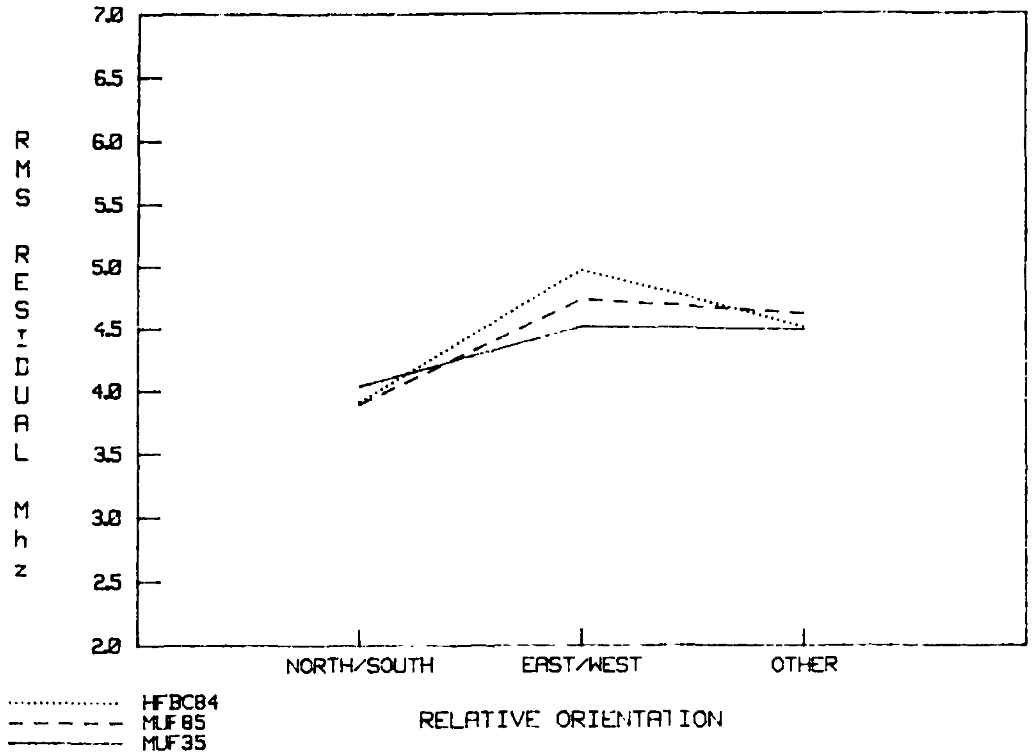

Figure 28. RMS error in MHz as a function of path orientation.

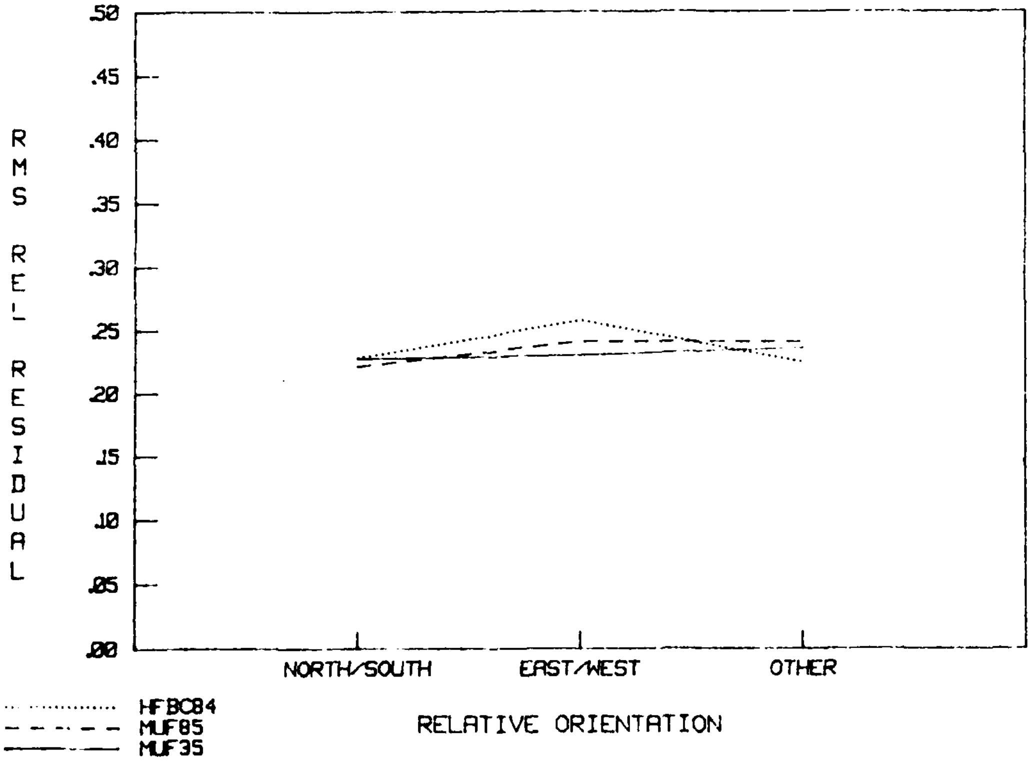

Figure 29. Relative RMS error as a function of path orientation.

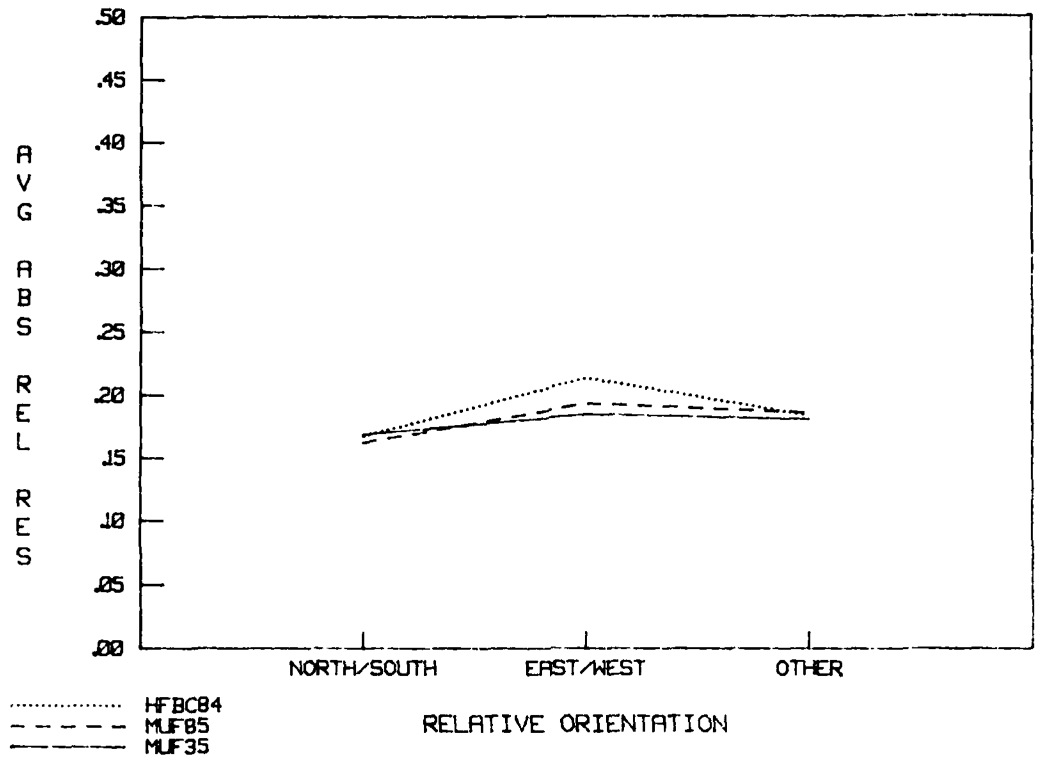

Figure 30. Magnitude of the error (average absolute relative residual) as a function of path orientation.

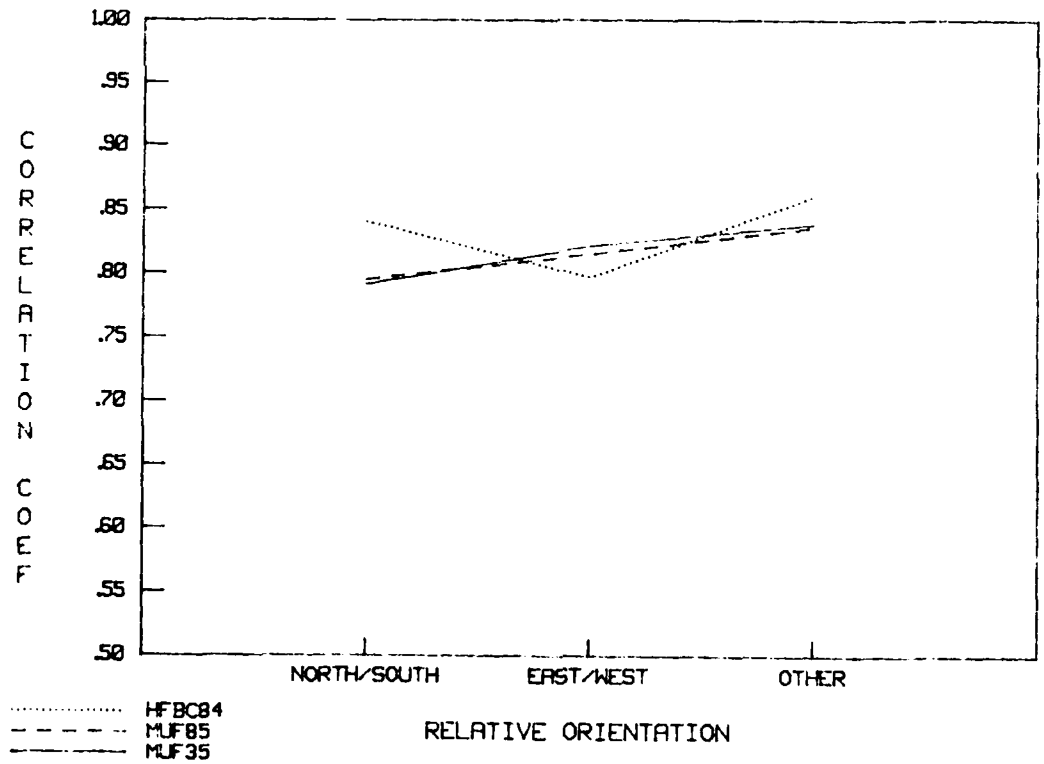

Figure 31. Correlation coefficients as a function of path orientation.

Table 16. Additional sounder path characteristics.

ID.	Transmission Path		Orientation	Latitude of Control Points	Geographic Region
1	GUAM	YOKOHAMA	No/So	LO	Ocean
2	FT MONMOUTH	PALO ALTC	E/W	M	Land
3	GUAM	HONOLULU	E/W	LO	Ocean
4	GUAM	KODIAK	E/W	M	Ocean
5	HONOLULU	KODIAK	No/So	M	Ocean
6	HONOLULU	WASHINGTON	E/W	M	Combined
7	MCCLELLAN	HONOLULU	Other	M	Ocean
8	PALO ALTO	FAIRBANKS	Other	H	Combined
9	BOULDER	BARROW	Other	H	Land
10	HONOLULU	YOKOHAMA	Other	M	Ocean
11	PHILIPPINES	YOKOHAMA	E/W	LO	Ocean
12	PHILIPPINES	HEH	E/W	TE	Combined
13	GUAM	HEH	Other	TE	Combined
14	DAVIS	KODIAC	Other	M	Ocean
15	HONOLULU	CORONA	E/W	M	Ocean
16	ANDOYA	THESSALONIKI	No/So	H	Land
17	MCCLELLAN	LA POSTA	Other	M	Land
18	FRANCE	GREECE	E/W	M	Combined
19	HONOLULU	LA POSTA	E/W	M	Ocean
20	COCO SOLO	STOCKBRIDGE	No/So	M	Ocean
21	ANDOYA	NEW DELHI	Other	H	Land
22	PALO ALTO	THULE	E/W	TA	Land
23	FRANCE	ICELAND	Other	H	Combined
25	FT MONMOUTH	ABERDEEN	Other	M	Land
26	FT MONMOUTH	CAMP DRUM	Other	M	Land
27	PUERTO RICO	MAYNARD	No/So	M	Ocean
28	THULE	STOCKBRIDGE	E/W	TA	Combined
29	ANDOYA	MAYNARD	Other	TA	Combined
30	BANGKOK	CHANTABURI	Other	LO	Land
31	OTTAWA	THE HAGUE	E/W	H	Combined
32	WINNIPEG	RESOLUTE BAY	No/So	TA	Land
33	OTTAWA	RESOLUTE BAY	No/So	TA	Land
34	OKINAWA	ST.KILDA	E/W	TE	Combined
35	OKINAWA	TOWNSVILLE	Other	TE	Combined
36	YAMAGAWA	ST.KILDA	E/W	TE	Combined
37	YAMAGAWA	TOWNSVILLE	Other	TE	Ocean
38	MONROVIA	ROTA	No/So	LO	Land
39	MONROVIA	LAMY	E/W	LO	Land
40	TRIPOLI	ACCRA	Other	LO	Land
41	OKINAWA	THESSALONIKI	E/W	H	Land
42	OKINAWA	NEW DELHI	E/W	LO	Combined
43	SAPPORO	AVIANO	E/W	H	Land

Table 16. Additional sounder path characteristics, continued.

ID.	Transmission Path		Orientation	Latitude of Control Points	Geographic Region
44	SAPPORO	KASSEL	E/W	H	Land
45	SAPPORO	THETFORD	E/W	H	Land
46	PHILIPPINES	BRINDIS	Other	M	Land
47	PHILIPPINES	AVIANO	Other	M	Land
48	PHILIPPINES	THETFORD	Other	H	Land
49	TOKOROZAWA	BRINDIS	E/W	M	Land
50	TOKOROZAWA	AVIANO	E/W	H	Land
51	TOKOROZAWA	KASSEL	E/W	H	Land
52	TOKOROZAWA	THETFORD	E/W	H	Land
53	THULE	PULLMAN	Other	TA	Combined
54	ANDOYA	PULLMAN	Other	TA	Combined
55	BROME	MIRIKATA	Other	TE	Land
56	ADELAIDE	TOWNSVILLE	No/So	TE	Land
57	KOLSAAS	USS MT WHITNEY	Other	H	Combined
58	SOL BUCHAN	USS MT WHITNEY	Other	H	Land
59	DRIVER	FT. BRAGG	Other	M	Land
60	HURLBERT FLD	FT. BRAGG	Other	M	Land
61	SHAW AFB	FT. BRAGG	Other	M	Land
62	MACDILL	FT. BRAGG	Other	M	Land
63	DRIVER	NORFOLK	Other	M	Land
64	HURLBERT FLD	NORFOLK	Other	M	Land
65	SHAW AFB	NORFOLK	Other	M	Land
66	MACDILL	NORFOLK	Other	M	Land
67	CAMP LEJUNE	NORFOLK	No/So	M	Land
68	ROBINS	NORFOLK	Other	M	Ocean
69	ISABELA	NORFOLK	Other	M	Ocean
70	R/V MOANA WAVE	NORFOLK	Other	M	Ocean

TE = Transequatorial
LO = Low latitude
M = Mid-latitude
H = High latitude
TA = Transauroral

No/So = North-South
E/W = East-West

Figures 26 and 27 illustrate the bias in the models. They show all models having a positive bias of about 1 MHz high as a function of path orientation. The HFBC84 model is most accurate for EAST/WEST orientation and least accurate for NORTH/SOUTH. The MINIMUF models are most accurate for NORTH/SOUTH and least accurate for EAST/WEST. Figure 27 shows the relative bias to be less than 8 percent for all cases.

Figures 28 and 29 illustrate the RMS error and relative RMS error, respectively. For all models the RMS error ranges between about 4.0 and 4.5 MHz. Figure 30 shows the average magnitude of the error. For the MINIMUF models it ranges between 17 and 21 percent; for the HFBC84 model the range was 18 to 23 percent. Figure 31 shows the correlation coefficients to be highest for the "OTHER" category for all models. When compared to the results from Reference 29, the overall correlation for the expanded database has decreased very little.

6.4 SEASON AND MONTH

Figures 32-37 summarize the performance of the models as a function of season, and Figures 38-43 provide additional information as a function of month. Here the seasons are defined as: (1) winter (November through February); (2) spring (March and April); (3) summer (May through August); and (4) autumn (September and October).

The average residual as a function of season is shown in Figure 32. This figure shows the MINIMUF models to have their lowest error during the summer, when the HFBC84 model has the highest error. This is also shown in more detail in Figure 38, in which the summer months of June, July and August have errors greater than 2 MHz for the HFBC84 model and less than 0.5 MHz for the MINIMUF-3.5 model. Relative errors are shown in Figure 33. MINIMUF 85 has errors of 7 percent or less for all seasons, while MINIMUF-3.5 and HFBC84 models have errors of 10 percent or less. Figure 39 shows relative error as a function of month. MINIMUF 85 has less than 9 percent error for all months, while the HFBC84 model has greater than 10 percent error for the summer months, and MINIMUF-3.5 has greater than 10 percent error for the winter months. Figure 34 shows RMS error as function of season. All three models have an RMS error of 4 to 5 MHz for all seasons, with MINIMUF-3.5 having a slightly lower overall RMS error. In Figure 40 the RMS error as a function of month is shown. The MINIMUF models show minimum RMS error during the summer months. The RMS relative error as a function of season is shown in Figure 35. Relative RMS errors for all models for all seasons was in the range 21 to 26 percent. The RMS relative error as a function of month is shown in Figure 41. Relative RMS error for all models for all months was in the range 20 to 28 percent.

The magnitude of the error as a function of season is shown in Figure 36. For MINIMUF-3.5 the results are within a few percent of values from the 25-path database, slightly lower in summer and a little higher in the fall. Results for MINIMUF 85 and HFBC84 are very close to MINIMUF-3.5. The magnitude of the error was in the range of 19 to 24 percent.

Correlation coefficients as a function of season are shown in Figure 37 and as a function of month in Figure 43. The graphs show the models to correlate better in winter than in summer, with HFBC84 model correlating better in the autumn than the MINIMUF models. When compared to the results from analysis of the 25-path database, the overall trend of the correlation as a function of month remains the same.

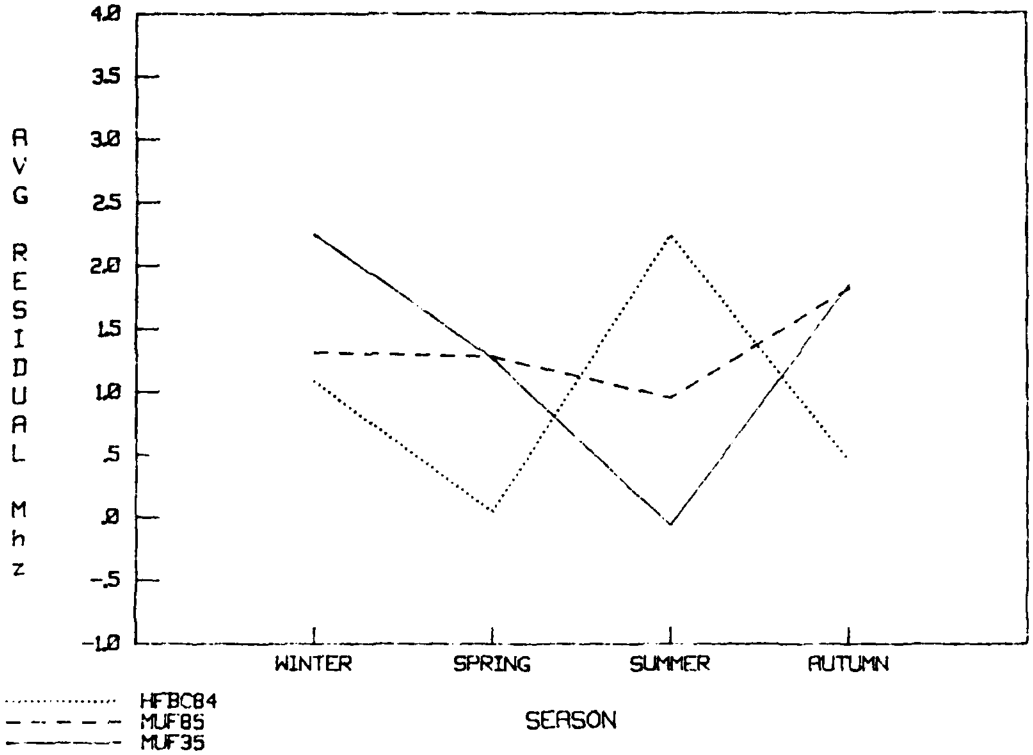

Figure 32. Average residual (bias) as a function of season.

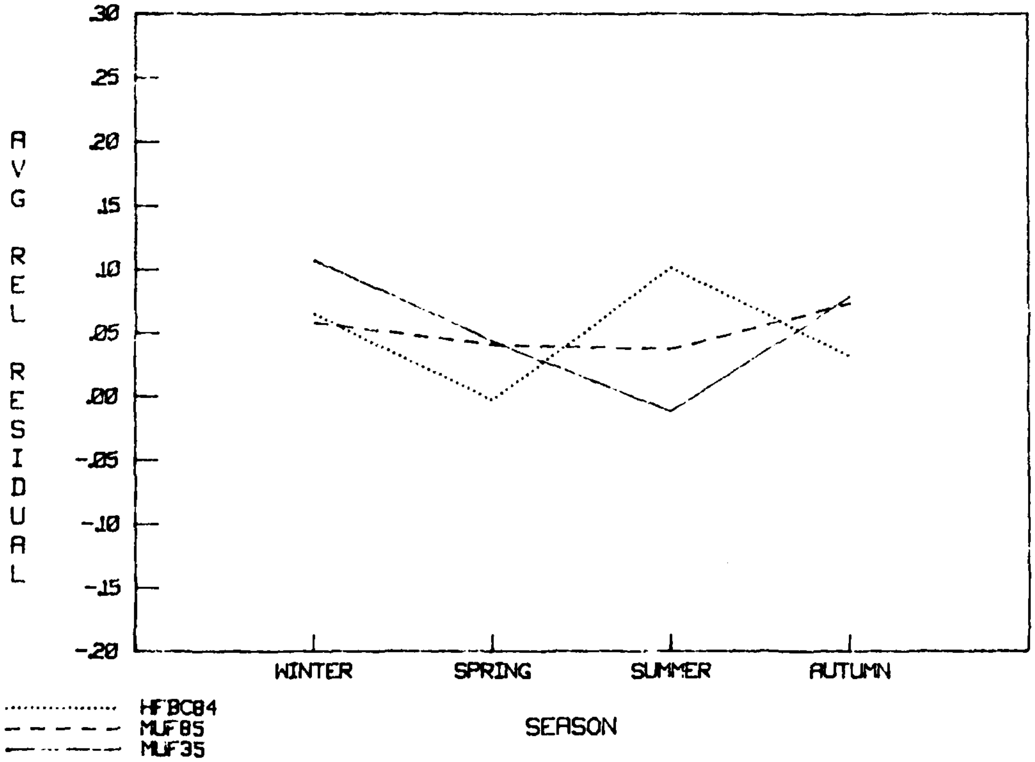

Figure 33. Average relative residual (relative bias) as a function of season.

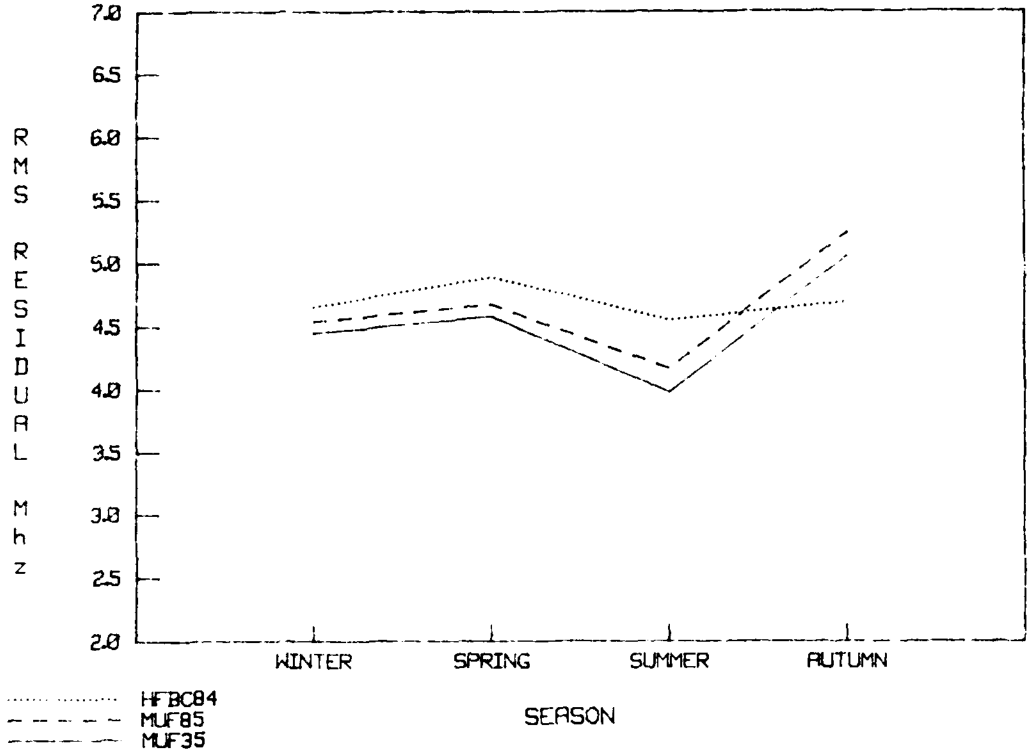

Figure 34. RMS error in MHz as a function of season.

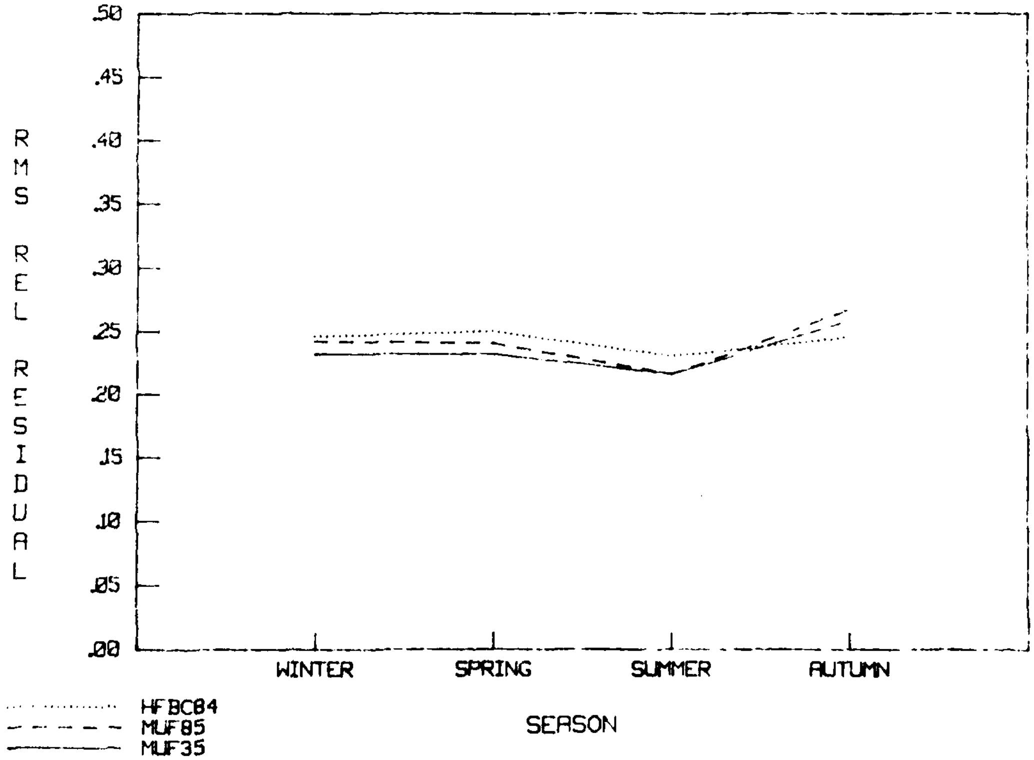

Figure 35. Relative RMS error as a function of season.

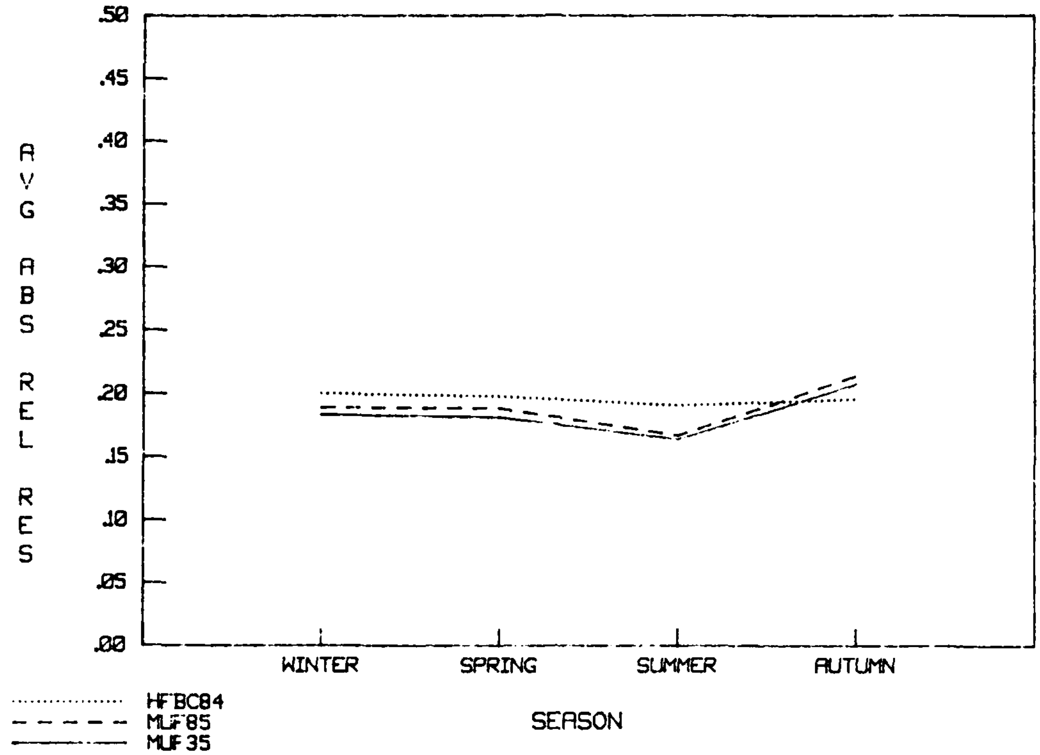

Figure 36. Magnitude of the error (average absolute relative residual) as a function of season.

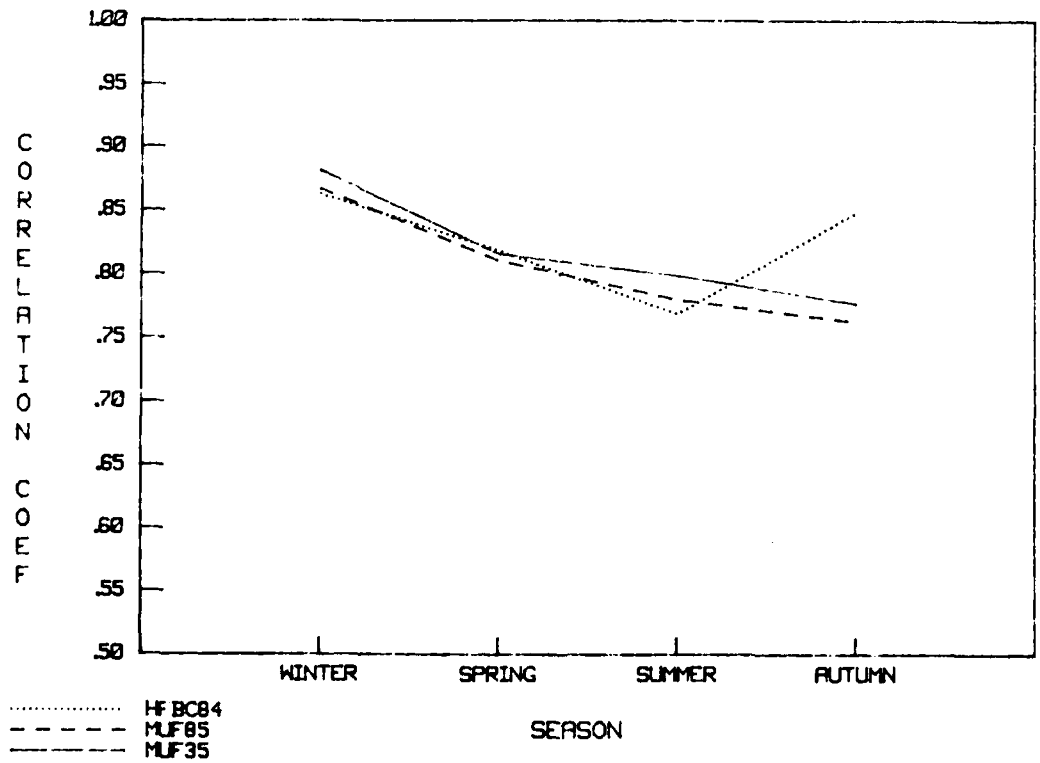

Figure 37. Correlation coefficients as a function of season.

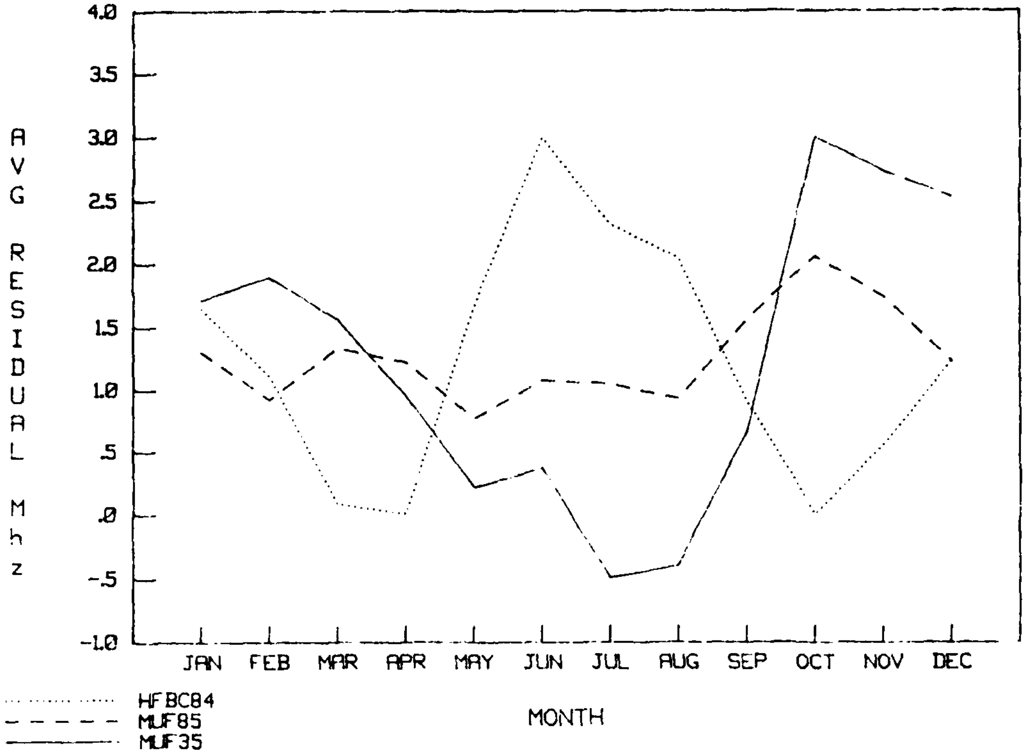

Figure 38 Average residual (bias) as a function of month.

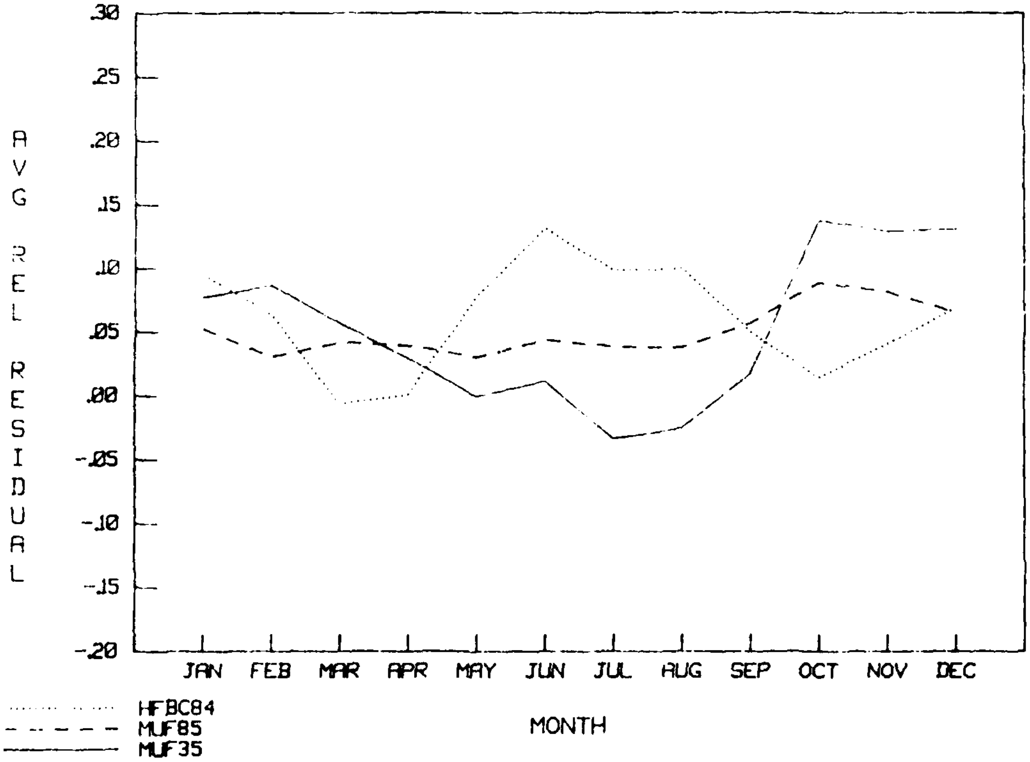

Figure 39 Average relative residual (relative bias) as a function of month.

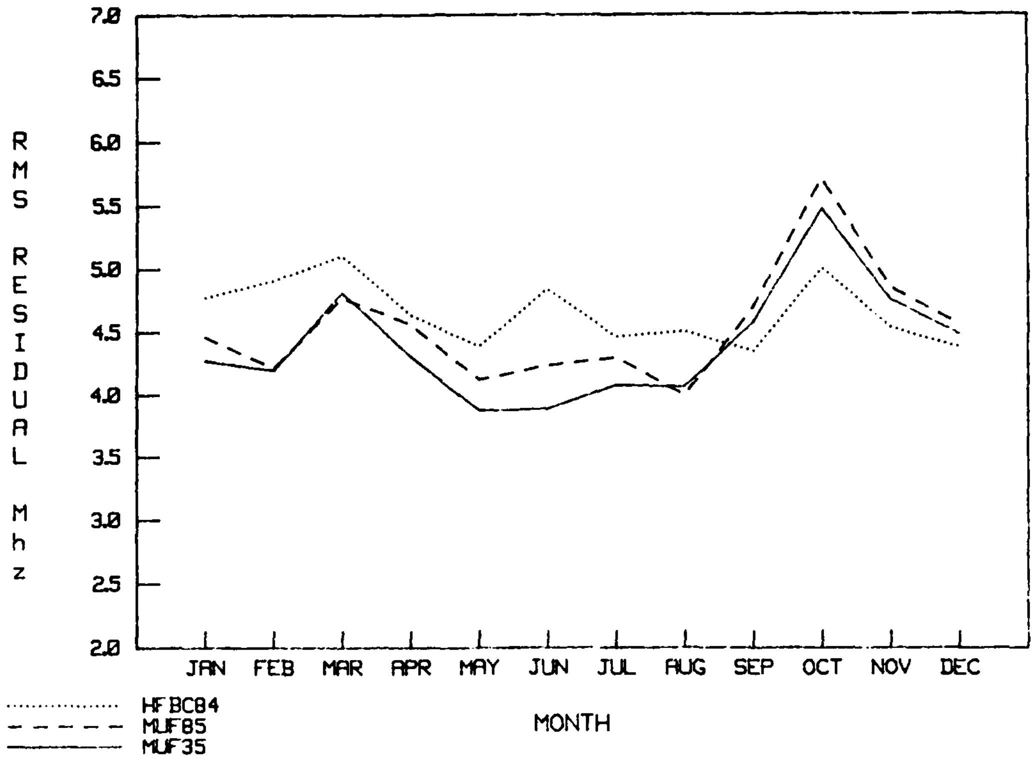

Figure 40. RMS error in MHz as a function of month.

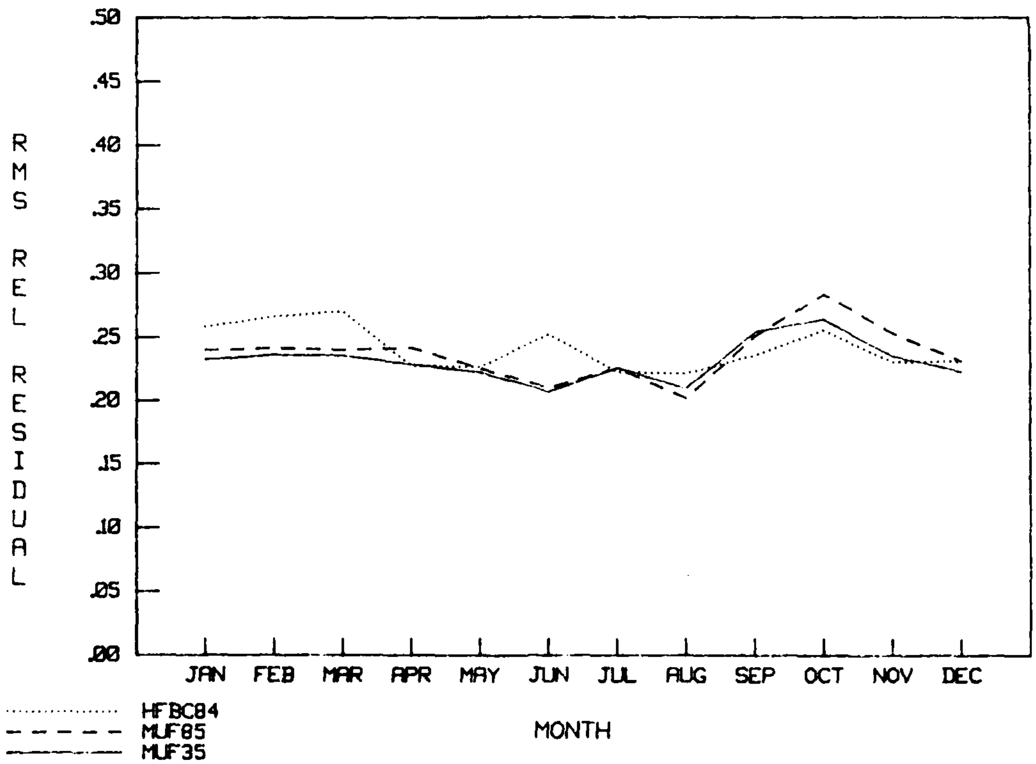

Figure 41. Relative RMS error as a function of month.

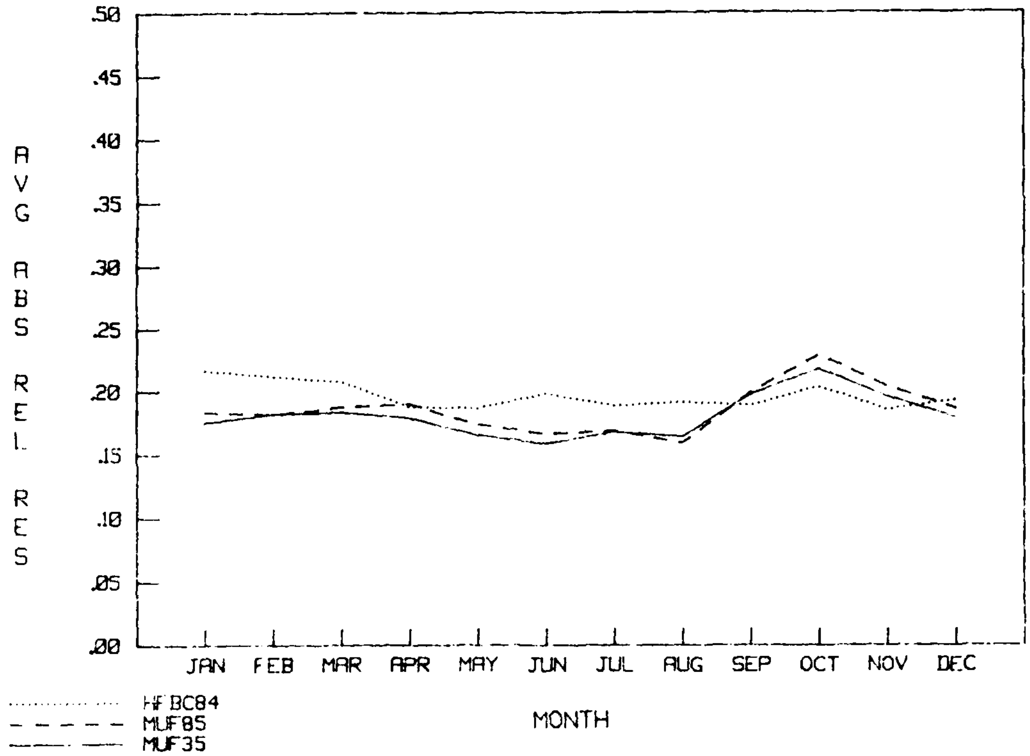

Figure 42. Magnitude of the error (average absolute relative residual) as a function of month.

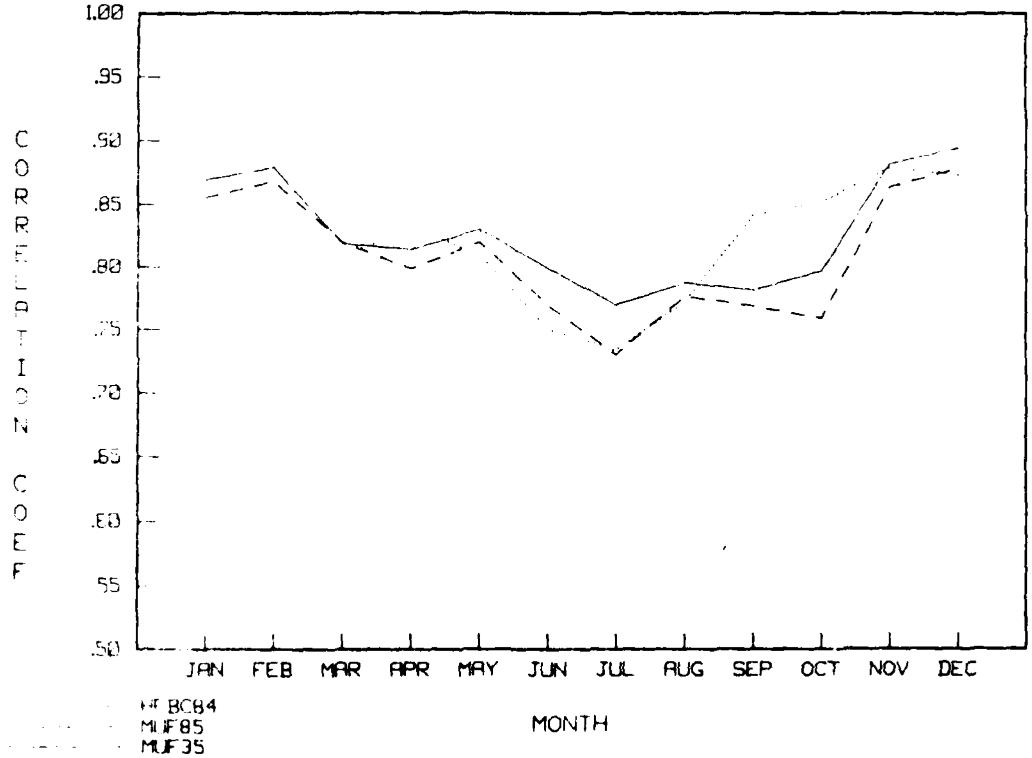

Figure 43. Correlation coefficients as a function of month.

6.5 GEOMAGNETIC LATITUDE

The next tests were made to determine error as a function of geomagnetic latitude. The five categories denote transequatorial (TE) propagation, low-latitude (LO) propagation, midlatitude (M) propagation, high-latitude (H) propagation, and transauroral (TA) propagation. These general areas have entirely different propagation characteristics and problems. Each path was categorized according to the geomagnetic latitude location of control points. The type determined for each path in the MOF database is given in Table 16.

Figures 44-49 illustrate the performance of MINIMUF as a function of geomagnetic latitude. Figures 44 and 45 show the average residual and average relative residual, respectively. The MINIMUF models had the lowest bias for transequatorial, low-latitude, and midlatitude paths, whereas their bias was highest for high-latitude paths. For transauroral paths MINIMUF 85 had the lowest bias. For low latitudes HFBC84 predicted high by about 1.7 MHz. When compared to the 25-path analysis, high-latitude bias has increased while transauroral bias has decreased. Figure 44 also shows the low-latitude and transauroral bias of the HFBC84 model to be much larger than the MINIMUF models.

Figures 46 and 47 show the RMS error and the relative RMS error, respectively, as a function of geomagnetic latitude of the control points. The MINIMUF models had the lowest RMS error for the transequatorial, low-latitude, and midlatitude paths. For transauroral paths MINIMUF 85 had lower RMS error than MINIMUF-3.5. HFBC84 had its lowest RMS error for transauroral paths.

Figure 48 shows the average magnitude of the error for the MINIMUF models to increase at high latitude and to have values less than 25 percent at all geomagnetic regions. Figure 49 shows the correlation coefficients. When compared to the 25-path analysis, the additional data at transauroral latitudes have dropped the correlation significantly. However, the previous result was based on analysis of only 1 percent of the database, while the present analysis is based on 7 percent.

6.6 SUNSPOT NUMBER

A major consideration in MUF prediction is the ability of a model to deal with different phases of the sunspot cycle. Ideally, it should produce consistent results for SSN values between 1 and 160. Model uncertainty was evaluated for both monthly median SSN (unsmoothed) and yearly running means (smoothed).

Figures 50 and 51 show the average residual (bias) and average relative residual as a function of monthly median SSN. The MINIMUF models have lower bias than the HFBC84 model at low SSN and slightly higher bias at higher SSN (greater than 100).

Figures 52 and 53 show the RMS error and relative RMS error, respectively. Note the gradual increase in RMS error with increasing monthly median SSN.

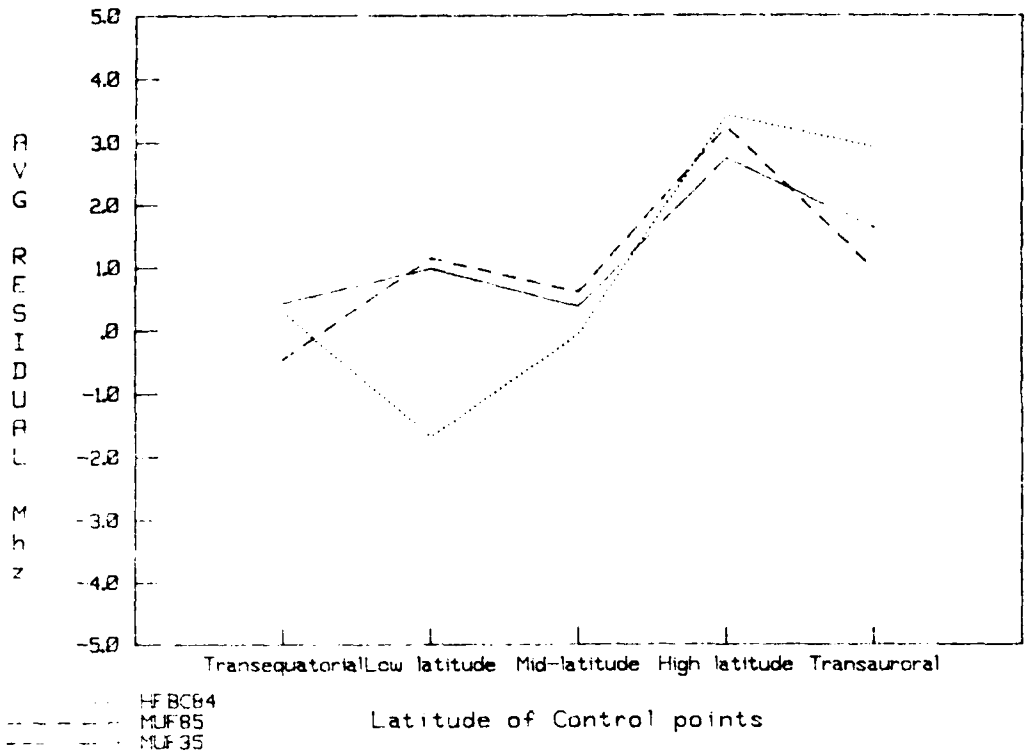

Figure 44 Average residual (bias) as a function of geomagnetic latitude of control points.

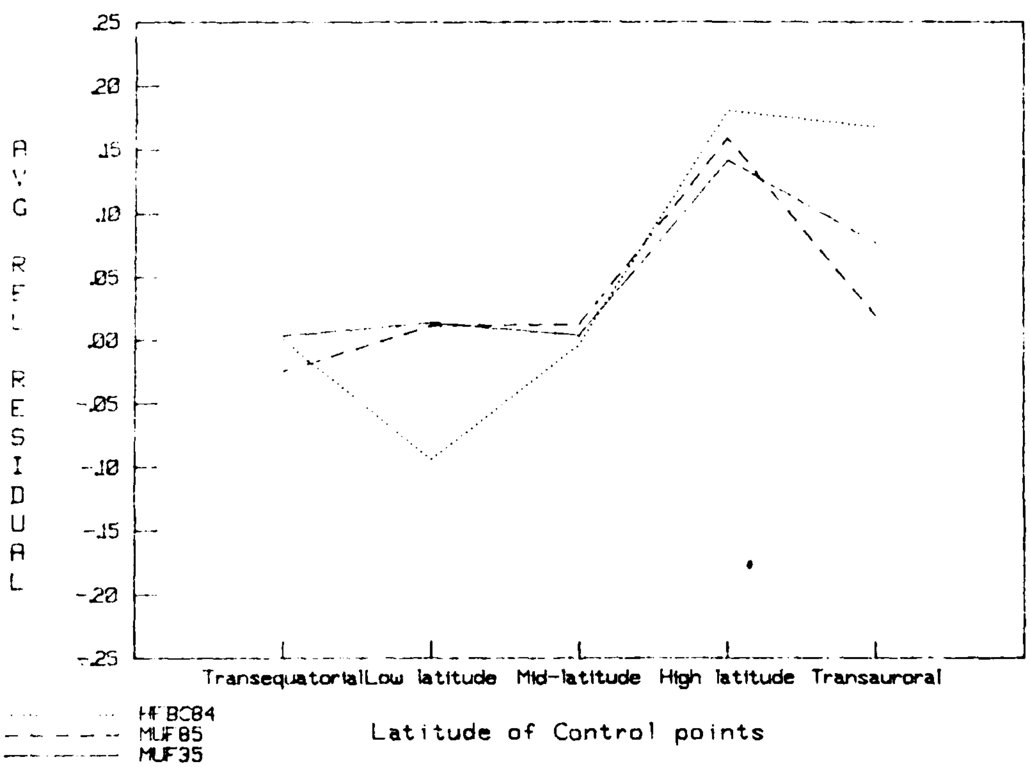

Figure 45 Average relative residual (relative bias) as a function of geomagnetic location of control points

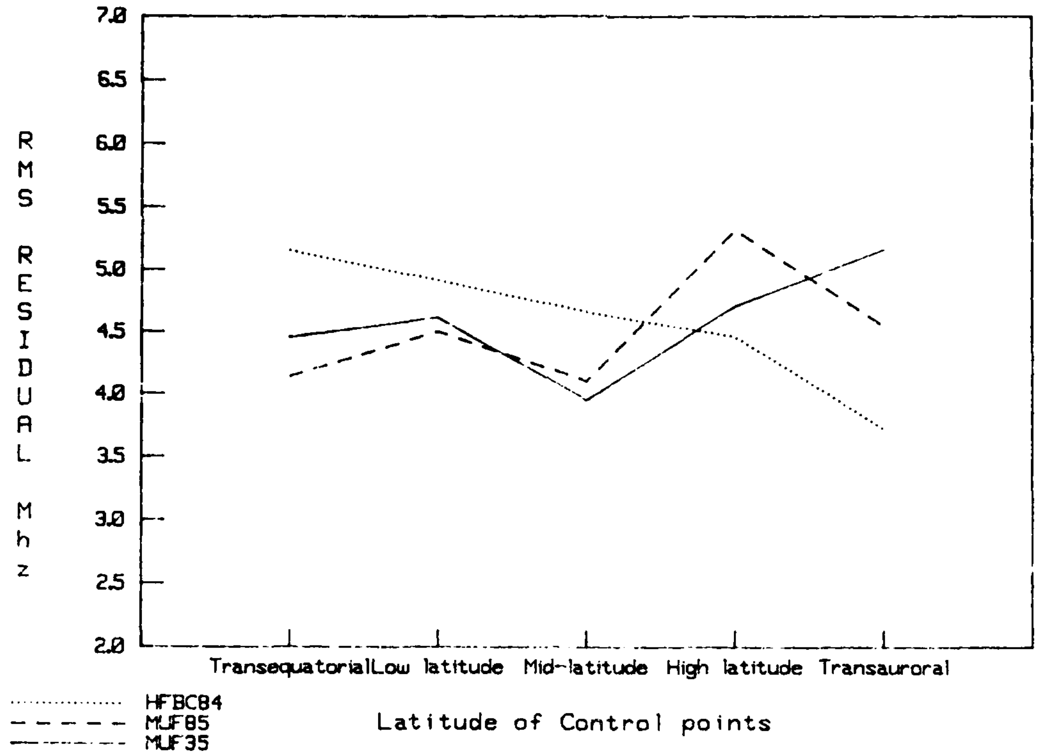

Figure 46. RMS error in MHz as function of geomagnetic latitude of control points.

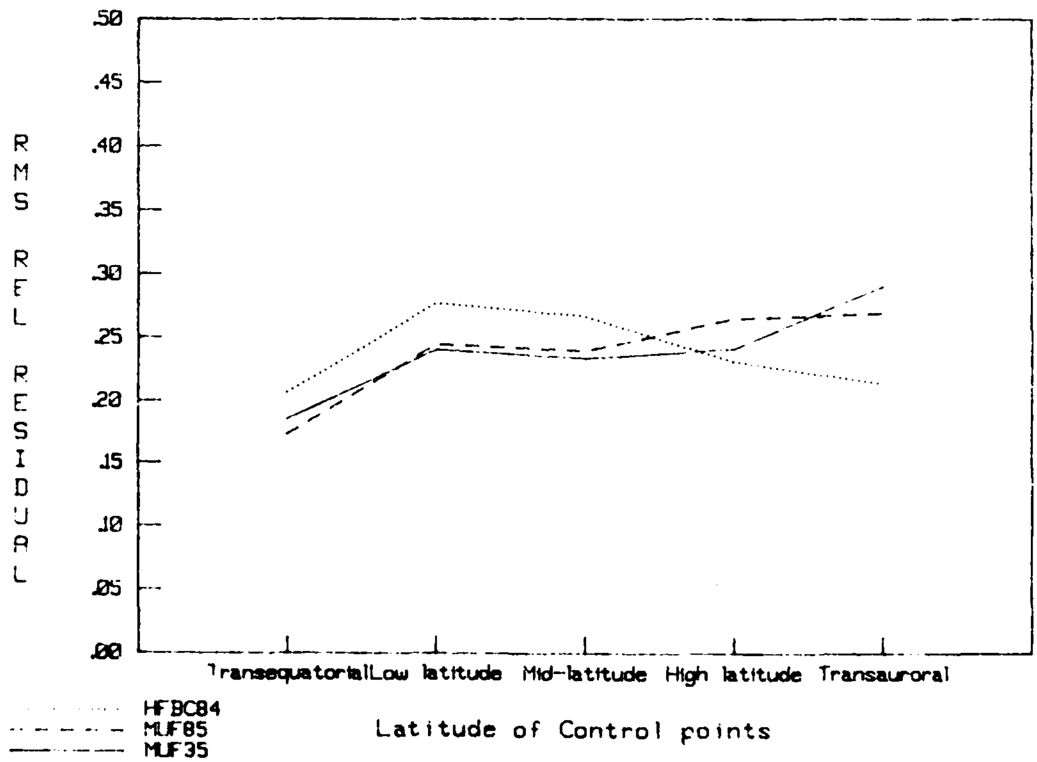

Figure 47 Relative RMS error as a function of geomagnetic latitude location of control points.

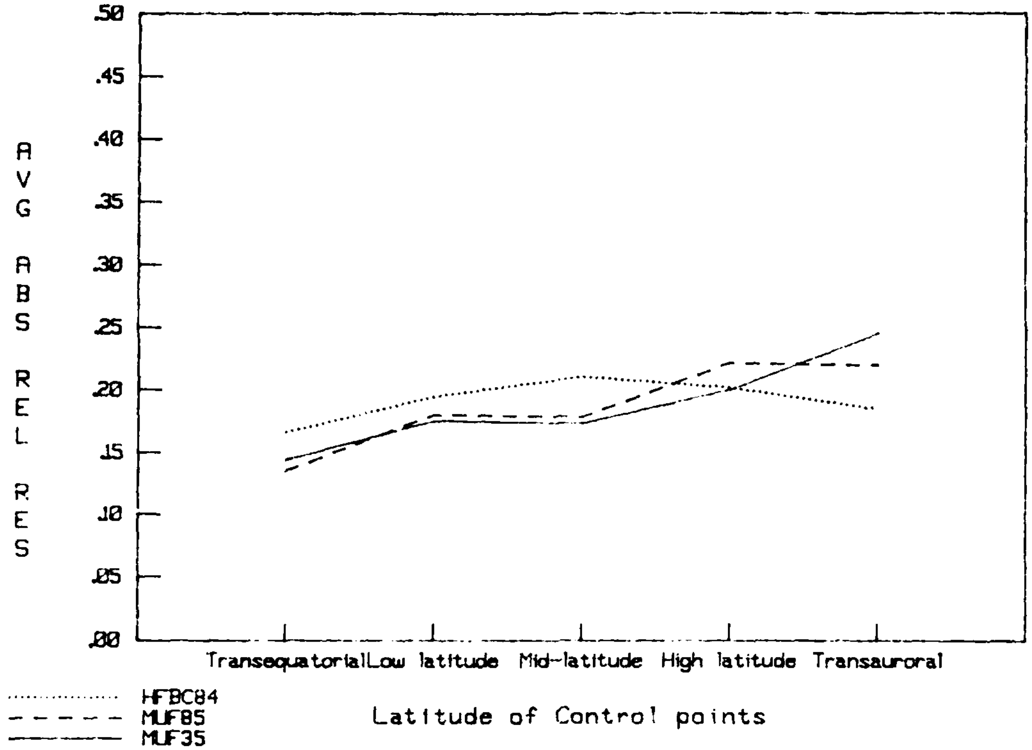

Figure 48 Magnitude of the error (average absolute relative residual) as a function of geomagnetic latitude location of control points.

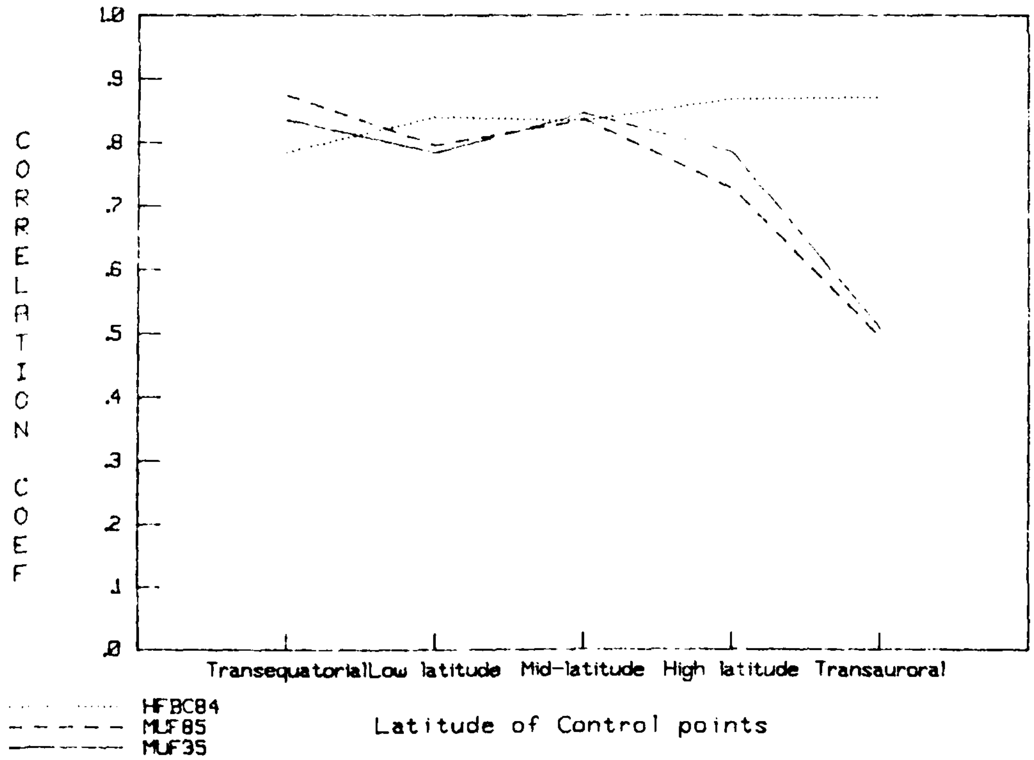

Figure 49 Correlation coefficients as a function of geomagnetic latitude location of control points.

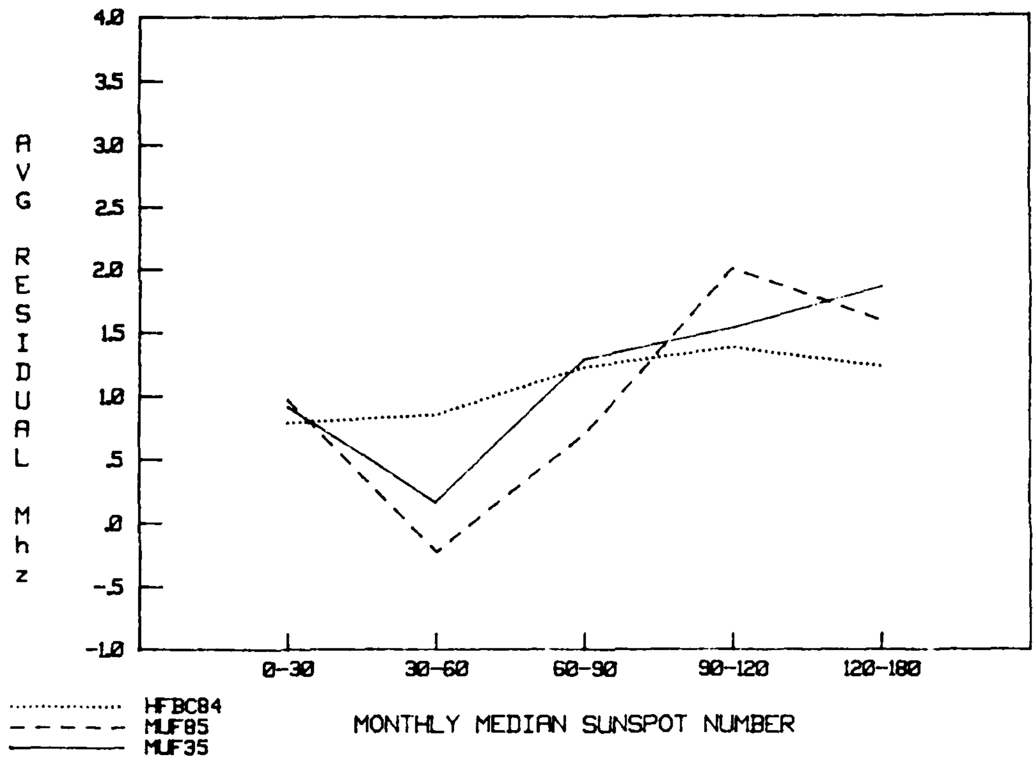

Figure 50. Average residual (bias) as a function of monthly median SSN.

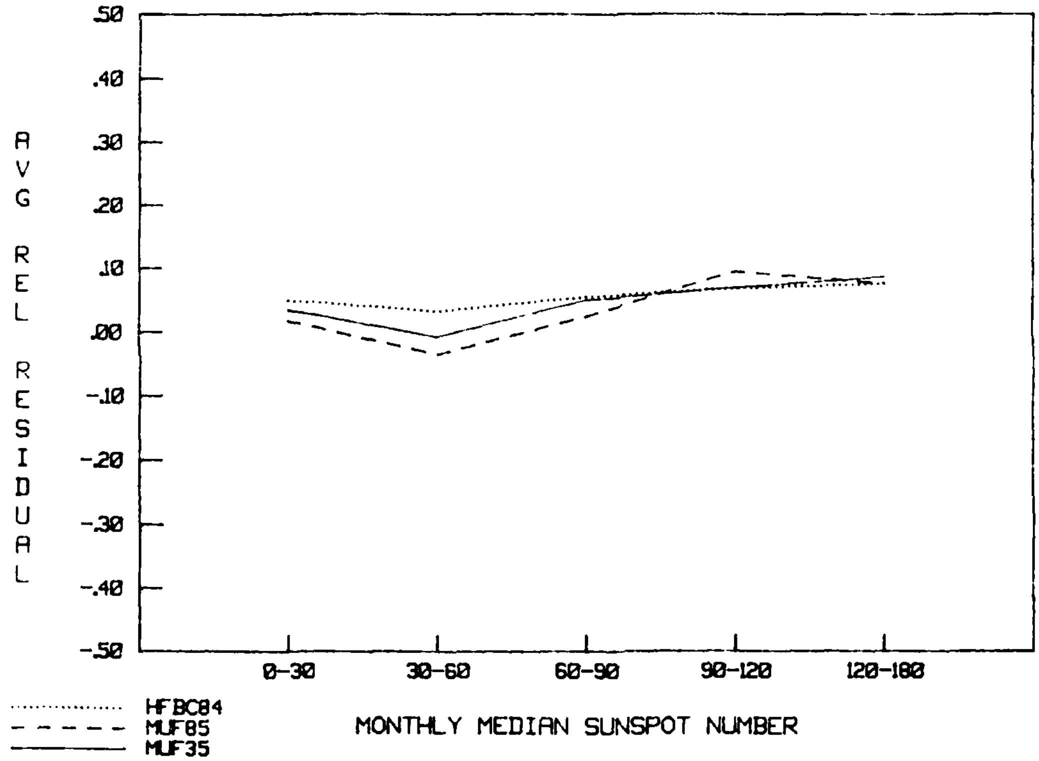

Figure 51. Average relative residual (relative bias) as a function of monthly median SSN.

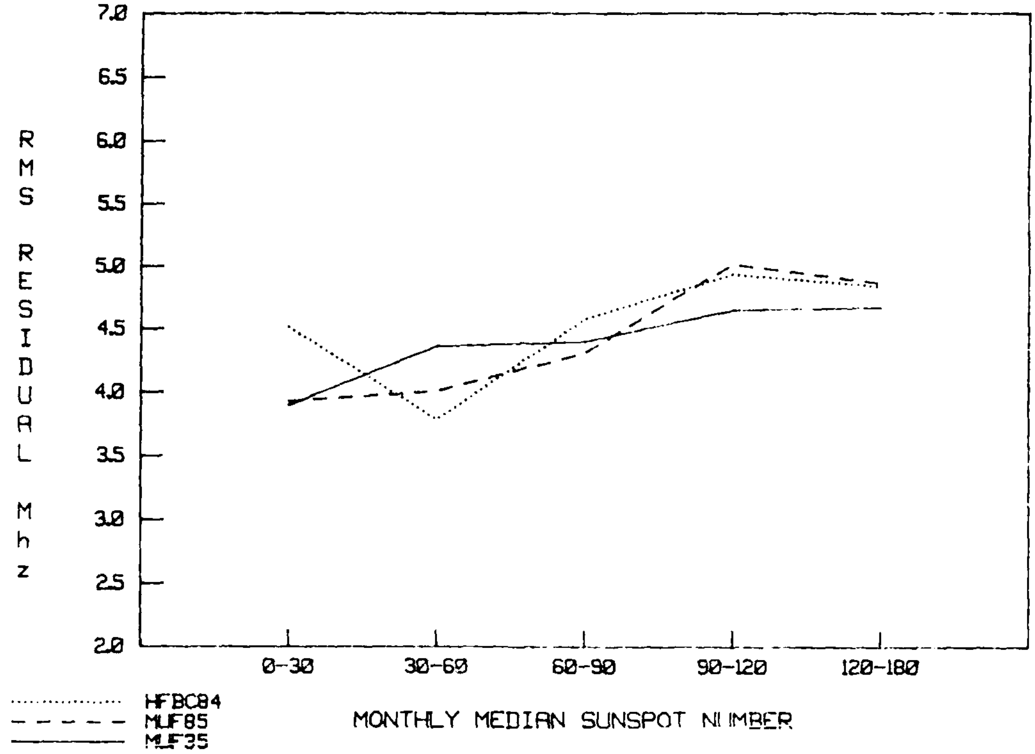

Figure 52. RMS error in MHz as a function of monthly median SSN.

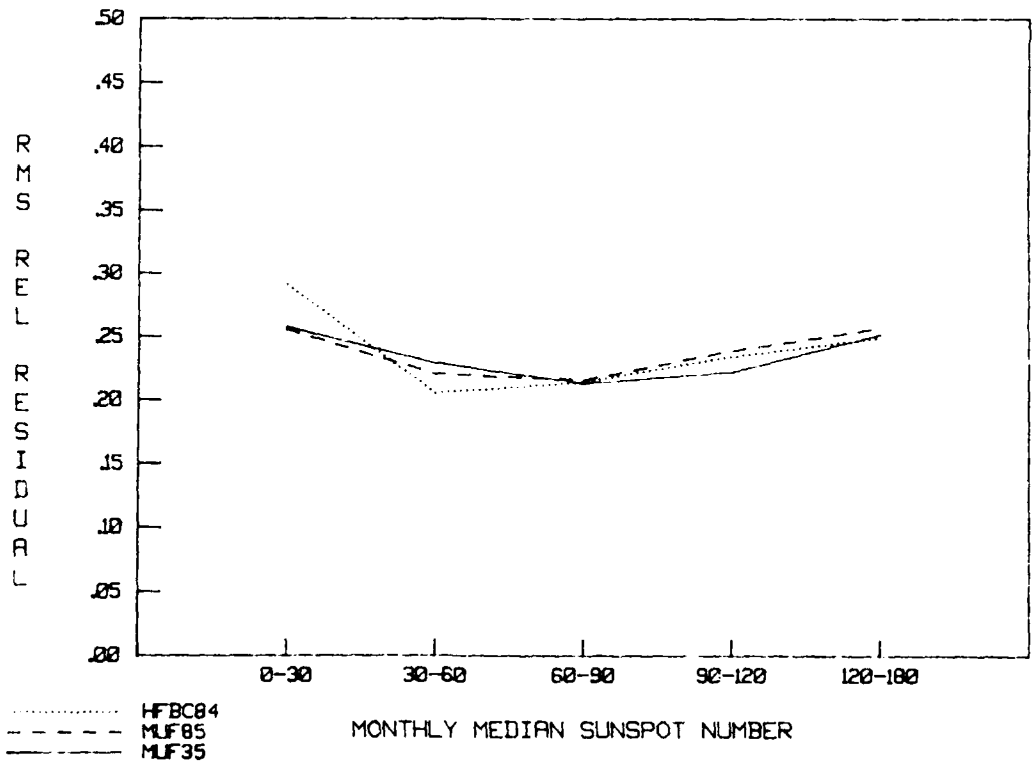

Figure 53. Relative RMS error as a function of monthly median SSN.

Figures 54 and 55 show the magnitude of the error and correlation coefficient, respectively. When compared to the 25-path analysis, correlation is unchanged except for a slight decrease at low SSN.

Figures 56 to 61 show similar analysis for yearly running mean SSNs. These SSNs, calculated using an averaging method other than monthly medians, were analyzed to determine if they provided less bias and better correlation.

Figures 56 and 57 show the average residual and average relative residual, respectively. When these figures are compared to figures 50 and 51, an increase in bias can be seen at high SSN.

Figures 58 and 59 show the RMS error and relative RMS error, respectively. When compared to the monthly median values in Figures 52 and 53, the MINIMUF results are basically unchanged, while a large decrease in RMS error is seen for the HFBC84 model at high SSN.

Figures 60 and 61 show the magnitude of the error and correlation coefficients, respectively. A comparison to the monthly median values in Figures 54 and 55 shows little change in the magnitude of the error and a decrease in MINIMUF correlation and an increase in HFBC84 correlation at high SSN.

6.7 DIURNAL TRENDS

One of the most important variations in path MOF is its diurnal variation. This section describes the accuracy of the model as a function of time of day. To do this, the entire data set was converted to local path time (i.e., the local time at the path midpoint).

Figures 62 and 63 show the average residual and the average relative residual, respectively. The bias of all three models has a strong diurnal variation. All models predict low, with the MINIMUF models having minimum error at 1200 midpath local time, while the HFBC84 model reaches a minimum 6 hours later at 1800. Maximum error is offset 12 hours from the minimum for all three models. When compared to the 25-path analysis MINIMUF minimum bias occurred 7 hours later at 1900.

Figures 64 and 65 show the RMS error and relative RMS error, respectively. The MINIMUF models have lower RMS error from 0700 to 1800 midpath local time, while the HFBC84 model has lower RMS error from 1800 to 0700.

Figure 66 shows average magnitude of the error, and Figure 67 shows the correlation coefficients for the three MUF models. The MINIMUF models are again shown to be better daytime models than the HFBC84 model in Figure 66. In Figure 67 the correlation of the MINIMUF models is shown to decrease rapidly during the morning transition period, while the HFBC84 model experiences little variation.

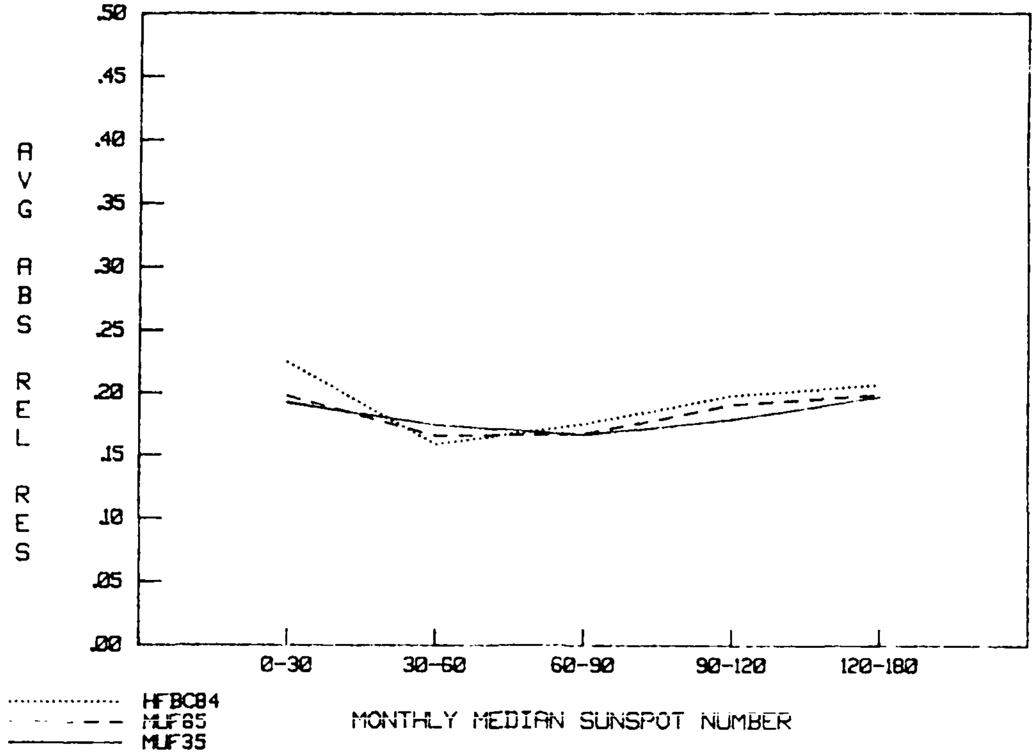

Figure 54. Magnitude of the error (average absolute relative residual) as a function of monthly median SSN.

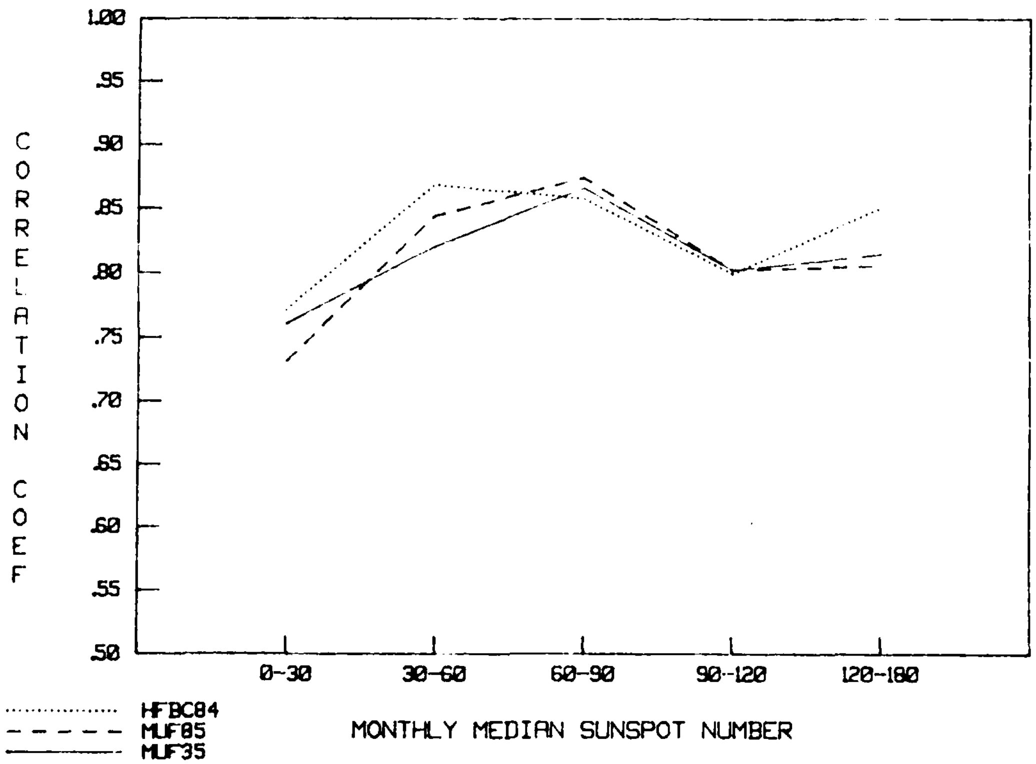

Figure 55. Correlation coefficients as a function of monthly median SSN.

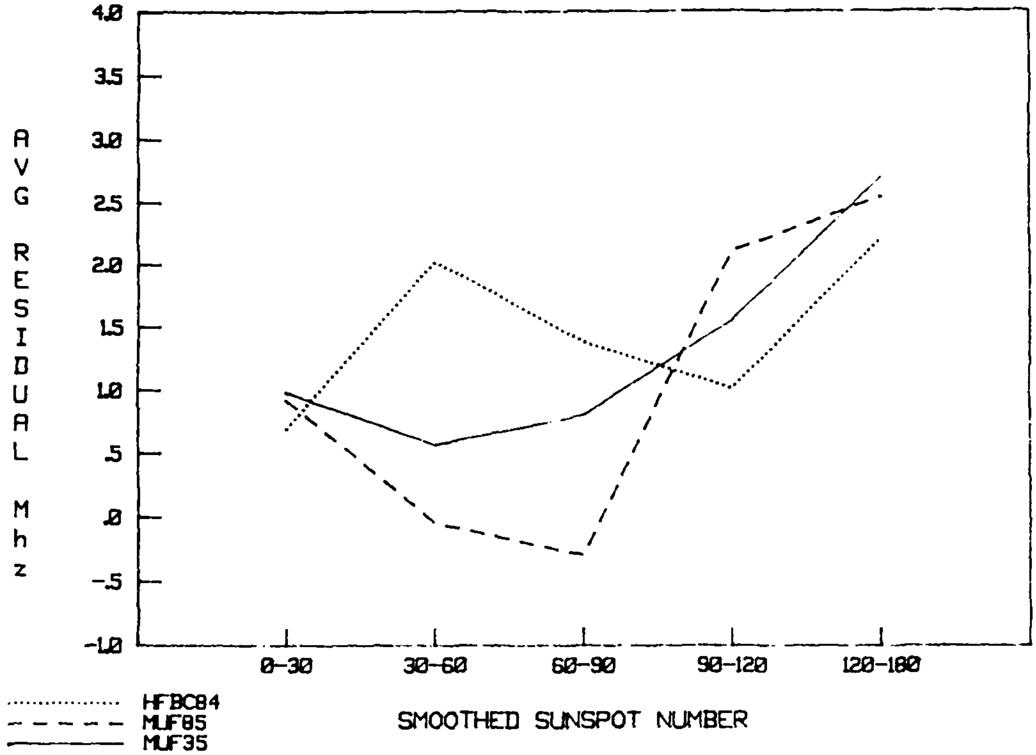

Figure 56. Average residual (bias) as a function of yearly running mean SSN.

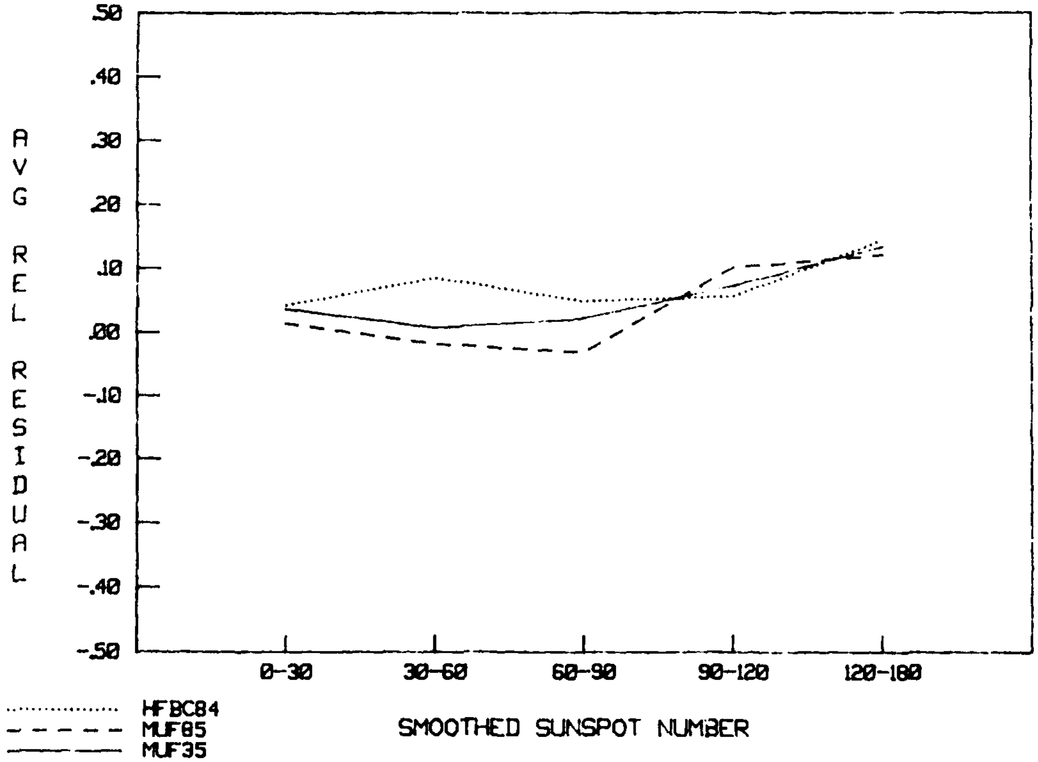

Figure 57. Average relative residual (relative bias) as function of yearly running mean SSN.

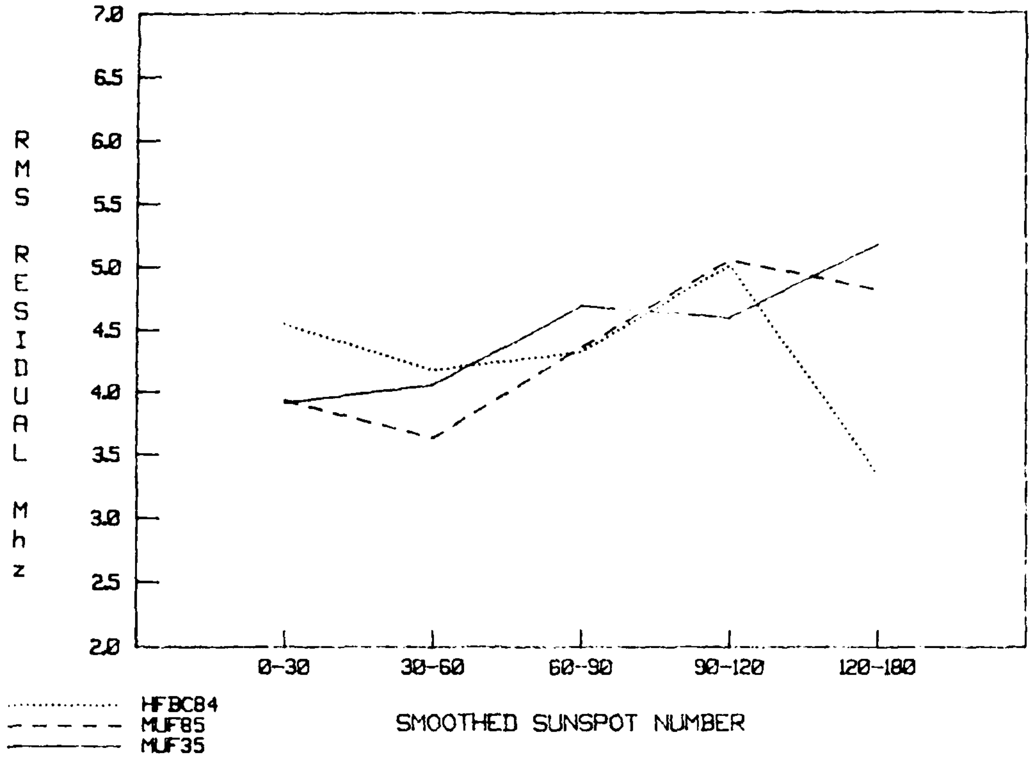

Figure 58. RMS error in MHz as a function of yearly running mean SSN.

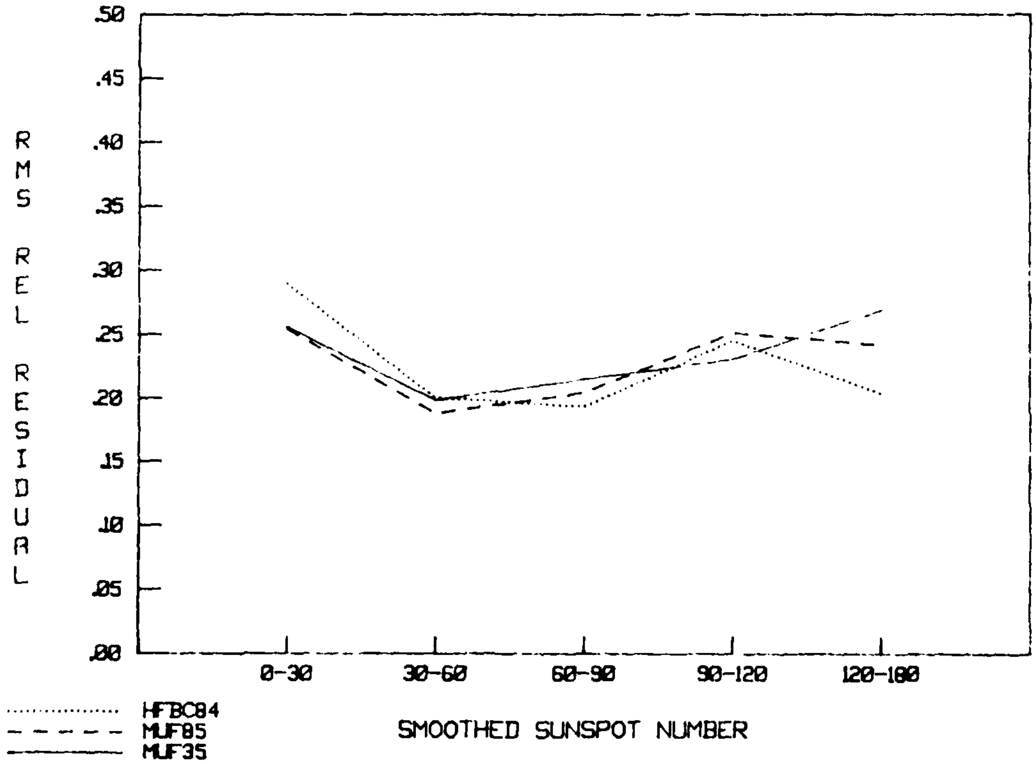

Figure 59. Relative RMS error as a function of yearly running mean SSN.

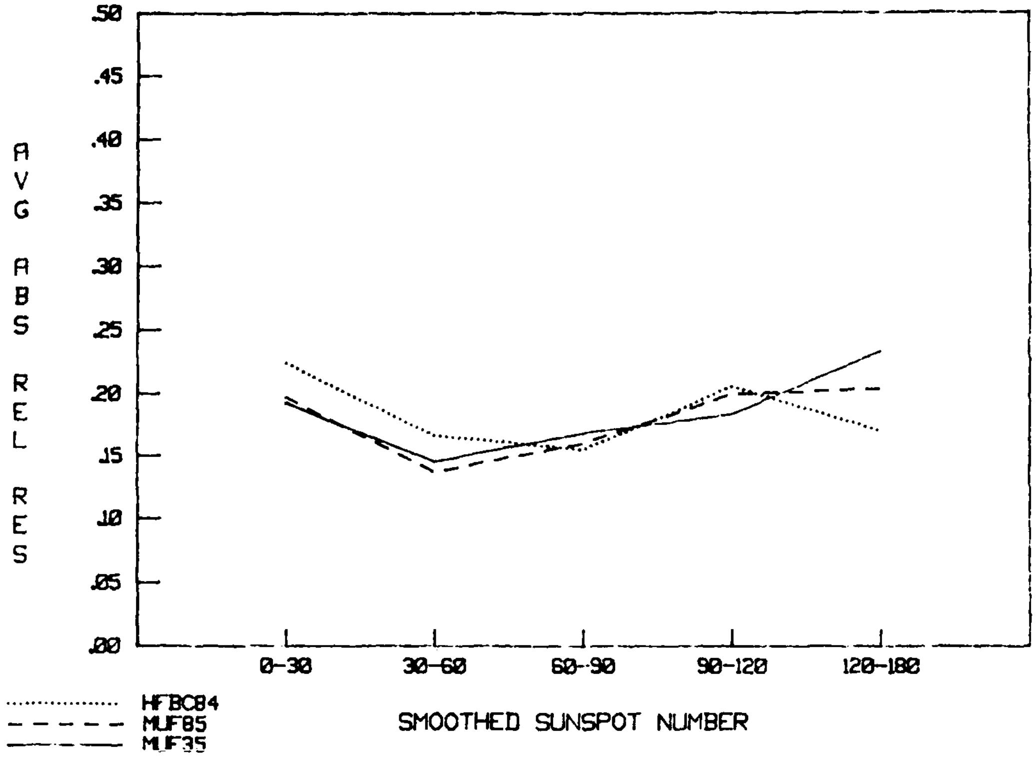

Figure 60. Magnitude of the error (average absolute relative residual) as a function of yearly running mean SSN.

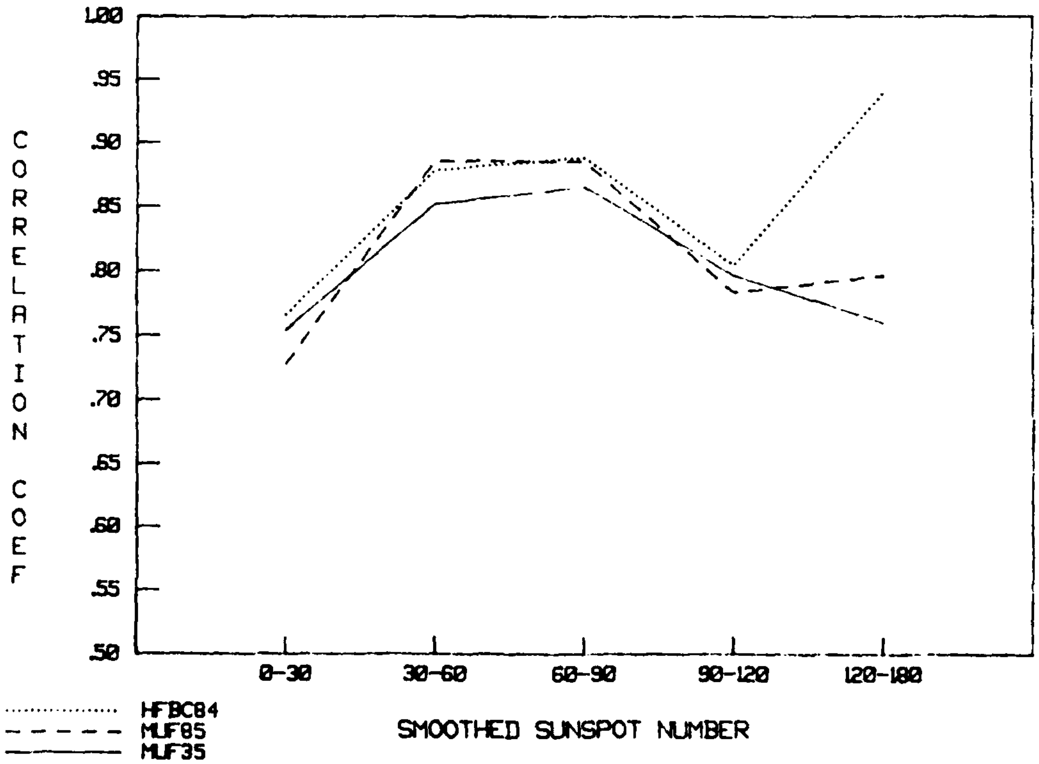

Figure 61. Correlation coefficients as a function of yearly running mean SSN.

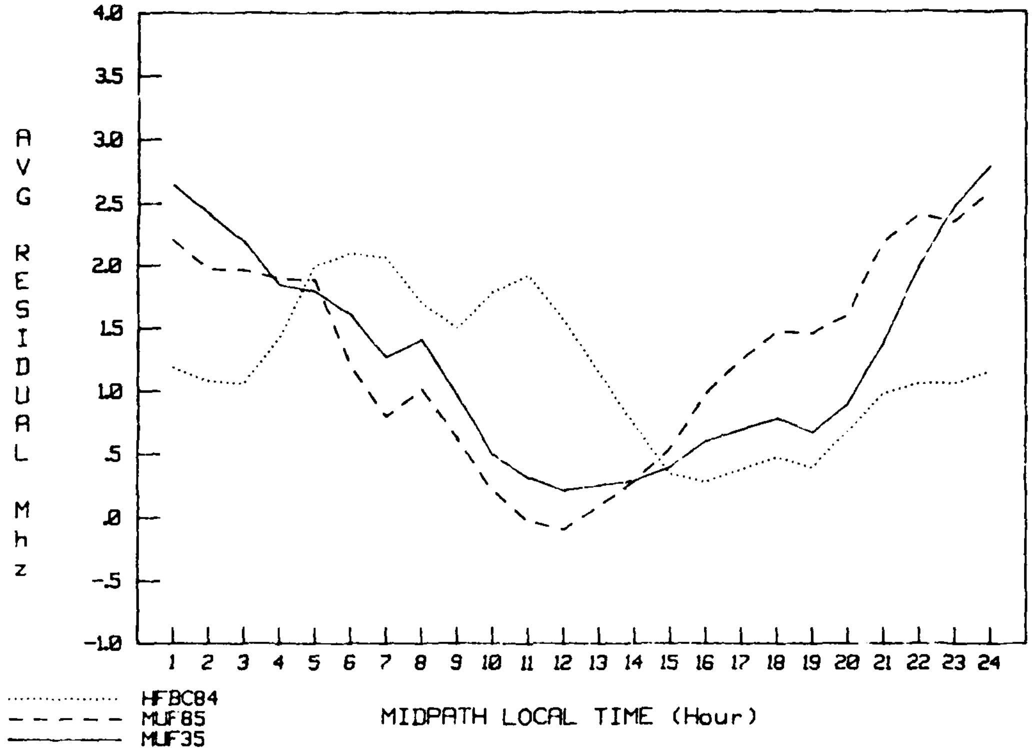

Figure 62. Average residual (bias) as a function of midpath local time.

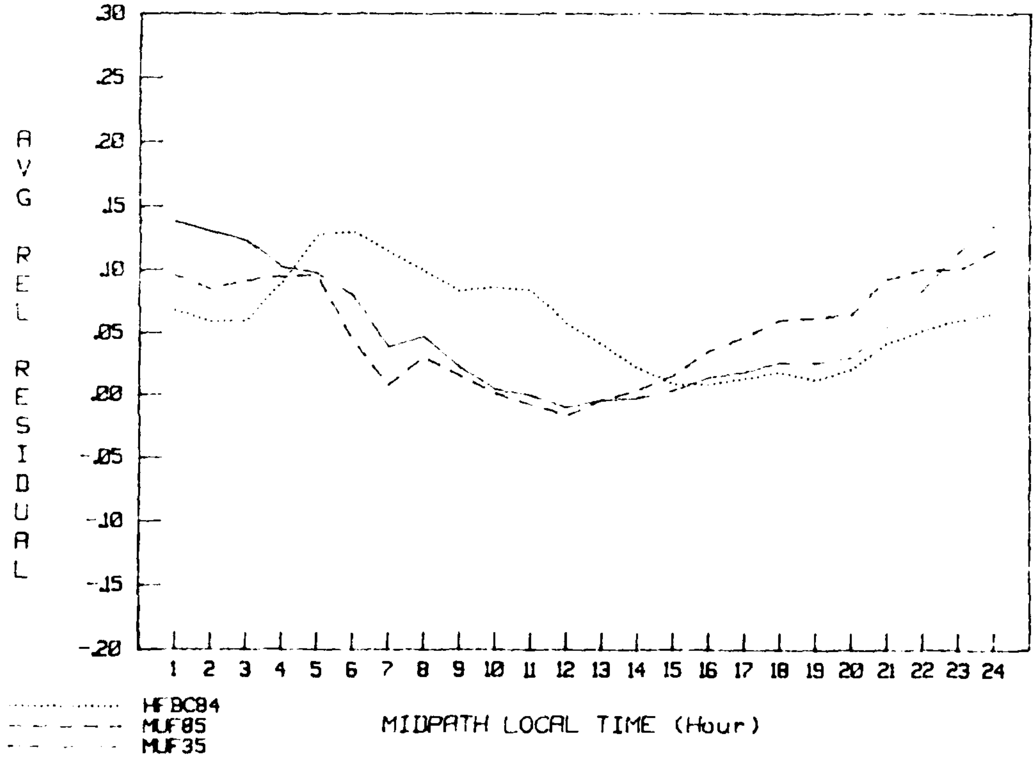

Figure 63. Average relative residual (relative bias) as a function of midpath local time.

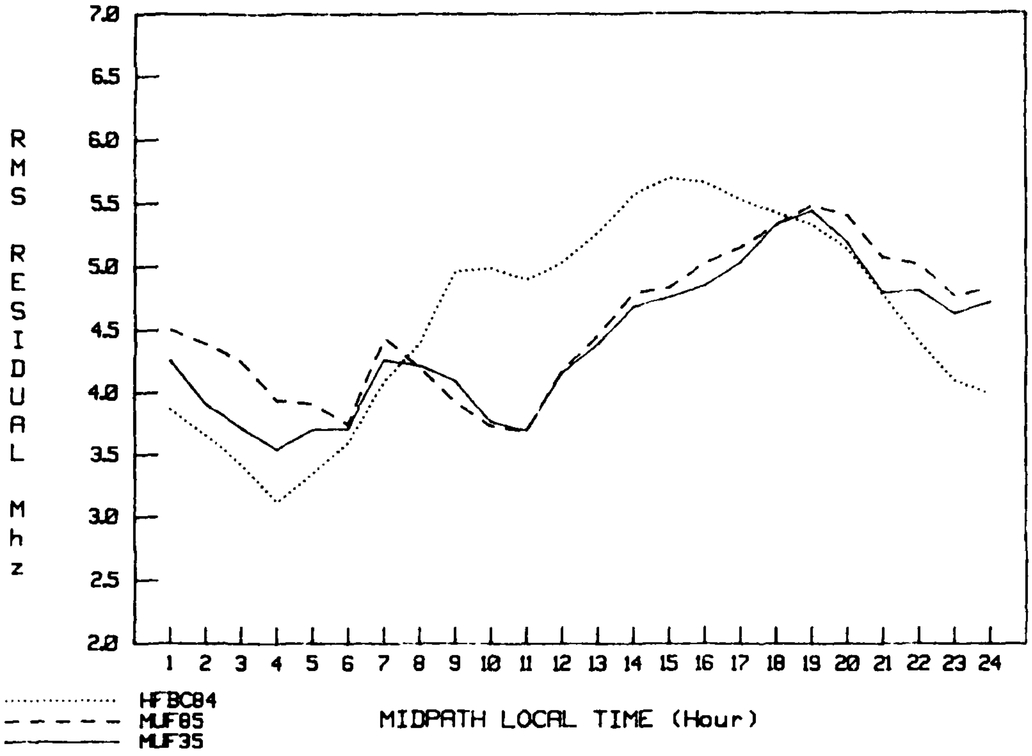

Figure 64. RMS error in MHz as a function of midpath local time.

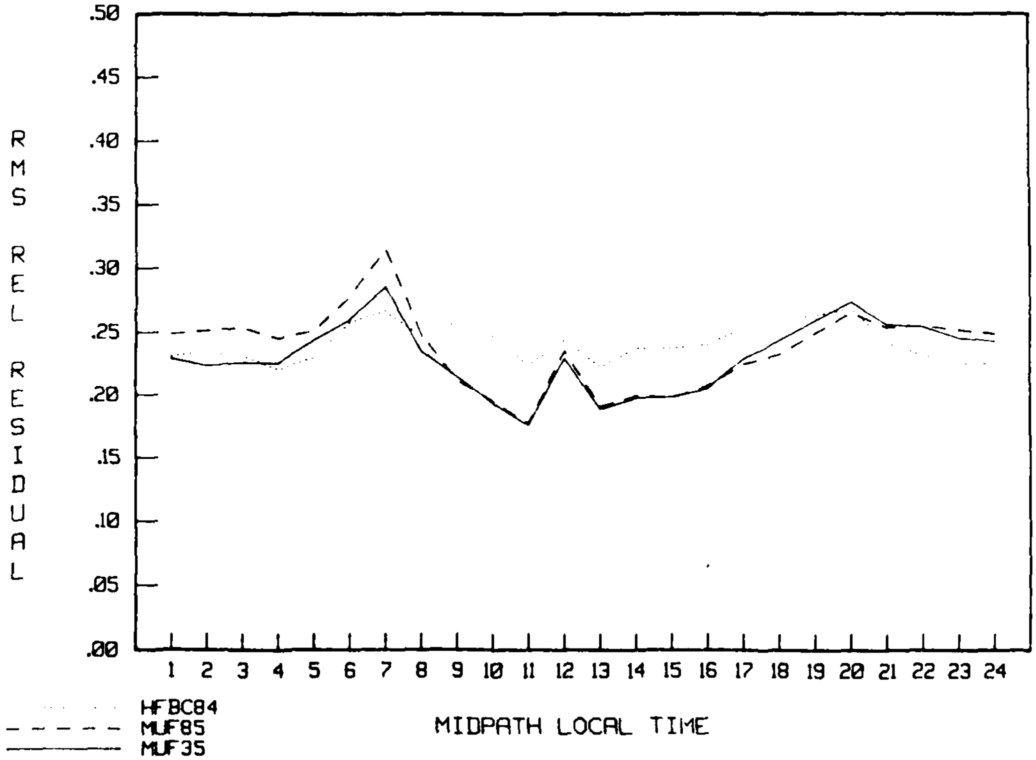

Figure 65. Relative RMS error as a function of midpath local time.

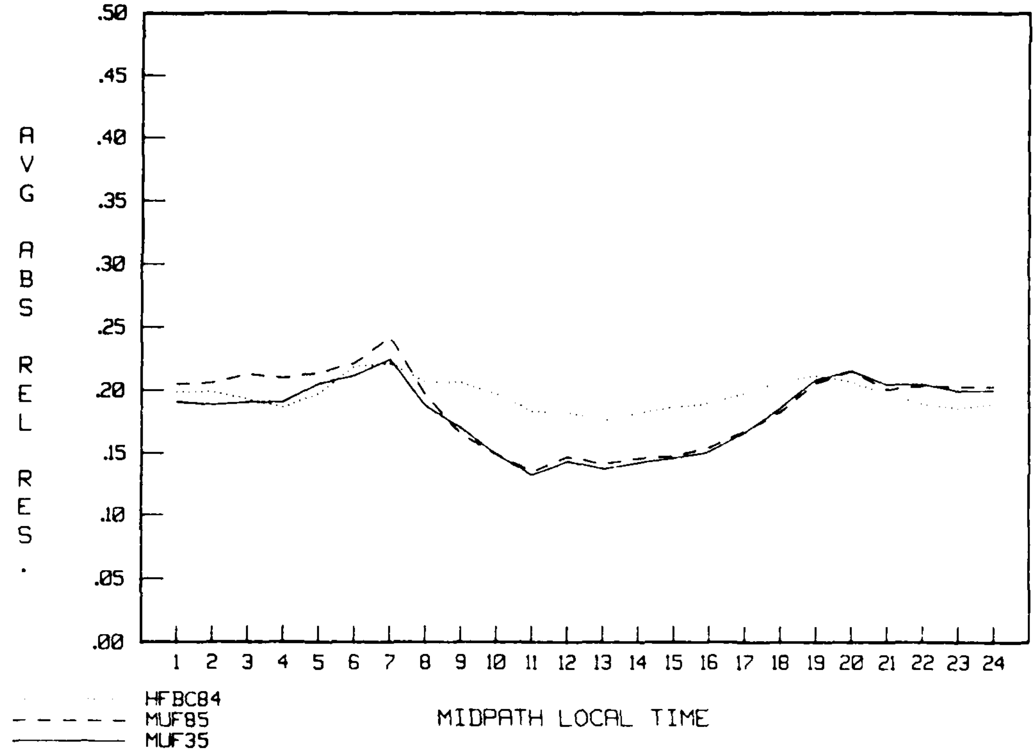

Figure 66. Magnitude of the error (average absolute relative residual) as a function of midpath local time.

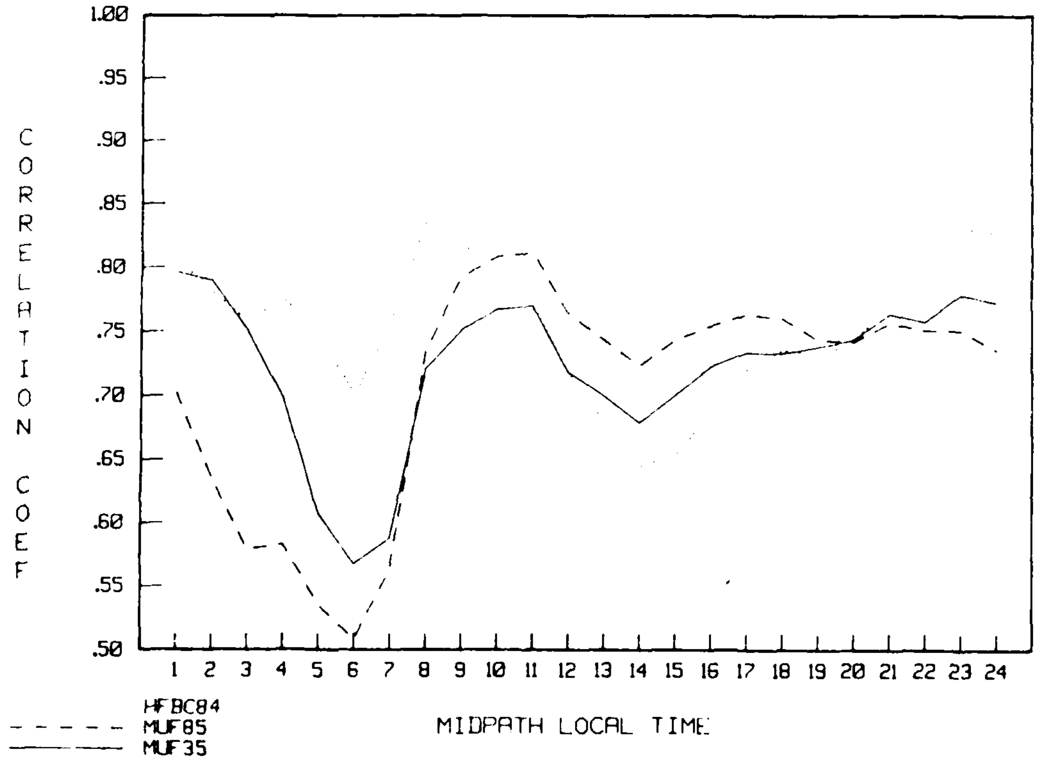

Figure 67. Correlation coefficients as a function of midpath local time.

6.8 GEOGRAPHICAL REGIONS

The last variation to be considered was the effect of different geographical regions on performance of the models. The subdivision chosen was defined as paths that were either entirely over land (continental), entirely over ocean (ocean), or partly over land and partly over ocean (combined). This division was chosen because the oblique sounder data over the ocean areas were used to calibrate MINIMUF-3.5. Table 16 indicates the percentage of the sample in each geographic area.

Figures 68-73 illustrate the performance of the models as a function of geographic region.

Figures 68 and 69 show the average residual and average relative residual, respectively. In the ocean areas MINIMUF models produce the best results, while the HFBC84 model shows a large negative bias. Figures 70 and 71 show the RMS error and relative RMS error, respectively. As expected, MINIMUF models have the lowest relative RMS error over ocean paths, while the HFBC84 model has an RMS error of almost 5.0 MHz. Figures 72 and 73 show the average magnitude of the error of the model and the correlation coefficients, respectively. When compared to the 25-path analysis, a slight decrease in the correlation for continental paths is seen.

6.9 SOUNDER PATH

Tables 12, 13, and 14 list the analysis results for each model for each sounder path in the MOF database. In figures 74 to 79 the results have been plotted to show the relative performance of each of the models. Figures 74 and 75 show the average bias and the relative bias, respectively. In Figure 74 a large bias is shown for paths 38, Monrovia, Liberia, to Rota, Spain, and 40, Tripoli, Lybia, to Accra, Ghana, for both MINIMUF models; however, the HFBC84 model shows a much smaller bias. This indicates the error is model-dependent. This is also shown in Figure 75 for path 18, France to Greece. The MINIMUF models show a relative residual of approximately -35 percent, while the HFBC84 model shows +35 percent relative residual.

Figures 76 and 77 show the RMS error and relative RMS error, respectively. Again paths 38 and 40 show much larger errors for the MINIMUF models than the HFBC84 model. Path 28, Thule, Greenland, to Stockbridge, New York, shows a large bias for all three models.

Figures 78 and 79 show the magnitude of the error and correlation coefficients, respectively. In Figure 79 paths 9, 16, 29, 39, and 54 show poor correlation for the MINIMUF models. Paths 16, Andoya, Norway, to Thessaloniki, Greece, and 29, Andoya, Norway, to Maynard, Massachusetts, show poor correlation for the HFBC84 model. Correlation for the rest of the paths was good, with coefficient values between 0.7 to 0.9.

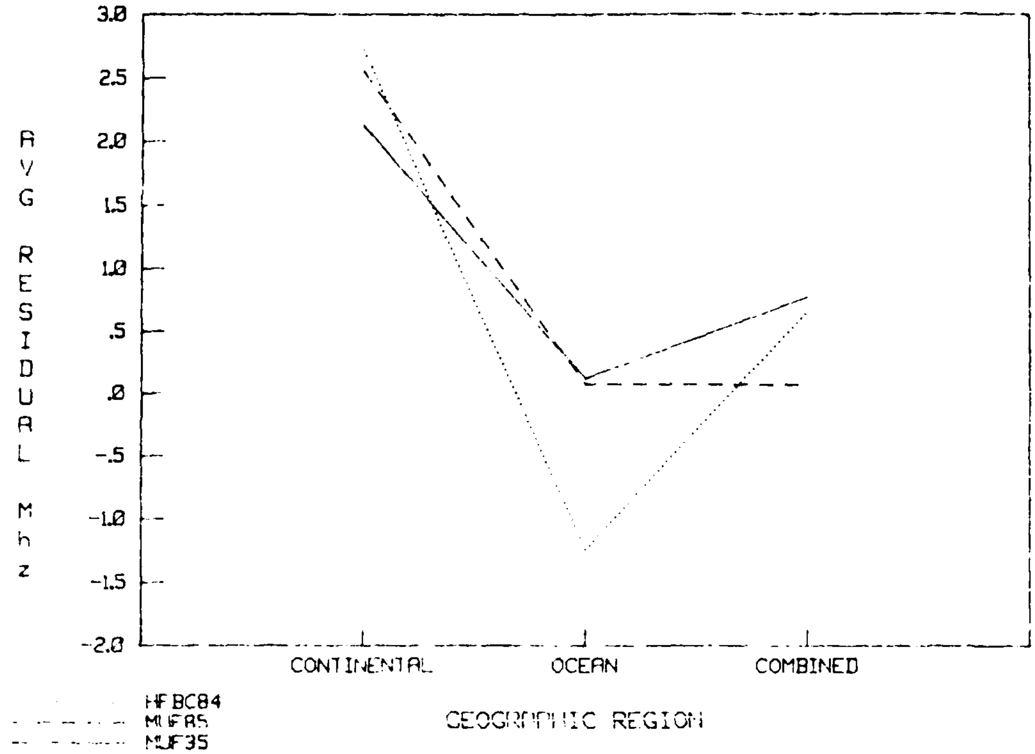

Figure 68 Average residual (bias) as a function of geographic region

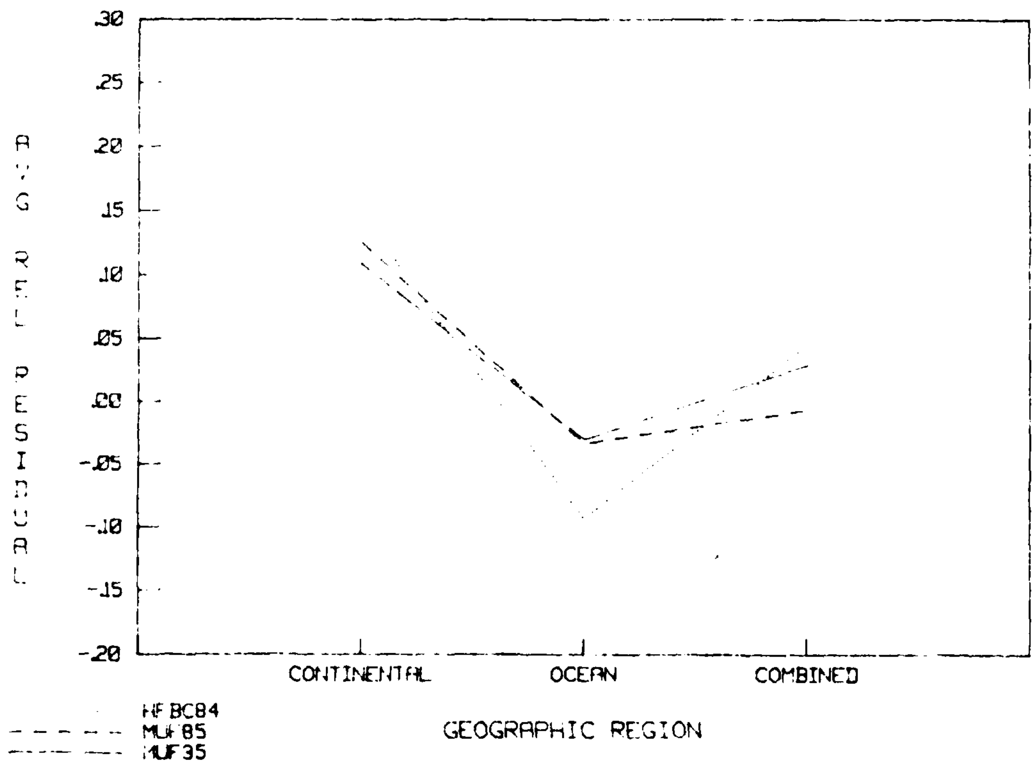

Figure 69 Average relative residual (relative bias) as a function of geographic region

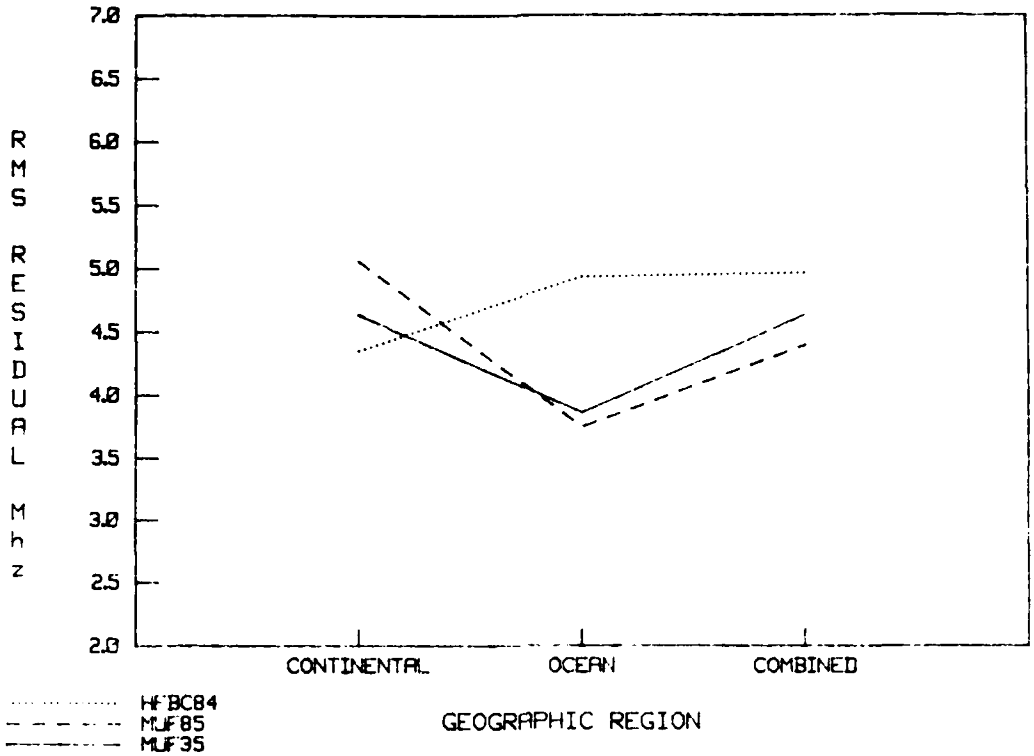

Figure 70 RMS error in MHz as a function of geographic region.

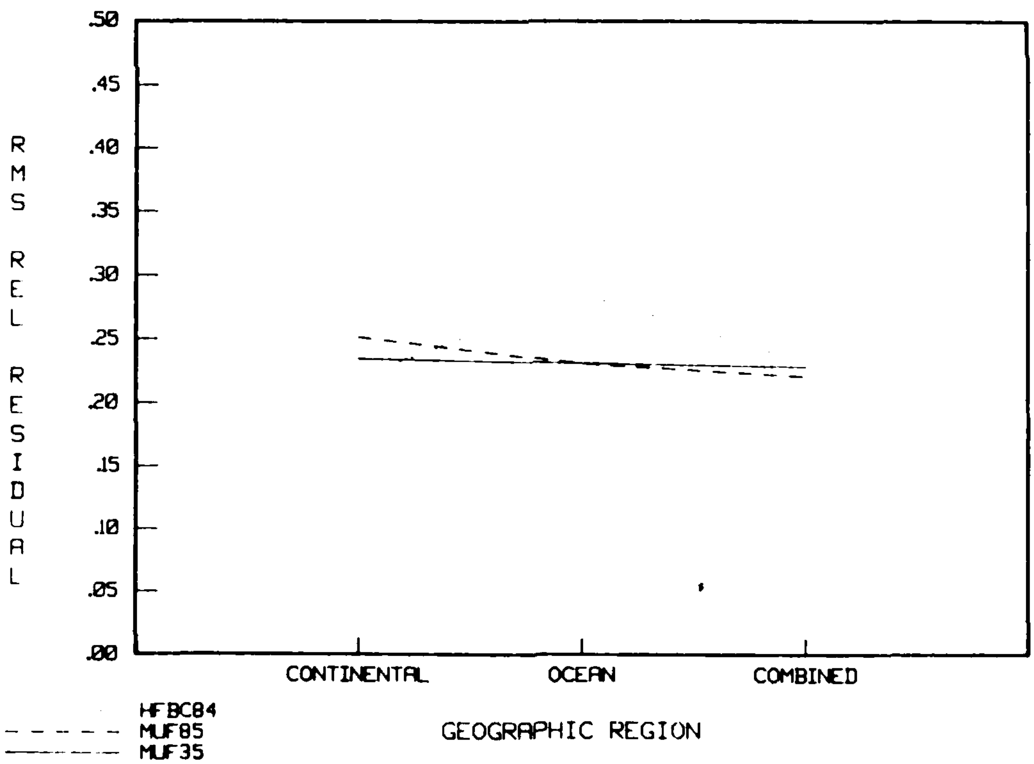

Figure 71 Relative RMS error as a function of geographic region.

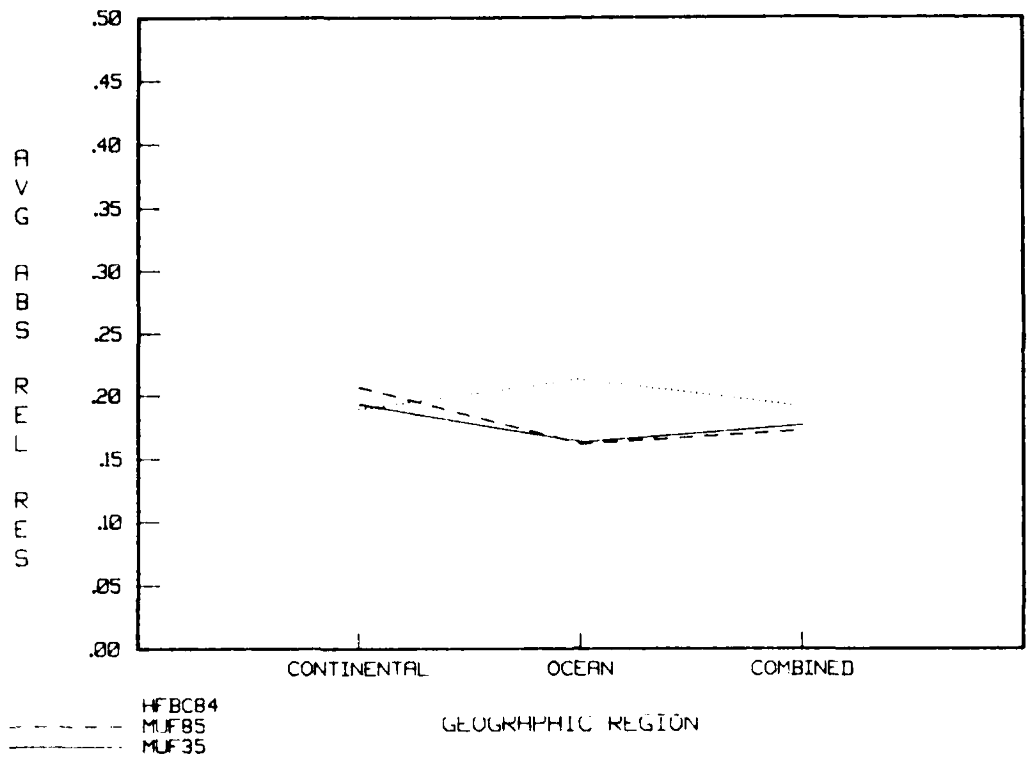

Figure 72. Magnitude of error (average absolute relative residual) as a function of geographic region

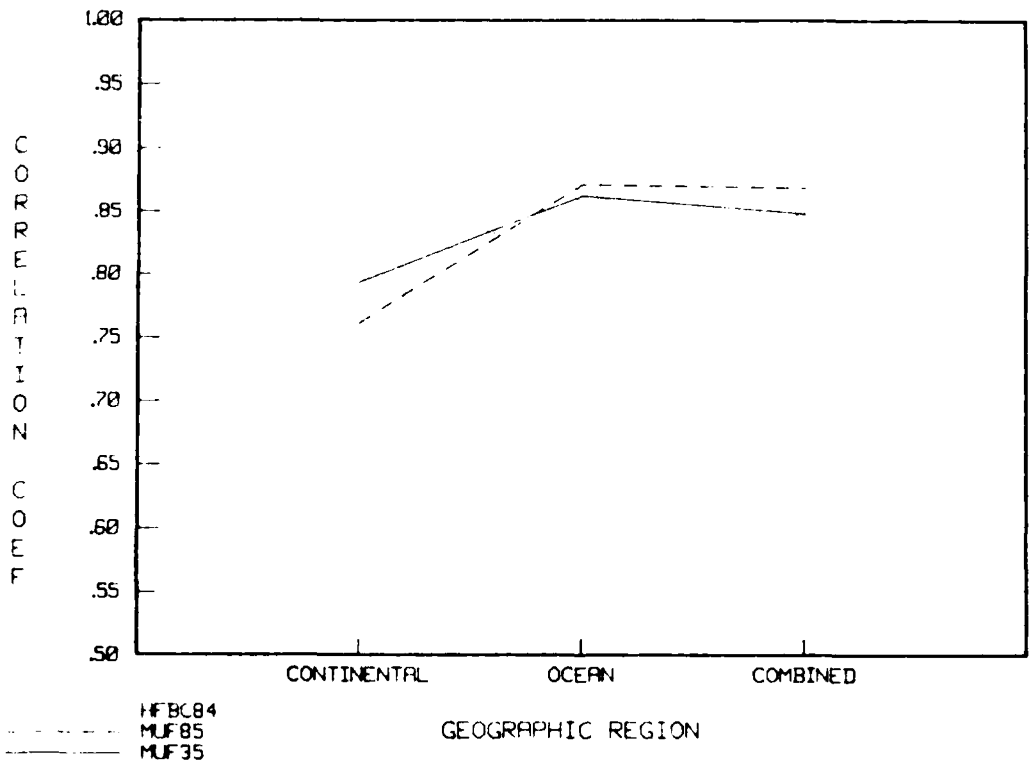

Figure 73. Correlation coefficients as a function of geographic region

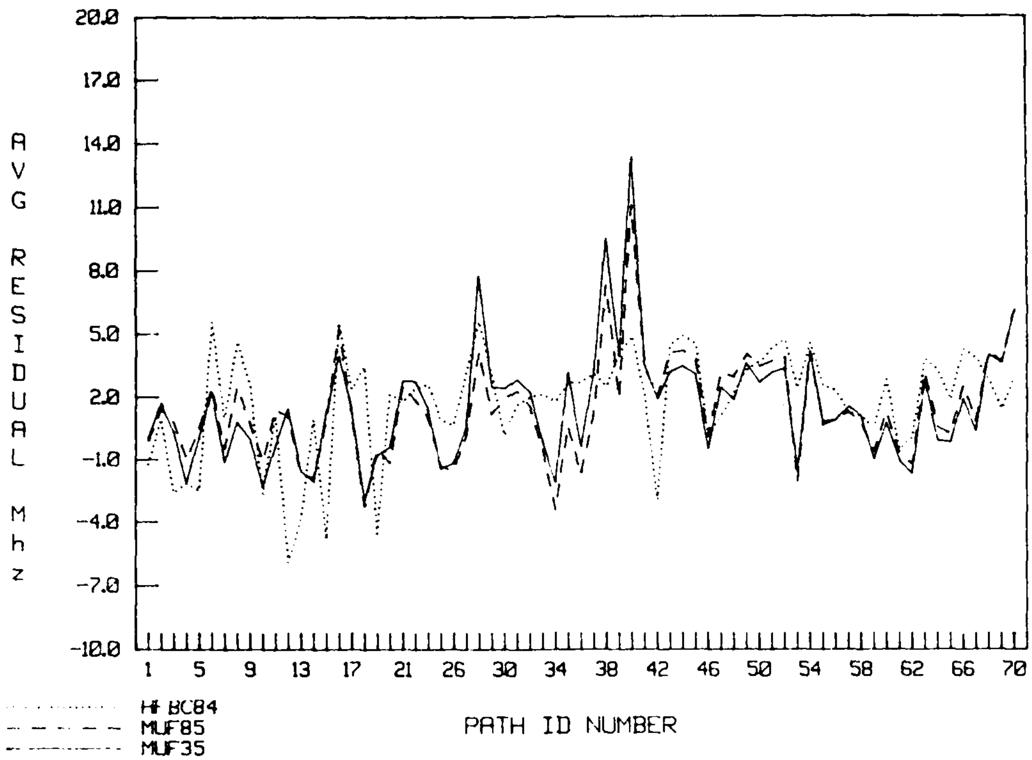

Figure 74. Average residual (bias) as a function of path identification.

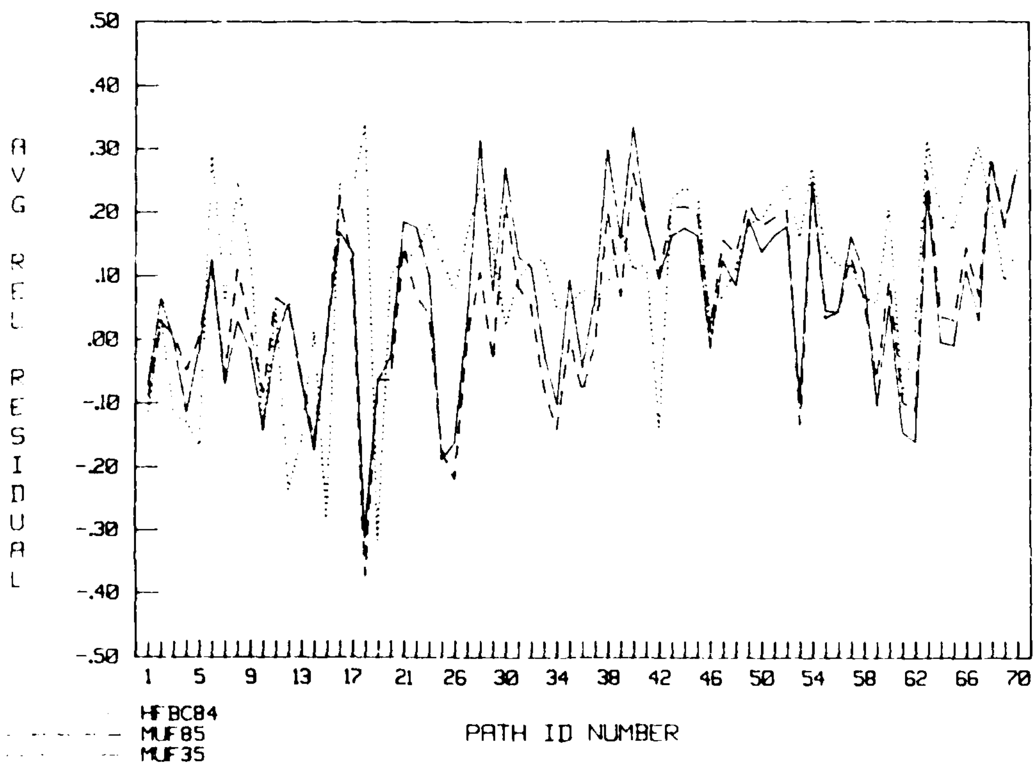

Figure 75. Average relative residual (relative bias) as a function of path identification.

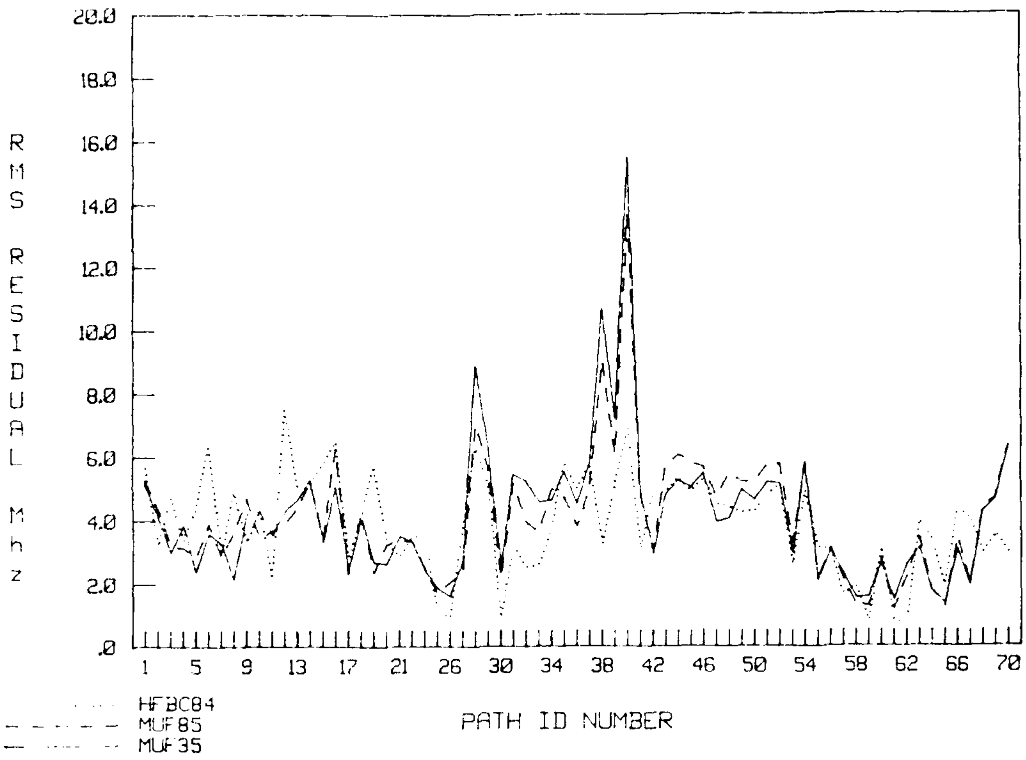

Figure 76 RMS error in MHz as a function of path identification.

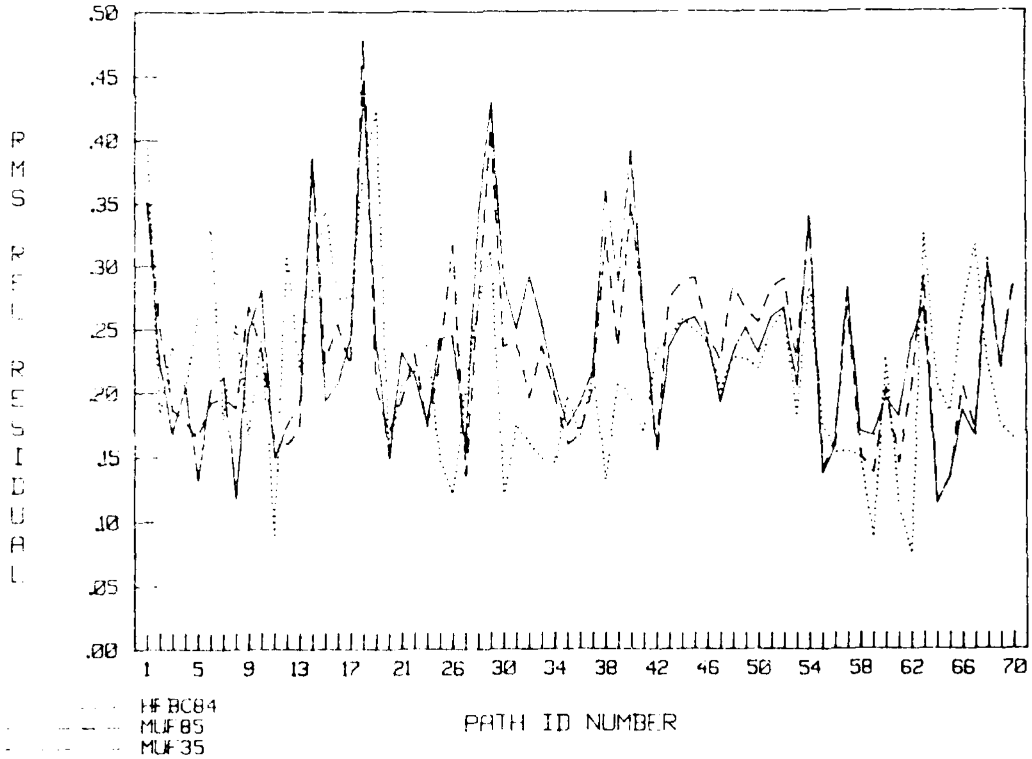

Figure 77 Relative RMS error as a function of path identification.

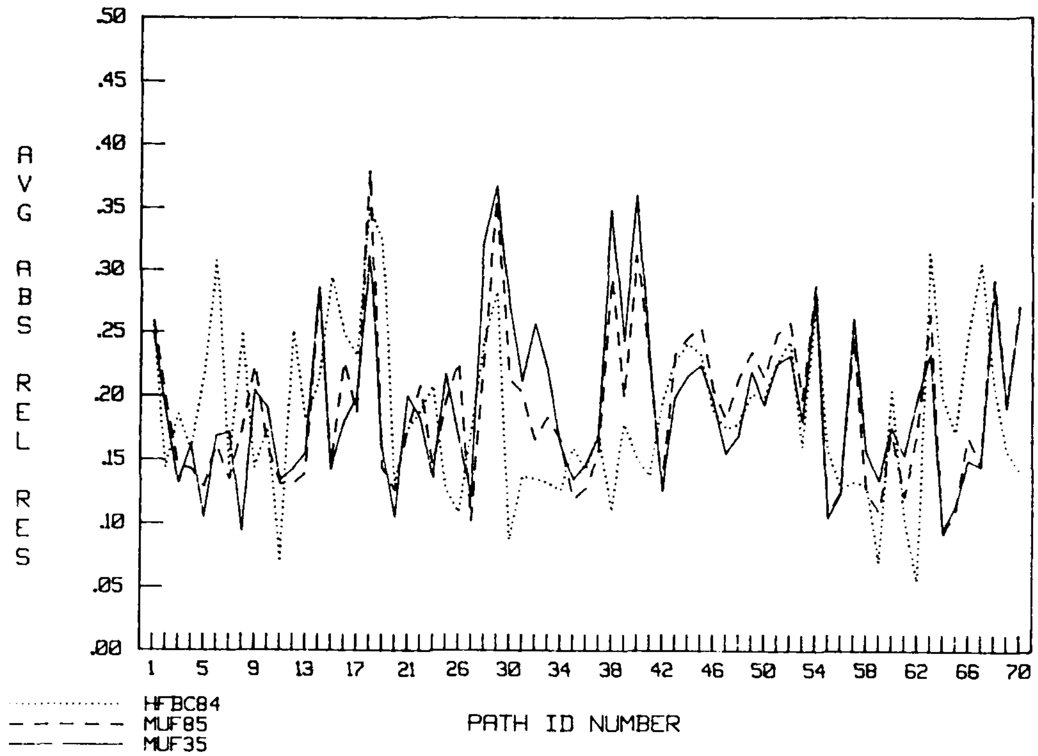

Figure 78. Magnitude of the error (average absolute relative residual) as a function of path identification.

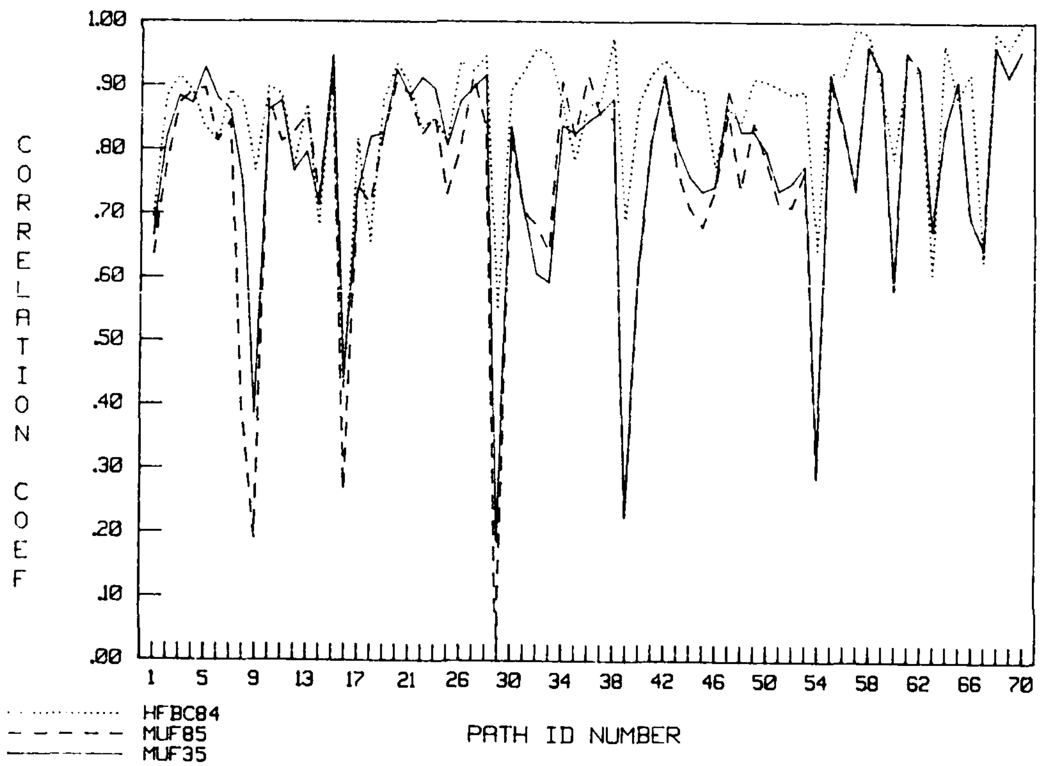

Figure 79. Correlation coefficients as a function of path identification.

7.0 CONCLUSIONS AND RECOMMENDATIONS

The performance of all three MUF models was almost identical overall. Bias was lowest for the HFBC84 model, 1.17 MHz compared to 1.26 MHz for MINIMUF-3.5 and 1.28 MHz for MINIMUF 85. The RMS error was lowest for MINIMUF-3.5, 4.44 MHz, compared to 4.58 MHz for MINIMUF 85 and 4.67 MHz for HFBC84.

The primary difference between MINIMUF-3.5 and MINIMUF 85 appeared when detailed analysis of the accuracies was conducted. When the variation in error was noted as a function of season, SSN, or range, for instance, there was less variation in the accuracy of MINIMUF 85. In some cases, MINIMUF-3.5 would exhibit high error, and in other cases it would exhibit low error.

A breakdown of the accuracies of the models is given as follows in the various categories studied:

1. Path length

The MINIMUF models have the lowest residuals in general, particularly for path lengths less than 5000 km, where MINIMUF 85 has the lower of the two MINIMUF models. HFBC84 has a large negative bias in the 4000- to 5000-km range. The RMS error increases with increasing path range for all these models.

2. Path orientation

All models predict low by about 1 MHz as a function of path orientation. The HFBC84 is most accurate for EAST/WEST orientation and least accurate for NORTH/SOUTH orientation, where MINIMUF 85 is most accurate. All models have an RMS error range between approximately 4.0 and 4.5 MHz.

3. Season

The MINIMUF models have their lowest error during the summer, when the HFBC84 model has its highest error. Here MINIMUF-3.5 has a bias of about zero MHz; MINIMUF 85 has a bias of about 1 MHz low; and HFBC84 has a bias of 2.2 MHz low. During the winter HFBC84 has a bias of about 1.1 MHz low; MINIMUF 85 has a bias of 1.2 MHz low; and MINIMUF-3.5 has a bias of 2.2 MHz low. All three models have an RMS error of 4 to 5 MHz, with MINIMUF-3.5 having a slightly lower overall RMS error.

4. Geomagnetic latitude

The MINIMUF models had their lowest bias and RMS error for transequatorial, low-latitude, and midlatitude paths, whereas their bias was highest for high-latitude paths. For transauroral paths MINIMUF 85 had the lowest bias. For low-latitude paths, HFBC84 predicted high by about 1.7 MHz. For transauroral paths MINIMUF 85 had a lower RMS error than MINIMUF-3.5. HFBC84 had its lowest RMS error for transauroral paths.

5. Sunspot number

Model uncertainty was evaluated for both monthly median SSNs (unsmoothed) and monthly mean smoothed SSNs. For the monthly median SSNs, the MINIMUF models have lower bias than HFBC84 at low SSN and slightly higher bias at high SSN (greater than 100). There is a general trend for all models to have higher bias at high SSNs. For monthly mean smoothed SSNs, an increase in bias at high SSN is indicated. For monthly median SSNs, there is a gradual increase in RMS error with increasing SSN, with MINIMUF 85 having a lower RMS error than MINIMUF-3.5 for SSNs less than 90. Using monthly smoothed SSNs in HFBC84 gives a large reduction in RMS error at high SSNs. The correlation of the models reflect the particular SSN used to develop the model. That is, MINIMUF-3.5 and HFBC84 have higher correlation coefficients with monthly smoothed SSNs, whereas MINIMUF 85 is more highly correlated with monthly median SSNs.

6. Diurnal trends

All models predict low, with the MINIMUF models having minimum error at 1200 midpath local time, while the HFBC84 model reaches a minimum 6 hours later at 1800. Maximum error is offset 12 hours from the minimum for all three models. The MINIMUF models have a lower RMS error from 0700 to 1800 midpath local time, while the HFBC84 model has a lower RMS error from 1800 to 0700.

7. Geographical regions

In ocean areas, the MINIMUF models produce the most accurate results, whereas continental data indicate HFBC84 to be more accurate there. For paths over both land and ocean, MINIMUF 85 appears to be most accurate.

8. Sounder type

Except for the non-NTSS types of sounders (the other category), the MINIMUF models had the lowest residuals. The non-NTSS types of sounders were used primarily on paths terminating in Canada and on transequatorial paths (paths difficult to predict). High residuals for all models for the BR Chirpsounder data indicate difficulty in modeling long paths in excess of 8000 km. The RMS error tended to be lowest for the MINIMUF paths for NTSS data and lowest for HFBC84 for the rest of the data.

9. Sounder path

Data for the paths Monrovia to Rota and Tripoli to Accra show both a larger bias and RMS error in the MINIMUF models than in HFBC84, as does the path France to Greece. The path Thule to Stockbridge shows a large bias for all three models.

As a result of this study, the following recommendations are made:

(1) Use MINIMUF 85 instead of MINIMUF-3.5.

(2) Make additional improvements in the MINIMUF model by adding geographical and time dependencies not accounted for in the effective zenith angle in the model.

(3) Improve the M-factor representation by introducing the effects of the underlying layers on F-region M-factor estimation.

(4) Continue to enhance the MOF database for regions of the world not represented.

(5) Test the MINIMUF models in the south polar region.

(6) Use the MOF database to validate other ionospheric prediction models such as IONOCAP.

8.0 REFERENCES

1. National Bureau of Standards Circular 462, Ionospheric Radio Propagation, 25 June 1948.

2. Stanford Research Institute, Technical Report 1, Contract DA 36-039 SC-66 381, IBM 704 Program to Determine the Maximum Usable Frequency (MUF) and the Lowest Useful High Frequency (LUF) for HF Radio Propagation, by E.A. Clark, March 1959.

3. Stanford Research Institute Final Technical Report 2, Contract DA 36-039 SC-85 052, The HF Propagation Prediction Programs for the IBM 7090 Computer, by E.M. Young and E.A. Clarke, May 1962.

4. Navy Electronics Laboratory Report 1358, A High Frequency Propagation Prediction Program for the CDC 1604 Computer, by D.B. Sailors, 28 February 1966.

5. National Bureau of Standards Technical Note 2, World Maps of F2 Critical Frequencies and Maximum Usable Frequency Factors, by D.H. Zacharisen, April 1959.

6. National Bureau of Standards Technical Note 2-2, Supplementary World Maps of F2 Critical Frequencies and Maximum Usable Frequency Factors, by D.H. Zacharisen, October 1960.

7. International Radio Consultative Committee 10th Plenary. Assembly, Geneva 1963, Report 322, World Distribution and Characteristics of Atmospheric Radio Noise, 1964.

8. National Bureau of Standards Report 6789, MUF-FOT Predictions by Electronic Computers, by D.L. Lucas and G.W. Haydon, 14 August 1961.

9. National Bureau of Standards Report 7619, Predicting the Performance of Band 7 Communication Systems Using Electronic Computers, by D.L. Lucas and G.W. Haydon, 15 October 1962.

10. Collins Radio Company Research Report 288, The Collins HF Propagation Prediction Program, by G. Bergemann and R. Decker, 1 September 1963.

11. F.T. Koide, "A Computer Method of HF Ionospheric Propagation Prediction and Analysis," IEEE Trans. on Antennas and Propagation, Vol. AP-11, pp 540-558, September 1963.

12. AVCO Corporation Technical Report RAD-TR-63-37, Contract AF 30 (602)-2809, Natural Communications Study Phase 1 Feasibility Study on a Reliable Polar High-Frequency Communications System, by G.E. Hill et al., 24 June 1964.

13. Environmental Sciences Services Administration Technical Report ITSA-1, Predicting Statistical Performance Indexes for High Frequency Ionospheric Telecommunication Systems, by D.L. Lucas and G.W. Haydon, 29 August 1966.

14. W.B. Jones and R.M. Gallet, "Methods for Applying Numerical Maps of Ionospheric Characteristics," J. Res. NBS, Vol. 66D, pp 649-662, November-December 1962.

15. National Bureau of Standards Technical Note 337, Advances in Ionospheric Mapping by Numerical Methods, by W.B. Jones, R.P. Graham, and M. Leftin, 12 May 1966. (Also Environmental Sciences Services Administration Technical Report ERL 1-7-ITS 75, May 1969.)

16. Commander, Naval Telecommunications Command, Naval Telecommunications Publication 6 Supp-1, Recommended Frequency Bands and Frequency Guide, 1980.

17. Bell Aerosystems Co. Report A70009-230, TR RADC-TR-67-396, HF and LF Propagation Models for Interference Prediction, by L.R. Spogen, Jr., J.L. Lloyd, and E.P. Moore, August 1967.

18. Environmental Sciences Services Administration Technical Report ERL 110-ITS 78, Predicting Long-Term Operational Parameters of High Frequency Sky-Wave Telecommunication Systems, by A.F. Barghausen, J.W. Finney, L.L. Proctor, and L.D. Schultz, May 1969.

19. Office of Telecommunications ITS Research Report 3, Global Representation of Annual and Solar Cycle Variation of foF2 Monthly Median 1954-1958, by W.B. Jones and D.L. Obitts, October 1970.

20. Office of Telecommunications ITS Research Report 2, World Maps of Atmospheric Radio Noise In Universal Time, by D.H. Zacharisen and W.B. Jones, October 1970.

21. Office of Telecommunications Report 76-88, Numerical Representation of Monthly Median Critical Frequencies of the Regular E Region (foE), by M. Leftin, May 1976.

22. Office of Telecommunications Report 76-102, Predicting the Performance of High Frequency Sky-wave Telecommunication Systems (The Use of the HFMUFES 4 Program), by G.W. Haydon, M. Leftin, and R. Rosich, September 1976.

23. Naval Ocean Systems Center Technical Report 186, MINIMUF-3. A Simplified HF MUF Prediction Agorithm, by R.B. Rose, J.N. Martin, and P.H. Levine, 1 February 1978.

24. Naval Ocean Systems Center Technical Report Document 201, MINIMUF 3.5, by R.B. Rose and J.N. Martin, 26 October 1978.

25. Naval Ocean Systems Center Technical Note 758, Further Verification of the MINIMUF-3.5 HF MUF Prediction Algorithm for: (1) Frequencies above 32 MHz., (2) Path Lengths of Less than 250 NMI, by R.B. Rose, 20 September 1979.

26. Stanford Research Institute Contract No. 3853(00), Technical Summary Report 4, Long Range Propagation Experiment, by A. Selby, February 1964.

27. National Bureau of Standards Report 7217, Boulder-Barrow Sweep Frequency Oblique Pulse Experiment, by L.H. Tveten, 8 January 1962.

28. Naval Ocean Systems Center Technical Report 695, Accuracy of High Frequency Maximum Usable Frequencies (MUF) Prediction, by D.B. Sailors, W.K. Moision and R.P. Brown, 15 September 1981.

29. D.L. Harnett, Introduction to Statistical Methods, Addisoı.-Wesley Publishing Co., 1st Edition, pp. 284-333, 1970.

30. Naval Ocean Systems Center Technical Report TR 1121, MINIMUF-85, by D.B. Sailors, R.A. Sprague, W.H. Rix, July 1986.

31. Y.T. Chiu, "An Improved Phenomenological Model of Ionospheric Density," J. Atmos. Terr. Physics, vol. 37, pp. 1563-1570, 1975.

32. T. Yonezawa and Y. Arima, "On the Seasonal and Non-seasonal Annual Variations and the Semi-annual Variation in the Noon and Midnight Electron Densities of the F2 Layer in Middle Latitudes," J. Radio Res. Lab. Japan, vol. 6, pp. 293-309, April 1959.

33. B.K. Ching and Y.T. Chiu, "A Phenomenological Model of Global Ionospheric Electron Density in the D-, F1-, and F2- regions," J. Atmos. Terr. Physics, vol. 35, pp.1615-1630, 1973.

34. Australian Government Department of Science, Operations and Management Division, Ionospheric Prediction Service Series R, A Critical Study of the NOSC HF Prediction Algorithm MINIMUF, by J. Caruana and M. W. Fox, May 1985.

APPENDIX A

BASIC PROGRAM FOR MINIMUF 85

The listing of MINIMUF 85 that follows is written in extended BASIC for the Tektronix 4052A computer. Statements 881-892 need to be placed in the routine that calls MINIMUF 85. The subroutine RAZGC determines the latitude and longitude of a point on a great circle path, given the range and bearing from the point. The subroutine GCRAZ gives the range and bearing between two points.

INPUT PARAMETERS

Z3 = transmitter latitude, radians ($\pi/2 \leq Z3 \leq \pi/2$)

Z4 = transmitter longitude, radians ($-2\pi \leq Z4 \leq 2\pi$)

Z5 = receiver latitude, radians ($\pi/2 \leq Z5 \leq \pi/2$)

Z6 = receiver longitude, radians ($-2\pi \leq Z6 \leq 2\pi$)

A0(1) = path length, radians

Z0(2) = azimuth of path, radians

M1 = month

D0 = day of month

H0 = hours, GMT

MO = minutes, GMT

S9 = monthly median sunspot number

PI = 3.141593

P0 = 1.5707963268

OUTPUT PARAMETER

The output is as follows:

J9 = MUF in MHz

```
100   ! MNIMUF85 TEST   "MNIMUFTEST"
110   !
120   ! INPUT DATA  DRIVER FOR MINIMUF
130 R1=PI/180
140 P1=2*PI
150 P0=PI/2
160 DIM Z0(8)
170 Z3=75*R1  ! TRANSMITTER LATITUDE
180 Z4=125*R1  ! TRANSMITTER LONGITUDE WEST POSITIVE
190 Z5=51.95*R1  ! RECEIVER LATITUDE
200 Z6=176.58*R1  !  RECEIVER LONGITUDE WEST POSITIVE
210 M1=1  ! MONTH  1= JAN
220 D0=15  ! DAY
230   !H0=0   HOUR
240 M0=0  !  MINUTE
250 S9=9  !  SMOOTH SUNSPOT NUMBER
260 A=Z5
270 B=Z6
280 C=Z3
290 D=Z4
300 CALL Gcraz
310 Z0(1)=R  !  RANGE BETWEEN TRANSMITTER-RECEIVER
320 Z0(2)=S  !  BEARING ANGLE
330 FOR H0=0 TO 23 STEP 1  !  LOOP FOR 24 HOURS
340    CALL Mnimuf
350    PRINT "LAT=";Z3/R1,"LON=";Z4/R1,"LAT=";Z5/R1,"LON=";Z6/R1
360    PRINT "MONTH=";M1,"DAY=";D0,"HOUR=";H0,"MINUTE=";M0
370    PRINT "SSN=";S9
380    PRINT ""
390    PRINT "MUF=";J9
400 NEXT H0
410 END
420   !
430 SUB Mnimuf
440    DIM Ssn(6),Scn(6)
450    Saa=0.814*S9+22.23
460    Sab=1.3022-0.00156*S9
470    FOR J=1 TO 6
480       Sar=2*J*PI*M1/12
490       Ssn(J)=SIN(Sar)
500       Scn(J)=COS(Sar)
510    NEXT J
520    Sac=0.9925+0.011*Ssn(1)+0.087*Scn(1)-0.043*Ssn(2)+0.003*Scn(2)
530    Sac=Sac-0.013*Ssn(3)-0.022*Scn(3)+0.003*Ssn(4)+0.005*Ssn(5)
540    Sac=Sac+0.018*Scn(6)
550    I=H0+M0/60
560    J=INT(Z0(1)/0.62784)+1
570    L=1/(2*J)
580    Ak6=1.59*Z0(1)
590    IF Ak6<1 THEN
600       Ak6=1
610    END IF
620    J9=100
630    IF Z0(1)>0.94174 THEN
640       Ak=2*J-1
```

```
650     ELSE
660        Ak=J
670     END IF
680     Kkk=1/Ak6
690     IF Kkk<>1 THEN
700        Kkk=0.5
710     END IF
720     FOR D9=1 TO Ak STEP 1
730        IF Z0(1)>0.94174 THEN
740           Ak1=D9*L
750        ELSE
760           Ak1=1/(2*Ak6)+(D9-1)*(0.9999-1/Ak6)
770        END IF
780        C=Ak1*Z0(1)
790        D=Z0(2)
800        A=Z5
810        B=Z6
820        CALL Razgc
830        E=R
840        F=S
850        IF F=>0 THEN 870
860        F=F+P1
870        G=0.0172*(10+(M1-1)*30.4+D0)
880        Slt=I-F/(R1*15)
890        IF Slt<24 THEN 910
900        Slt=Slt-24
910        IF Slt>0 THEN 930
920        Slt=Slt+24
930        A=E
940        B=F
950        Smg=0.9792*SIN(A)+0.2028*COS(A)*COS(B-1.2043)
960        Sdg=ASN(Smg)
970        IF ABS(Sdg)<0.95993 THEN
980           Sgf=0
990        ELSE
1000          Sgf=0.7578*SQR(1+3*Smg*Smg)*0.5-0.5
1010       END IF
1020       H=0.409*COS(G)
1030       P=3.82*F+12+0.13*(SIN(G)+1.2*SIN(2*G))
1040       IF P<=24 THEN 1070
1050       P=P-24
1060       GO TO 1090
1070       IF P=>0 THEN 1090
1080       P=P+24
1090       Q=2.5*Z0(1)*Kkk MIN P0
1100       Q=SIN(Q)
1110       Q=1+2.5*Q*SQR(Q)
1120       IF COS(E+H)>-0.26 THEN 1170
1130       G=0
1140       S=0
1150       Sad=1
1160       GO TO 1610
1170       S=(-0.26+SIN(H)*SIN(E))/(COS(H)*COS(E)+1.0E-3)
1180       S=S MAX -1 MIN 1
1190       S=12-ASN(S)*7.6394
```

```
1760     Rltm=Sdg
1770     Rlgm=COS(A)*SIN(B-1.2043)/COS(Rltm)
1780     Rlgm=Rlgm MAX -1 MIN 1
1790     Rlgm=ASN(Rlgm)
1800     X=(2.2+(0.2+S9/1000)*SIN(Rltm))*COS(Rltm)
1810     Ff=EXP(-(X^6))
1820     Gg=1-Ff
1830     T=PI*Tmo/12
1840     V=SIN(T)
1850     U=COS(T+T)
1860     Y=SIN(Rlgm/2)
1870     Ys=COS(Rlgm/2-PI/20)
1880     Z=SIN(Rlgm)
1890     Za=SQR(ABS(Z))
1900     Am=1+V
1910     IF Sdg<0 THEN 1960
1920     C=-23.5*PI/180
1930     W=EXP(-1.2*(COS(Rltm+C*COS(Phi))-COS(Rltm)))
1940     Plr=(2+1.2*S9/100)*W*(1+0.3*V)
1950     GO TO 2000
1960     B=V*(0.5*Y-0.5*Z-Y^8)-Am*U*(Z/Za)*EXP(-4*Y*Y)
1970     Plr=2.5+2*S9/100+U*(0.5+(1.3+0.2*S9/100)*Ys^4)
1980     Plr=Plr+(1.3+0.5*S9/100)*COS(Phi-PI*(1+B))
1990     Plr=Plr*(1+0.4*(1-V*V))*EXP(-1*V*Ys^4)
2000     T=Gg*H^2/8.12+0.66*Ff*Plr
2010     IF T<0 THEN 2040
2020     Ff2=T^0.5*2.85
2030     H=Ff2*Q*Sae
2040 END SUB
2050 SUB Gcraz
2060     IF ABS(A-C)>1.0E-5 OR ABS(B-D)>1.0E-5 THEN 2100
2070     R=1.0E-6
2080     S=0
2090     GO TO 2290
2100     IF ABS(A-P0)>1.0E-5 THEN 2140
2110     R=P0-C
2120     S=PI
2130     GO TO 2290
2140     IF ABS(A+P0)>1.0E-5 THEN 2180
2150     R=P0+C
2160     S=0
2170     GO TO 2290
2180     E=SIN(A)
2190     F=COS(A)
2200     G=SIN(C)
2210     H=E*G+F*COS(C)*COS(B-D)
2220     H=H MAX -1 MIN 1
2230     R=ACS(H)
2240     S=(G-E*H)/(F*SIN(R))
2250     S=S MAX -1 MIN 1
2260     S=ACS(S)
2270     IF SIN(B-D)>0 THEN 2290
2280     S=PI-S
2290 END SUB
2300 SUB Razgc
```

```
1200        T=P-S/2
1210        IF T=>0 THEN 1230
1220        T=T+24
1230        U=P+S/2
1240        IF U<=24 THEN 1260
1250        U=U-24
1260        V=ABS(COS(E+H))
1270        W=9.7*V^9.6
1280        W=W MAX 0.1
1290        X=I
1300        IF U<T AND (I-U)*(T-I)>0 THEN 1440
1310        IF U=>T AND (I-T)*(U-I)<=0 THEN 1440
1320        IF T<=I THEN 1340
1330        X=X+24
1340        Y=PI*(X-T)/S
1350        Z=PI*W/S
1360        F=(T-X)/W
1370        F=F MAX -100 MIN 100
1380        G=V*(SIN(Y)+Z*(EXP(F)-COS(Y)))/(1+Z^2)
1390        P=V*(Z*(EXP(-S/W)+1))*EXP((S-24)/2)/(1+Z^2)
1400        IF G=>P THEN 1420
1410        G=P
1420        Sad=1.11-0.01*Slt
1430        GO TO 1610
1440        IF U<=I THEN 1460
1450        X=X+24
1460        Stt=X-U
1470        Stu=14*Stt/(24-S)
1480        Sag=PI*(Stu+1)/15
1490        Sah=2*Sag
1500        Sai=1.0195-0.06*SIN(Sah)-0.037*COS(Sah)+0.018*SIN(2*Sah)
1510        Saj=-0.003*COS(2*Sah)+0.025*SIN(3*Sah)+0.018*COS(3*Sah)
1520        Sak=0.007*SIN(4*Sah)-0.005*COS(4*Sah)+0.006*SIN(5*Sah)
1530        Sal=0.017*COS(5*Sah)-0.009*SIN(6*Sah)-0.004*COS(6*Sah)
1540        Sad=Sai+Saj+Sak+Sal
1550        Z=PI*W/S
1560        F=(U-X)/2
1570        F=F MAX -100 MIN 100
1580        Y=-S/W
1590        Y=Y MAX -100 MIN 100
1600        G=V*(Z*(EXP(Y)+1))*EXP(F)/(1+Z^2)
1610        Sae=Sab*Sac*Sad
1620        H=SQR(6+Saa*SQR(G))+Sgf
1630        H=H*(1-0.1*EXP((S-24)/3))
1640        H=H*(1+(1-SGN(Z5)*SGN(Z3))*0.1)
1650        H=H*(1-0.1*(1+SGN(ABS(SIN(A
1660        CALL Fof2
1670        J9=J9 MIN H
1690    NEXT D9
1700    J9=J9 MAX 2 MIN 50
1710 END SUB
1720 SUB Fof2
```

END

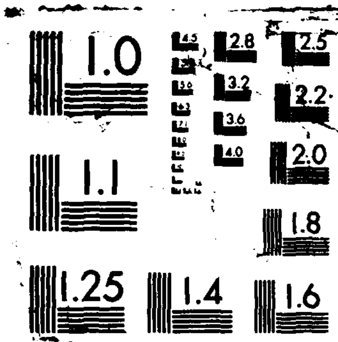
1.0
2.8
2.5
3.2
2.2
3.6
4.0
2.0
1.1
1.8
1.25
1.4
1.6

```
2310    IF C>1.0E-5 THEN 2350
2320    R=A
2330    S=B
2340    GO TO 2610
2350    IF ABS(A-PO)>1.0E-5 THEN 2390
2360    R=PO-C
2370    S=B
2380    GO TO 2610
2390    IF ABS(A+PO)>1.0E-5 THEN 2430
2400    R=C-PO
2410    S=B
2420    GO TO 2610
2430    E=SIN(A)
2440    F=COS(A)
2450    G=COS(C)
2460    H=E*G+F*SIN(C)*COS(D)
2470    H=H MAX -1 MIN 1
2480    P=ACS(H)
2490    Q=(G-E*H)/(F*SIN(P))
2500    Q=Q MAX -1 MIN 1
2510    Q=ACS(Q)
2520    R=PO-P
2530    IF SIN(D)>0 THEN 2560
2540    S=B+Q
2550    GO TO 2570
2560    S=B-Q
2570    IF S<=P1 THEN 2590
2580    S=S-P1
2590    IF S=>-P1 THEN 2610
2600    S=S+P1
2610 END SUB
```

APPENDIX B

FORTRAN PROGRAM FOR MINIMUF 85

The listing of MINIMUF 85 that follows is written in FORTRAN 77 for the HP 9050 computer. The parameters passed to the subroutine and those returned by it are described in the comments portion of the routine.

```
      subroutine muf85 (tlat, tlon, rlat, rlon, itime, cpnt, ssn,cmuf)
cp
c     subroutine muf85
c
c       update nov 1985
c       an improved version of muf35 which includes ssn,season and
c       diurnal dependence in the M-factor plus an improved FOF2 model
c       call muf85(tlat,tlon,rlat,rlon,itime,ssn,cmuf)
c
c       *******  this version modified 3/20/86 to return thru common
c           /sun/ the local mean time at the control pt (lmt)
c        this routine computes the maximum usable frequency (cmuf) for
c        a given propagation path.  the required input is:
c
c        parameters passed:
c          tlat  - transmitter latitude in radians
c          tlon  - transmitter west lingitude in radians
c          rlat  - receiver latitude in radians
c          rlon  - receiver west longitude in radians
c          itime - six element array containing the month, day
c                  hour, minute, julian day, and year
c          ssn   - sunspot number
c
c        parameters returned:
c          cpnt  - path control point info in radians
c          cmuf  - classical muf in megahertz.
c
c        called by subroutine or function:  mufluf
c
c        subroutines and functions called:  fof2
c                                           path
c                                           razgc
c                                           sygn
c
c        common blocks referenced:          hite
cz
      logical        v, first
      integer        itime(6)
      real           cpnt(8), k5, l0, lmt, k8, k9, m9, mlat,sn(6),cn(6)
c
c      lmt added to common /sun/ and common added for this exercise
c      common /sun/dum1,dum2,lmt
      common /hite/ h,v,ym
cm
c      common /hite/  h, v, ym
c
c                    h   is the height of the path
c                     v   is a logical variable which decides if the
c                         path length is calculated from 1000 km f
c                         end points and if the multilayered ionospheric
c                         model is to be used.  these will be performed
c                         if v is true.
c                    ym  is the f layer thickness.
c
cz
```

```
      data   pi/3.14159265/,twopi/6.2831853/,halfpi/1.57079632/,
     &       dtr/0.017453293/,rtd/57.2957795/,r0/6371./
      data   s8 /250.0/, fml /0.728/, fms /0.52998/,
     &       fm2 /0.00356/, fm3 /63.75/, fm4 /0.00178/,
     &       first /.true./
c
      t5 = float( itime(3) ) + float( itime(4) )/60.0
c
c   convert 10.7 cm flux to sunspot number
c
c     ssn = ( sqrt( fms - fm2*( fm3 - flux10 ) ) - fml )/fm4
c     ssn = amax1( amin1( ssn, 250.0 ), 0.0 )
c
c   determine number of hops
c   1 hop for path length <= 4000 km ( 0.6278 radians )
c   2 hop otherwise
c
c      a3 is a 6th order fourier series based on month which is part
c         of the new M-factor
c      a2 is a linear function of ssn in the M-factor
c      al is a linear function of ssn in the critical frquency
c         expression
c
      do 500 n = 1,6
      qn = float(2*n)
      arg = pi*qn*itime(1)/12.0
      sn(n) = sin(arg)
      cn(n) = cos(arg)
  500 continue
      a3 = .9925+.011*sn(1)+.087*cn(1)-.043*sn(2)
     1    +.003*cn(2)-.013*sn(3)-.022*cn(3)
     2    +.003*sn(4)+.005*sn(5)+.018*cn(6)
      al = .814*ssn+22.23
      a2 = 1.3022-.00156*ssn
      call path(tlat,tlon,rlat,rlon,cpnt)
      gl = cpnt(1)
      azim = cpnt(8)
c
c      control point changes for muf85
c
      if(.not. v)then
         h3=1.59
         ak6 = h3*cpnt(1)
         if(ak6 .lt.1.0)ak6=1.0
         k5 = 1.0/ak6
         if(k5 .ne. 1.0) k5 = .5
         khop = int(cpnt(1)/.62784)+1
         kkhop = khop
         if(cpnt(1) .gt. 0.94174)kkhop = 2*khop-1
      else
c
c      old control point method for raytrace
c
         khop = 1
         if ( gl .gt. 0.62784 )  khop = 2
```

```
         k5 = 1.0/float( khop )
         kkhop = khop
      end if
c
      cmuf=100.0
      ym = 100.0
      do 160 kl = 1,kkhop
c
c   l0, w0 = latitude and west longitude of control points
c   mid-point for 1 hop case; points 2000 km from each
c   end for 2 hop case.
c
        if ( khop .eq. 1 )  pl = gl/2.0
        if ( khop .eq. 2 .and. kl .eq. 1 )  pl = 0.31392
        if ( khop .eq. 2 .and. kl .eq. 2 )  pl = gl - 0.31392
c
c   if v is .false., do cntrl pt calculations like in apes
c
        if(v) go to 600
c
c
c       control point method for muf85
c
      if(cpnt(1) .gt. .94174) then
         xkl = kl
         xhop = khop
         akl = xkl/(2.0*xhop)
      else
         akl = 1.0/(2.0*ak6)+float(kl-1)*(.9999-1.0/ak6)
      end if
c
      pl = gl*akl
c
  600   call razgc( rlat, rlon, pl, azim, l0, w0 )
c
c    lmt = local mean time in hours at the control point
c    mlat = geomagnetic latitude at the control point
c
        if ( w0 .ge. 0.0 )  then
          lmt = w0
        else
          lmt = w0 + twopi
        end if
        lmt = t5 - lmt*rtd/15.0
        if ( lmt .lt. 0.0 )  then
          lmt = lmt + 24.0
        else if ( lmt .ge. 24.0 )  then
          lmt = lmt - 24.0
        end if
        smg = 0.9792*sin( l0 ) + 0.2028*cos( l0 )*cos( w0 - 1.2043 )
        smg = amax1( amin1( smg, 1.0 ), -1.0 )
        mlat = asin( smg )
c
c      gyro frequency for lat > 55deg
c
```

```
         if ( abs( mlat ) .lt. 0.95993 )  then
           gyro = 0.0
         else
           gyro = 0.3789*sqrt( 1.0 + 3.0*smg*smg) - 0.5
         end if
c
c   y1 = 2*pi*date/365.25
c   y2 = -solar declination
c   k8 = time of local noon
c
         y1=0.0172*( 10.0 + float(itime(1)-1)*30.4 + itime(2) )
         y2=0.409*cos(y1)
c
         k8=3.82*w0+12.0+0.13*(sin(y1)+1.2*sin(2.0*y1))
         if ( k8 .gt. 24.0 )  then
           k8 = k8 - 24.0
         else if ( k8 .le. 0.0 )  then
           k8 = k8 + 24.0
         end if
c
c   m9 = m-factor = muf/f0f2
c
         m9 = amin1( 2.5*gl*k5, halfpi )
         m9 = sin( m9 )
         m9 = 1.0 + 2.5*m9*sqrt( m9 )
c
c   changes to include altitude of the f-layer variations
c   for diurnal,latitude, and solar cycle
c   (if v is .false. bypass all this variation stuff)
c
         if(.not.v) go to 50
51       cchi=sin(l0)*sin(-y2)+cos(l0)*cos(-y2)*cos((t5-k8)*15.*dtr)
         chi=acos(cchi)
c
c   altitude variations of f-layer
c
         chil=((chi+0.349)/.873)**2
         xl=(l0/0.524)**2
         xmax=3.-(ssn-25.)*5.e-3+1.25*cos((l0-0.96)*0.045)
         delx=2.*cos(chi-0.873+.698*cos((l0-0.96)*0.045))
      &        +(ssn-25.)*0.01*exp(-chil)*exp(-xl)
         xll=xmax - delx
c
50      continue
         if ( cos( l0 + y2 ) .gt. -0.26 )  go to 100
c
c   no daylight on path at any time during the day
c
         g0 = 0.0
         k9 = 0.0
         go to 140
100      continue
c
c   k9 = length of daylight
c   t  = time of sunrise
```

```
c   t4 = time of sunset
c
        k9 = ( -0.26 + sin(y2)*sin(10) )/( cos(y2)*cos(10) + 1.0e-3 )
        k9 = amax1( amin1 ( k9, 1.0 ), -1.0 )
        k9 = 12.0 - asin( k9 )*7.6394
        t = k8 - k9/2.0
        if ( t .lt. 0.0 )  t = t + 24.0
        t4 = k8 + k9/2.0
        if ( t4 .gt. 24.0 )  t4 = t4 - 24.0
        c0 = abs( cos( 10 + y2 ) )
        t9=9.7*(amax1(c0,.1))**9.6
        t9 = amax1( t9, 0.1 )
        t6 = t5
        if ( ( t4 .lt. t .and. (t5-t4)*(t-t5) .gt. 0.0 ) .or.
     &          ( t4 .ge. t .and. (t5-t)*(t4-t5) .le. 0.0 ) )  go to 120
c
c   day time at control point
c
        if ( t .gt. t5 )  t6 = t6 + 24.0
c
c      local time conversion
c      t5 is local time, w0 is longitude in radians
c
      z = w0*(180.0/3.14159265)
c
c      local time dependent factor for M-factor
c
      hrlcl  = t5 - z/15.0
      if(hrlcl .ge. 24.0)hrlcl = hrlcl - 24.0
      if(hrlcl .lt. 0.0) hrlcl = hrlcl + 24.0
      a4 = 1.11-.01 * hrlcl
c
        g9 = pi*( t6 - t )/k9
        g8 = pi*t9/k9
        u = ( t - t6 )/t9
        u = amin1( amax1( u, -87.0 ), +87.0 )
        u1 = -k9/t9
        u1 = amin1( amax1( u1, -87.0 ), +87.0 )
        g0=c0*(sin(g9)+g8*(exp(u)-cos(g9)))/(1.0+g8*g8)
        g3 = c0*( g8*( exp( u1 ) + 1.0 ) )
     &          *exp( ( k9 - 24.0 )/2.0 )/( 1.0 + g8*g8 )
        g0 = amax1( g0, g3 )
        if(v) ym = 100.0*(1.0 + 0.2*cos(pi*((t6-t)/k9 - 0.5)))
        go to 140
120     continue
c
c   night time at control point
c
c
c      6th order fourier series night time factor for M-factor,
c          based on hours after sunset,t2
c
        if ( t4 .gt. t5 )  t6 = t6 + 24.0
      t1 = t6 - t4
      t2 = 14.0*t1/(24.0-k9)
```

```
      ag = pi *(t2+1.0)/15.0
      ag1 = 2.0*ag
      ag2 = 4.0*ag
      ag3 = 6.0*ag
      ag4 = 8.0*ag
      ag5 = 10.0*ag
      ag6 = 12.0*ag
      a14 = 1.0195 -.06*sin(ag1)-.037*cos(ag1)+.018*sin(ag2)
      a24 = -.003*cos(ag2)+.025*sin(ag3)+.018*cos(ag3)
      a34 = .007*sin(ag4)-.005*cos(ag4)+.006*sin(ag5)
      a44 = .017*cos(ag5)-.009*sin(ag6)-.004*cos(ag6)
      a4  = a14+a24+a34+a44
c
        g8=pi*t9/k9
        u = ( t4-t6)/2.0
        u = amin1( amax1( u, -75.0 ), +75.0 )
        u1 = -k9/t9
        u1 = amin1( amax1( u1, -75.0 ), +75.0 )
        g0=c0*(g8*(exp(u1)+1.0))*exp(u)/(1.0+g8*g8)
140     continue
        if(.not.v) go to 150
        h = amin1(350.0,amax1(250.,x11*ym))
c   the slope of the mfactor variation
        xm=-1.e-3*amin1(6.0*g1/(khop*.31),6.)
c   the new mfactor
        m9=m9+xm*(h-290)
c
c   g2 = muf at control point
c
150     continue
        g2 = sqrt(6.0 +a1 * sqrt(g0)) + gyro
        g2 = g2*( 1.0 - 0.1*exp( ( k9 - 24.0 )/3.0 ) )
        g2 = g2*( 1.0 + ( 1.0 - sygn( tlat )*sygn( rlat ) )*0.1 )
        g2 = g2*( 1.0 - 0.1*( 1.0 + sygn( abs( sin( l0 ) )
     &       - cos( l0 ) ) ) )
        if ( abs( mlat ) .ge. 0.95993 )  then
c
c     FOF2 corrects for plar region FOF2.  result is G2 if
c         not in polar regiond
c
c
          g2 = m9*fof2( g2, lmt, itime, l0, w0, mlat, ssn )
        else
          g2 = g2*m9
        end if
c
      g2 = g2 * a2*a3*a4
        cmuf = amin1( cmuf, g2 )
160   continue
      cmuf = amin1( amax1( cmuf, 2.0 ), 50.0 )
c
      return
      end
```

```
      function fof2( ff2, lmt, itime, lat, lon, mlat, ssn )
cp
c     function fof2
c
c       x = fof2( ff2, lmt, itime, lat, lon, mlat, ssn )
c
c       this function corrects the f2-layer critical frequency
c       computed by muf35 for polar latitudes using the chiu model.
c
c       reference (to be supplied when available)
c
c       input:
c         ff2     critical frequency from muf35 in mhz - real
c         lmt     local mean time at lat,lon in hours  - real
c         itime   integer array containing month, day,
c                 hour, minute, julian day, and year   - integer
c         lat     geographic latitude in radians       - real
c         lon     geographic west longitude in radians - real
c         mlat    magnetic latitude in radians         - real
c         ssn     sunspot number                       - real
c
c       output:
c         fof2    the f2-layer critical frequency in mhz - real
c
c       called by subroutine or function:  muf35
c
c       subroutines and functions called:  none
c
c       common blocks referenced:          none
cz
      integer       itime(6)
      real          lat, lmt, lon, mlat, mlon
c
      data          pi /3.1415926/
c
      phi = lmt*pi/12.0
      tmo = itime(1) + ( itime(2) + itime(3)/24.0 + itime(4)/1440.0 )/30.0
     &      - 0.5
      cmlat = cos( mlat )
      mlon = cos( lat )*sin( lon - 1.2043 )/cmlat
      mlon = amax1( amin1( mlon, 1.0 ), -1.0 )
      mlon = asin( mlon )
      x = ( 2.2 + ( 0.2 + ssn/1000.0 )*sin( mlat ) )*cmlat
      ff = exp( -( x**6 ) )
      gg = 1.0 - ff
      t = pi*tmo/12.0
      v = sin( t )
      if ( mlat .ge. 0.0 )  then
        w = exp( -1.2*( cos( mlat - 0.41015*cos( phi ) ) - cmlat ) )
        plr = ( 2.0 + 0.012*ssn )*w*( 1.0 + 0.3*v )
      else
        u = cos( t+t )
        y = sin( mlon/2.0 )
        ys = cos( mlon/2.0 - pi/20.0 )
        z = sin( mlon )
```

```
          za = sqrt( abs( z ) )
          am = 1.0 + v
          b = v*( ( y - z )/2.0 - y**8 ) - am*u*( z/za )*exp( -4.0*y*y )
          ys4 = ys**4
          plr = (2.5 + ssn/50.0 + u*( 0.5 + ( 1.3 + 0.002*ssn )*ys4 )
     &              + ( 1.3 + 0.005*ssn )*cos( phi - pi*( 1.0 + b ) ))
     &              * ( 1.0 + 0.4*( 1.0 - v*v ) )*exp( -v*ys4 )
        end if
c
        fof2 = gg*ff2*ff2/8.12 + 0.66*ff*plr
        if (fof2 .gt. 0.0)  then
         fof2 = 2.85*sqrt(fof2)
        else
         fof2 = ff2
        end if
        return
        end
```

```
      subroutine path (tlat, tlon, rlat, rlon, cpnt)
cp
c      subroutine path
c
c        call path(tlat,tlon,rlat,rlon,cpnt)
c
c        this routine computes the range,azimuth, and control point
c        coordinates for a given propagation path.  the method assumes
c        a spherical earth with a radius of 6371 km.  the required
c        input for this module is:
c             tlat    transmitter latitude in radians
c             tlon    transmitter west longitude in radians
c             rlat    receiver latitude in radians
c             rlon    receiver west longitude in radians
c        this subroutine returns the following information in an 8 word
c        real array (cpnt):
c             cpnt(1) distance between the receiver and transmitter in
c                     radians
c             cpnt(2) latitude of midpoint in radians
c             cnpt(3) west longitude in radians
c             cpnt(4) latitude of point 1000km from the receiver in radians
c             cpnt(5) west longitude of point 1000km from receiver in
c                     radians
c             cpnt(6) latitude of point 1000km from transmitter in radians
c             cpnt(7) west longitude of point 1000km from transmitter
c                     in radians
c             cpnt(8) azimuth from receiver to transmitter in radians
c
c        cpnt(4) through cpnt(7) will not be computed for paths less than
c        1000 km (0.15696 radians) in length.
c
c        subroutines and functions used:  gcraz
c                                         razgc
c
c        common blocks:  none
c
cz
c
      dimension cpnt(8)
c
c    get range and azimuth
c
      call gcraz( rlat, rlon, tlat, tlon, cpnt(1), cpnt(8) )
c
c    get mid-point coordinates
c
      p1 = cpnt(1)/2.0
      call razgc( rlat, rlon, p1, cpnt(8), cpnt(2), cpnt(3) )
c
c    is path length >= 1000 km?
c
      if ( cpnt(1) .lt. 0.15696 )  go to 100
c
c    yes - get coordinates of 1000 km points
c
```

```
      pl = 0.15696
      call razgc( rlat, rlon, pl, cpnt(8), cpnt(4), cpnt(5) )
      pl = cpnt(1) - 0.15696
      call razgc( rlat, rlon, pl, cpnt(8), cpnt(6), cpnt(7) )
100   continue
      return
      end
```

```
      subroutine razgc( lat1, lon1, range, azim, lat2, lon2 )
cp
c      subroutine razgc
c
c        call razgc(lat1,lon1,range,azim,lat2,lon2)
c
c        this routine computes the latitude and west longitude
c        (lat2, lon2) of a point a specified range from a given
c        point on the earth's surface.  also required for input
c        is the azimuth (azim) to the new point in radians.  this
c        method assumes a spherical earth and recognizes the
c        degenerate cases of the given point being at the north
c        or south pole.  for the degenerate cases, azim should be 0
c        or pi and lon2 is undefined.  however, azim is not checked,
c        and lon2 is arbitrarily set equal to lon1.  this routine
c        recognizes the degenerate case when range is set to zero.
c        all coordinates are in radians.
c
c        subroutines and functions used:  none
c
c        common blocks:  none
c
cz
c
      real        lat1, lon1, lat2, lon2
c
      data  pi/3.14159/,twopi/6.28318/,halfpi/1.570796/
      data  rtd/57.295779/,dtr/0.017453/
c
c   test for degenerate cases
c
      if ( abs( lat1 - halfpi ) .gt. 1.0e-5 )  go to 100
c
c   the given point is the north pole
c
      lat2 = halfpi - range
      lon2 = lon1
      go to 200
100   continue
      if ( abs( lat1 + halfpi ) .gt. 1.0e-5 )  go to 120
c
c   the given point is the south pole
c
      lat2 = range - halfpi
      lon2 = lon1
      go to 200
120   continue
      if ( range .gt. 0.0 )  go to 130
c
c   point 2 coincident with point 1
c
      lat2 = lat1
      lon2 = lon1
      go to 200
130   continue
```

```
c
c   general case
c
      s1 = sin( lat1 )
      c1 = cos( lat1 )
      c2 = cos( range )
      ca = s1*c2 + c1*sin( range )*cos( azim )
      ca = amin1( amax1( ca, -1.0 ), +1.0 )
      a = acos( ca )
c
c   test if destination ends up on the poles
c
      if( abs(a).gt.1.0e-5 ) go to 140
      lat2 = halfpi
      lon2 = lon1
      go to 200
140   continue
      if( abs(a-pi) .gt. 1.0e-5 ) go to 150
      lat2 = -halfpi
      lon2 = lon1
      go to 200
150   continue
c
c   everything seems ok, get destination coordinates
c
      cg = ( c2 - s1*ca )/( c1*sin( a ) )
      cg = amin1( amax1( cg, -1.0 ), +1.0 )
      g = acos( cg )
      lat2 = halfpi - a
      sa = sin( azim )
      if ( sa .ge. 0.0 )  lon2 = amod( lon1 - g, twopi )
      if ( sa .lt. 0.0 )  lon2 = amod( lon1 + g, twopi )
200   continue
      return
      end
```

```
      function sygn ( y )
cp
c      real function sygn
c
c        x=sygn(y)
c
c        this function returns the value of 0 if y is 0, -1. if y is
c        less than zero and a +1. if y is greater than zero.
c
c        subroutines and functions used:  none
c
c        common blocks:  none
c
cz
c
      if  (y)  100, 200, 300
100   sygn = -1.0
      go to 999
200   sygn = 0.0
      go to 999
300   sygn = 1.0
c
999   return
      end
```

APPENDIX C

FORTRAN PROGRAM FOR HFBC84

The listing of HFBC84 that follows is written in FORTRAN 77 for the HP 9050 computer. Coefficients required for running this routine are not included in the listing.

```
      SUBROUTINE CURMUF
      COMMON / CON / D2R, DCL, GAMA, PI, PI2, PIO2, R2D, RZ, VOFL
      COMMON / FRQ / FREL(14), NUMFREL, FREQ, JMODE, FXEMAX
      COMMON /GEOG/ CLAT(5),CLONG(5),GLAT(5),GMDIP(5),GYZ(5)
     A ,HPF2(5),RD(5),KM,BTR,BTRD,BRTD,GCD,GCDKM,LATFL
      COMMON /PARM/PWR,PWRDB,RLATD,RLONGD,TLATD,TLONGD,SSN,MONTH
     A ,IHR1,IHR2,NMODE,XLY,XLZ
      COMMON /FSTAB/ TAB(6,24,12),ALLMUF(24),EMIN(24,12),CIREL(24,12)
      COMMON /TVAR/ FI(3,5),CYCEN(5),IT,ACAV,ASM
      COMMON/MODES/ DELMOD(2,6),ITMOD(2,6),ZMFMOD(2,7)
C     RECEIVER SITE SAMPLE AREA
      IF (KM-3)  100,105,110
C  ONE SAMPLE
  100 KE=1
      KEMAX = 1
      KF=1
      GO TO 117
C    THREE SAMPLES
  105 KF=2
      KE=1
      KEMAX = 3
      IF(FI(1,1) - FI(1,3)) 117, 117, 106
  106 KE=3
      KEMAX = 1
      GO TO 117
C  FIVE SAMPLES
C.....SEPARATE TESTS FOR SELECTION OF LOWEST CRITICAL FREQUENCIES
  110 KE = 1
      KEMAX = 5
      IF(FI(1,1) - FI(1,5)) 115, 115, 112
  112 KE = 5
      KEMAX = 1
  115 KF = 2
      IF(FI(3,2) - FI(3,4)) 117, 117, 116
  116 KF = 4
  117 CONTINUE
C
C  ELAYER MUF
C
C.....SEE SUBROUTINE ITS FOR FOE CALCULATION (IWP6/12 DECISION 36)
      FXE = FI(1,KE)
      FXEMAX = FI(1,KEMAX)
      HPE = 110.
      DEL  = 0.0
      PHE=ASIN(RZ*COS(DEL)/(RZ+HPE))
      NHOPS = .5 * GCDKM / ((PIO2 - DEL - PHE) * RZ)
      NHOPSE = 0
      IF(GCDKM.GT.2000.) NHOPSE = 1
      NHOPS = MAX0(NHOPS,NHOPSE)
      DO 123 J=1,6
      EHOPS=NHOPS+1
      PSI=GCDKM/((2.*RZ)*EHOPS)
      CPSI = COS(PSI)
      SPSI = SIN(PSI)
      TANP = SPSI / (1. - CPSI + HPE / RZ)
```

```
      PHE = ATAN(TANP)
      DEL = PIO2 - PHE - PSI
      CDEL = COS(DEL)
      SPHE = RZ*CDEL/(RZ+ HPE)
      SECP = 1./SQRT(1.-SPHE*SPHE)
121   DELMOD(1,J)=DEL*R2D
      ITMOD(1,J)=NHOPS+1
      ZMFMOD(1,J)=FXE*SECP
123   NHOPS=NHOPS+1
      ZMFMOD(1,7)=FXEMAX
      EMUF=ZMFMOD(1,1)
C
C F2  LAYER MUF
C
      FLFC = 1.
      IF(GCDKM - 4000.) 130, 135, 135
  130 FLFC = 1.64E-7 * GCDKM * GCDKM
      IF(GCDKM - 800.) 135, 135, 132
  132 FLFC = 1.26E-14 * GCDKM ** 4 - 1.3E-10 * GCDKM ** 3
     A + 4.1E-7 * GCDKM ** 2 - 1.2E-4 * GCDKM
  135 CONTINUE
      JMODE=KF
      FX2 = 0.96*FI(3,KF)
C.....SET ZENITH ANGLE TO DETERMINE OPERATIONAL MUF FACTOR
      HP2 = HPF2(KF)
      DEL = 0.0
      PHE=ASIN(RZ*COS(DEL)/(RZ+HP2))
      NHOPS = .5 * GCDKM / ((PIO2 - DEL - PHE) * RZ)
      NHOPSF = 0
      IF(GCDKM.GT.4000.) NHOPSF = 1
      IF(GCDKM.GT.7000.) NHOPSF = 2
      NHOPS = MAX0(NHOPS,NHOPSF)
      DO 137 J=1,6
      XHOPS=NHOPS+1
      PSI=GCDKM/((2.*RZ)*XHOPS)
      CPSI = COS(PSI)
      SPSI = SIN(PSI)
      TANP = SPSI / (1. - CPSI + HP2 / RZ)
      PHE = ATAN(TANP)
      DEL = PIO2 - PHE - PSI
      CDEL = COS(DEL)
      SPHE = RZ*CDEL/(RZ+ HP2)
      SECP = 1./SQRT(1.-SPHE*SPHE)
136   DELMOD(2,J)=DEL*R2D
      ITMOD(2,J)=NHOPS+1
      ZMFMOD(2,J)=FX2*SECP
137   NHOPS=NHOPS+1
      F4 = FI(3,KF)*FI(2,KF)*1.1
      FZ = FI(3,KF) + .5*GYZ(KF)
      F2MUF = FZ + (F4-FZ)*FLFC
      IF(GCDKM-4000.) 160,160,140
  140 IF(KF-2) 145,145,150
  145 KFF = 4
      GO TO 155
  150 KFF = 2
```

```
  155 F44 = FI(3,KFF)*FI(2,KFF)*1.1
       F2MUF = AMIN1(F4,F44)
  160 CONTINUE
      ZMFMOD(2,1)=F2MUF
C
C  CIRCUIT MUF
C
      IF(GCDKM.GT.4000.) EMUF = 0.0
      ALLMUF(IT) = AMAX1(EMUF,F2MUF )
      RETURN
      END
```

ATE

LMED

8